공학박사 학위논문

Advancement of Regulatory Atmospheric Dispersion Model for Nuclear Power Plants

원자력 발전소 규제를 위한 대기확산평가 모델 고도화

2021년 8월

서울대학교 대학원

에너지시스템공학부

신 지 용

Advancement of Regulatory Atmospheric Dispersion Model for Nuclear Power Plants

지도 교수 김 은 희

이 논문을 공학박사 학위논문으로 제출함
2021년 8월

서울대학교 대학원
에너지시스템공학부
신 지 용

신지용의 공학박사 학위논문을 인준함
2021년 8월

위 원 장 _____ 심 형 진

부위원장 _____ 김 은 희

위 원 _____ 서 경 석

위 원 _____ 정 재 학

위 원 _____ 김 주 열

Abstract

Nuclear reactors with smaller capacities than conventional power reactors, such as research reactors and small modular reactors, can designate shorter boundaries for exclusion areas. For the shortened boundary distances, elevated release is preferred to ground release since the radionuclides emitted from tall stacks are diluted until dispersed to the ground surface. Previous studies have pointed out the limitations of the current dispersion model for elevated release when combined with complex terrain conditions. To minimize regulatory confusions, substitution for a newer enhanced model should be considered. This research aims to evaluate the current model and draw out possible improvements.

To analyze the major components of the model, an atmospheric dispersion code based on XOQDOQ was written. Instead of horizontal transport of plumes, an adjusted plume height approach to simulate a plume centerline that responds to terrain heights and atmospheric stabilities was added. Instead of using the relative deposition rate function, site-specific deposition velocities were derived to calculate the deposition factor.

Preliminary assessments were carried out assuming routine elevated release at Wolsong and Kori sites between 2016 and 2018. The effects of correction factors for recirculation and wind speeds were analyzed, and mixed release cases were compared to the elevated release cases. Maximum dispersion factors from the elevated release increased with terrain heights, and the maximum points moved to elevated locations. Under mixed release conditions, the maximum dispersion factor at 300 m exceeded the maximum values under elevated release conditions.

The modeling results were then compared with AERMOD, a reference model for environmental impact assessment. A set of meteorological preprocessing codes was developed so that the on-site measurements can be combined with the surface and upper-air data from the weather stations. Without terrain elevation, the

difference between the models was minimal, but when terrain elevation was considered, the maximum dispersion factor from XOQDOQ was increased by eight to twenty-seven times, while in AERMOD, the increment was less than two times compared to the no terrain case. When plume heights were adjusted, the increments were less than four times the base case and the maximum locations shifted closer to the AERMOD cases.

To evaluate the dispersion model, the predicted concentrations of air pollutants were compared with the observed concentrations obtained from air monitors in the region. Compared to the annual distribution of 1-hour averaged concentrations, the current dispersion model performed well for the prevailing wind directions within the factor of 2 ranges. The model results fluctuated between over and underprediction, while for several receptors, the terrain elevation reinforced the overprediction by the model. The validation is limited due to severe uncertainties in the source locations, release heights, and emission rates.

In this research, the dispersion modeling for elevated release with complex terrain conditions was performed. As there have been few domestic cases that assumed elevated release, the components of the model and the changes in dispersion pattern due to terrain heights were thoroughly reviewed. This research can be used as a reference in determining the employability of elevated releases.

Secondly, the current dispersion model was evaluated with various approaches such as model intercomparison, sensitivity analysis, and long-term validation. It was confirmed that the discrepancies between the models were minimal without terrain elevation, but the current model can lead to higher concentrations when terrain elevation is factored in.

Keyword: dispersion model, model evaluation, environmental impact assessment, Gaussian plume model, complex terrain
Student Number: 2015-21319

Table of Contents

Chapter 1. Introduction

1.1. Dispersion Models in Regulation

The atmospheric dispersion model is a mathematical model describing the transport of gaseous material. For nuclear installations, the dispersion model plays an essential role in the regulatory processes. The factors calculated from the model include dispersion factor and deposition factor, both of which are input parameters for the external and internal dosimetry. This research aims to evaluate the current atmospheric dispersion model for elevated releases under complex terrain conditions.

Calculating dispersion and deposition factors is a crucial step in determining the Exclusion Area Boundary (EAB). The modeling results are included in the Preliminary Safety Analysis Report (PSAR) submitted for the construction permit. In the report, the applicant should confirm that the expected dose due to radioactive effluents at the EAB does not exceed the established limit. Another regulatory process that requires dispersion modeling is Probabilistic Safety Assessment (PSA) level-3, which includes off-site dose assessment due to gaseous effluents. The dispersion modeling is also applied to justify the total amount of radionuclides to be released.

Reactors with a smaller capacity than conventional power reactors, such as research reactors and small modular reactors, usually establish shorter EAB distances. In that case, the applicant may prefer elevated releases to ground releases since the radionuclides emitted from tall stacks are diluted until they disperse to the ground surface. However, the current atmospheric dispersion model for regulatory purposes may not be suitable for elevated releases combined with complex terrain conditions and there have been few domestic installations that assumed elevated release conditions. Thus, both applicants and regulatory bodies should consider modifying or upgrading the current model. For that purpose, the current model design was evaluated, and possible improvements were drawn out.

1.1.1. Regulatory Framework regarding Gaseous Effluents in Nuclear Installations.

The Nuclear Safety Act and Nuclear Safety and Security Commission (NSSC) Rules state domestic regulations regarding elevated releases and EAB criteria for nuclear installations. Article 11 and 21 of the Nuclear Safety Act specifies the population's health and prevention of environmental hazards as requirements for construction and operation permit. According to Article 89 of the same law, the exclusion area is set for preventing radiation hazards. Thus, access and residence in the exclusion area can be prohibited.

According to Article 129 of the Enforcement Decree of the Nuclear Safety Act, the NSSC and relevant offices set the exclusion area considering orographic and other environmental conditions. Article 174 of the same decree requires safety limits established by NSSC to be met for liquid and gaseous radioactive effluents to prevent public risk. Furthermore, article 5 of Rule No. 24 of the NSSC specifies that the location of the nuclear installation should be apart from the populated area so that the total dose to the public in case of a nuclear accident may not exceed the safety limit established by the NSSC.

Public Notices Radiation01 “Standards for Radiation Protection” and Reactor04 “Technical Standards for the Location of Nuclear Installations” of the NSSC specify the dose constraint for normal and accidental situations. According to Article 2 of Reactor04 and the Attached Table, the 10 Code of Federal Regulations (CFR) Part 100.11 is applied. It stipulates that the dose constraint assuming possible accident scenarios to be 250 mSv to whole−body and 3000 mSv to thyroid during two hours of exposure at the EAB. Article 16 of Radiation01 specifies the annual dose constraint due to gaseous effluents at the EAB. The limits are divided into specific pathways, as in Table 1.1. The limits are the same as in Appendix I of 10 CFR part 50.

Table 1.1. Dose constraints at EAB under operating conditions

Pathways	Dose constraint
Annual air dose due to gamma radiation[1)]	0.1 mGy
Annual air dose due to beta radiation[1)]	0.2 mGy
Annual dose to an individual (Whole-body)[2)]	0.05 mSv
Annual dose to an individual (Skin)[3)]	0.15 mSv
Annual dose or dose commitment to organs[4)]	0.15 mSv

[1)] absorbed dose in the air
[2)] effective dose due to external exposure
[3)] equivalent dose due to external exposure
[4)] an estimated annual dose or dose commitment

10 CFR Part 100 specifies the regulations regarding the location of the nuclear installations. As Part 100 was revised in 1996, the nuclear power reactors whose licensing applications were made before January 10th, 1997, and the testing reactors are subject to the dose constraints stated in Part 100.11. Part 100.21, where the dose constraint at the EAB follows 10 CFR 50.34(a)(1) as 250 mSv TEDE (total effective dose equivalent), is used for the rest of the power reactors. The method for establishing source term in accident scenario (substantial meltdown of core) has also been changed in Part 100.21.

As domestic dose constraints for accidental conditions still refer to the 10 CFR Part 100.11, revision for Public Notice Reactor04 is necessary. Previous research (KINS, 2016) suggested three options for modification: (1) continued referring to Part 100.11, (2) Updating the current regulation to meet Part 100.21, and (3) Specifying the minimum EAB distance for each reactor type (e.g., 560 m for PWRs). Revisions to the legislations and related regulatory guides are still under review.

Article 17 of the NSSC Public Notice Reactor29 “Standards for Measurement and Evaluation of Meteorological Conditions at the Site of Nuclear Installations” describes the methodologies for assessing atmospheric dispersion and dilution of radionuclides. Paragraph 3 of the Article states that when the emission height is greater than twice the surrounding building structures, an applicant should assume the elevated release type. Paragraphs 4 and 5 specify the calculation

requirements for accidental and routine conditions. For long-term, normal operating conditions, an applicant should estimate the dispersion factor for specific distances, including the boundaries of exclusion area, closest residential area, emergency planning area, and low population zone (LPZ).

Regulatory Guide (RG) 1.3 of the Korea Institute of Nuclear Safety (KINS) describes standard procedures for regulatory dispersion modeling. The parts in the regulatory guide that deals with modeling details refer to the RG 1.111 (long-term, routine) and 1.145 (short-term, accidental) of the US Nuclear Regulatory Commission (NRC). The technical details of the KINS RG 1.3 and NRC RG 1.111 are elaborated in Chapter 2.

1.1.2. Construction Permit for Ki-Jang Research Reactor

One of the recent regulatory cases regarding dispersion modeling is the construction permit of the Ki-Jang Research Reactor. The applicant for the permit is Korea Atomic Energy Research Institute (KAERI). Tables 1.2 and 1.3 are the model estimates of dose due to gaseous effluents at the planned EAB distance for accidental and operating conditions.

Table 1.2. Short-term dose assessment results (NSSC, 2019)

Pathways	Dose constraint	Model Calculation	
		EAB (160 m)	LPZ (400 m)
Whole body (mSv)	250	42.21	7.37
Thyroid (mSv)	3000	84.45	60.2

For accidental cases, emission of radionuclides due to the maximum hypothetical accident is assumed. The above case is based on a fuel assembly blockage scenario. The doses at the boundaries of EAB and LPZ are compared with the regulatory limit. As the ground release is assumed, the dispersion and deposition factors tend to decrease as the distance to the source is increased.

Table 1.3. Long-term dose assessment results (NSSC, 2019)

Pathways	Dose constraint	Model Calculation	
		EAB (160 m)	Maximum
Annual Air Dose due to Gamma Radiation (mGy/y)	0.1	3.52E-03	2.08E-02*
Annual Air Dose due to Beta Radiation (mGy/y)	0.2	6.19E-03	3.67E-02*
Annual Dose to Whole Body (mSv/y)	0.05	1.48E-03	8.74E-03*
Annual Dose to Skin (mSv/y)	0.15	4.42E-03	2.61E-02*
Annual Dose or Dose Commitment to Organ (mSv/y)	0.15	2.62E-02	4.17E-02**

* Dispersion factor at 300 m, ** Deposition factor at 400m

For operating cases, effluents are assumed to be routinely emitted through the gaseous waste treatment system. The annual dose at the EAB is compared with the regulatory limit. Due to elevated release, it was found that the maximum dispersion and deposition factors have been estimated beyond the EAB distance. Thus, the regulatory body required additional assessment regarding the maximum values.

As in the above case, it is conventional to set the EAB first and verify that the dose estimated from the model calculation meets the dose constraint. And when the elevated release under normal operation results in the maximum value located beyond the exclusion area, the additional verification that the maximum values are still below the limit might be required.

1.2. Gaussian Plume Model

Leelossy et al. (2018) reviewed the numerical models to assess the atmospheric dispersion of radionuclides for various purposes. The models can be divided into Gaussian, Eulerian, and Lagrangian models, corresponding to analytic, deterministic, and stochastic solutions to the diffusion equation (Leelossy et al., 2018; Stockie, 2011). Gaussian plume model assumes a single source in the homogenous and stationary wind and turbulence intensity. The model provides good results for the local scale of 1 to 10 km and has become the standard of regulatory modeling for industrial stack releases and several environmental applications (Cimorelli et al., 2005; Romanov et al., 2020).

Gaussian plume model is a powerful tool for regulatory or policy-related decision-making because it can work with only a few parameters. The key inputs to a Gaussian plume model, other than wind speed and direction, are the lateral and vertical turbulence intensities that define the spread of the two-dimensional normal distribution (Leelossy et al., 2018). A simplified approach to estimate the turbulent spreads of the plume is to use empirical values categorized with stability classes (Turner, 1996). A more sophisticated approach uses a physical parameterization of turbulence based on planetary boundary layer characteristics; mixed layer depth, friction velocity, sensible heat flux, and Monin-Obukhov length (Moreira et al., 2005; Stull, 1988).

1.2.1. Gaussian Plume Model in Regulatory Practice

The Nuclear Safety Act requires that the exclusion area boundary is set considering the distance that meets the dose constraint during two hours of a possible accident. However, it is customary to set EAB distances for each reactor type in advance and verify that the dose constraints for both accidental and normal operating conditions are met at the assumed EAB.

Public Notice Radiation 01 requires that the annual dose due to gaseous effluents during normal operation be estimated at the EAB. In Appendix I of 10 CFR 50, on the other hand, annual air dose is calculated at "any location near ground level which could be occupied by individuals in unrestricted areas," and the annual individual dose is calculated for "individual in an unrestricted area."

The Final or Preliminary Safety Analysis Report (FSAR/PSAR) submitted by several nuclear power plants in Korea and the United States were reviewed. Gaussian plume model had been a standard dispersion model applied to nuclear power plants for both accidental and normal operating conditions. Tables 1.4 and 1.5 summarize the details of the reports. Most applicants employed similar methodologies for dispersion modeling as described in NRC RG 1.111. In the United States, several cases used stack emission, and despite the guides in Appendix I of 10 CFR 50, the dose at the EAB was compared to the dose constraints. For domestic nuclear power plants, however, the ground release was adopted for the cases reviewed here.

For PWRs, the short-term and long-term dose assessment results for gaseous effluent are in Chapter 2 of the FSAR. Wolsong Units 2-4, which are CANDU reactors, reported the assessment results in Chapter 11 (long-term) and Chapter 15 (short-term). As Shin-Kori Units 5 and 6 are yet to acquire the operating permit, the PSAR and the inspection report were reviewed.

Table 1.4. Regulatory dispersion modeling for domestic nuclear installations

Reactor Unit	Construction Permit	Reactor Type	EAB (m)	Dispersion Model	
				Normal	Accidental
Kori 1	1972.05.31	WH-60	700	-	PAVAN
Kori 2	1978.11.18	WH-F	700	-	-
Kori 3, 4	1979.12.24	WH-F	700	-	-
Shin-Kori 1, 2	2005.07.01	OPR-1000	560	AZAP	AZAP
Shin-Kori 3, 4	2008.04.15	APR-1400	560	AZAP	AZAP
Shin-Kori 5, 6	-	APR-1400	560	AZAP	AZAP
Wolsong 2	1992.08.28	CANDU	914	XOQDOQ	-
Wolsong 3, 4	1994.02.26	CANDU	914	XOQDOQ	-
Shin-Wolsong 1, 2	2007.06.04	OPR-1000	560	AZAP	AZAP
Hanbit 1, 2	1981.12.17	WH-F	700	WINDIFF	WINDIFF
Hanbit 3, 4	1989.12.21	System 80	700	AZAP	AZAP
Hanbit 5, 6	1997.06.14	OPR-1000	560	AZAP	AZAP
Hanul 1, 2	1983.01.25	France CPI	700	-	AZAP
Hanul 3, 4	1993.07.16	OPR-1000	700	AZAP	AZAP
Hanul 5, 6	1999.05.17	OPR-1000	560	AZAP	AZAP
Shin-Hanul 1, 2	2011.12.02	APR-1400	560	AZAP	AZAP

Kori Unit 1 has been permanently shut down since June 2017. The dose due to dispersion was reassessed, assuming that fuels were unloaded. A straight-line Gaussian plume model as in RG 1.111 was applied, correcting radioactive decay, depletion, and wake effects. Meteorological data from 2012 to 2014 were used as input. It was not mentioned whether the recirculation factor was applied or not. The same approaches were applied for Kori Units 2-4 for long-term, routine operations.

In Wolsong Units 2-4, the dispersion model includes terrain elevation data as input. However, it is assumed that the ground or mixed release type would have been selected from the stack and building heights. It is also mentioned that the dispersion toward the ocean has been excluded in the dose calculation.

The EAB distances for domestic nuclear reactors had been collectively set as 700 and 914 m for PWRs and CANDUs, respectively. However, starting from the construction permit of Hanbit Units 5 and 6, the EAB distance for PWRs was reduced to 560 m.

AZAP is the dispersion code based on the NRC RGs for short-term and long-term modeling (Na et al., 2000). ARCON96 is a plume dispersion code to assess effluent concentrations inside a reactor control room. The NRC RG 1.194 specifies the regulatory details.

Table 1.5. Regulatory dispersion modeling for nuclear installations in the United States

Name	Reactor	Release Height (m)	EAB (m)	Dispersion Model	
				Normal	Accidental
Dresden 1, 2, 3	BWR-1, BWR-3	95	800	-	PAVAN, ARCON96
LaSalle 1, 2	BWR-5	113	510	-	PAVAN, ARCON96
Nine Mile Point (cancelled)	EPR	62	677	AEOLUS3	AEOLUS3
Oyster Creek	BWR-2	112	414	-	-
Peach Bottom 2, 3	BWR-4	58	823	-	PAVAN, ARCON96
Turkey Point 6, 7	AP-1000	Ground	435	XOQDOQ	PAVAN, ARCON96

In Dresden Units 1, 2, and 3, more than 98% of the hourly wind direction measurements showed variations over 60 degrees. The FSAR assumes it is unlikely that the gaseous release in accidental situations will lead to high concentrations. The long-term modeling results of the site are separately reported through the Offsite Dose Calculation Manual (ODCM). The modeling methodology described in the ODCM follows NRC RG 1.111. It is also mentioned that the terrain elevation is not considered as the site is in a relatively flat region.

La Salle Units 1 and 2 assume stack height of 113 m, while the maximum release height is 100 m in the dispersion model described in RG 1.111. Therefore, the modeling assumed 100 m release height, as the results will be more conservative by setting lower release heights than the actual value.

Nine Mile Point Units 1 and 2 are Boiling Water Reactors (BWR). And the construction plan for Unit 3, the US European Pressurized Reactor (EPR), was canceled. The FSAR for Unit 3 is a combined Construction and Operating License (COL) document containing technical details, including long-term dispersion modeling. AEOLUS3 code based on NRC RG 1.111 was applied for dispersion modeling under normal operating conditions. The AEOLUS3 code can model dry deposition and wet deposition, but wet deposition was not assumed for this case. The default recirculation factor of XOQDOQ was applied, and the dispersion coefficients followed XOQDOQ as well. The effective stack heights calculation included terrain elevation, and the mixed release was assumed. The factors for dispersion and deposition were estimated for several receptor locations, including the site boundary. The dispersion toward Ontario Lake was ignored for the dose calculation process.

Turkey Point Units 6 and 7 are Advanced Passive 1000 (AP-1000) reactors under construction. In FSAR, XOQDOQ was used to calculate the dispersion factor. Even though the site employs stack release, the ground release was assumed for the modeling since the stack height is less than twice the surrounding building heights. The wind speed levels were divided into 13 classes. The default recirculation factor of the XOQDOQ code was assumed to consider the meteorological characteristics of the site, which is in the coastal region.

To sum up, several regulatory cases for stack releases were reviewed by the FSAR and other regulatory documents submitted to the US NRC. In most cases, the dispersion modeling according to the NRC RG 1.111 was performed for long-term and normal operating conditions. In addition, several instances in which terrain elevation was considered and recirculation factor was applied were found.

1.2.2. Case of Nuclear Installations in European Countries

According to KINS (2016), most European countries do not explicitly set exclusion areas. Instead, they set up emergency planning areas for administrative purposes. The restriction area set around the nuclear installations can be regarded as equivalent to the EABs, and the establishment and management of the restriction area are up to each facility. When dose assessment assuming possible accident is performed, the dose to the residents is realistically assessed.

European Commission (2007) published Radiation Protection 144, guidance on assessing collective doses due to routine releases. The guidance implemented PC-CREAM (Health Protection Agency, UK) based on Gaussian plume model. In addition, PC-CREAM 08 was also used for calculating the collective dose due to nuclear installations in the UK (Nelson et al., 2002; Jones et al., 2013).

1.2.3. IAEA Guidelines on Dispersion Modeling

International Atomic Energy Agency (IAEA) published a set of requirements and guidelines regarding dispersion modeling. For example, requirement 25 of the SSR-1 requires dispersion modeling near the expected nuclear power plant before site selection. For atmospheric dispersion modeling, the orographic and meteorological characteristics should be considered. And weather data should be measured at relevant height and location for at least a year.

The SRS No. 19 mentions Gaussian plume model as one of the conventional methods adopted for long-term continuous emitting situations. And according to the GSG-10, Gaussian plume model is suitable for relatively flat terrain where a residential area is located 10-20 km from the source point.

1.3. Limitations of Gaussian Plume Model

It has been frequently pointed out that the current regulatory dispersion model is not suitable for complex terrain conditions. For domestic nuclear power plants (Shin-Kori Reactor Units 5 and 6), the regulatory body required additional information that supports applying conventional dispersion coefficient for the site. The same was required for Ki-Jang Research Reactor.

International Atomic Energy Agency (IAEA), during its SALTO review, also pointed out the suitability of the dispersion modeling of Wolsong Reactor Unit 1. It is recommended that the application of the dispersion coefficients defined in KINS RG 1.3 and NRC RG 1.111 be limited for ground release cases within a kilometer radius of rural and flat areas. Thus, whether its application can be expanded to the releases with terrain elevation considered should be evaluated.

NRC (2014) published a periodic review on the RG 1.111 which has not been revised since 1977. The content of the review includes issues raised regarding the model formulations and meteorological input processing.

On model formulation and assumptions, the review suggested applying dispersion models developed by other institutions. Also, the need for revisions on wake effect, calm state, terrain-recirculation effects, mixed release, and corrections for non-vertical stack releases was mentioned. On meteorological input, using hourly data instead of joint frequency distribution was suggested. Additionally, the need for the recommended measurement period, the limitations due to non-time-series data, wet deposition modeling, and analyzing seasonal variation in addition to the annual prediction were proposed.

The NRC review also mentions that as of 2014, there is no upcoming licensing for power reactors in three to five years. Thus, revising RG 1.111 is not a pressing issue. As for small modular reactors and research reactors, which emit smaller amounts of radionuclides than power reactors, the continued use of RG 1.111 can be recommended.

The US National Council on Radiation Protection &

Measurements (NCRP) developed a screening method at the request of the US Environmental Protection Agency (EPA) in 1985 to screen small facilities using radioactive materials complying with the Clean Air Act. NCRP Commentary No. 3 proposed a methodology for evaluating the concentration of radioactive substances in the ground using Gaussian plume model. Like RG 1.111, NCRP Commentary No. 3 also limits the use of the model for the purpose of evaluating average values over a long period of time. NCRP Commentary No. 8 (NCRP, 1993) discusses the uncertainty of the model components and correction factors such as atmospheric stability, diffusion coefficient, release height, duration of wind direction, wind speed, mixing layer height, and terrain effect. The degree of model uncertainty quantified by comparing the predicted concentration with the measured value is presented in Table 1.6. The predicted/measured values range based on the annual average ranges from 0.25−4 times (flat terrain) to 0.1−10 times (complex terrain). Over a short period of time, the fluctuation of the predicted value is even larger and can range from 0.1−10 times up to 0.01−100 times.

Table 1.6. Range of uncertainties in dispersion model (NCRP, 1993)

Conditions	Range
• Highly instrumented site: ground−level centerline concentration within 10 km of a continuous point source	
Ground−level releases	0.8 to 1.2
Elevated releases	0.65 to 1.35
Maximum air concentration for elevated releases	0.51 to 1.5
• Annual average for a specific point, flat terrain, within 10 km downwind of the release point	0.5 to 2
• Annual average for a specific point, flat terrain, 10 to 150 km downwind of the release point	0.25 to 4
• Specific hour and receptor point, flat terrain, steady meteorological conditions	
Elevated releases without building wake effects	0.1 to 10
Elevated releases with building wake effects	0.01 to 100
• Short−term, surface−level releases with building wake effects using temperature gradient method of estimating atmospheric stability	
Wind speeds > 2 m/s	0.7 to 100
Wind speeds < 2 m/s	1 to 100
• Short−term, surface−level releases without building wake effects using temperature gradient method of estimating atmospheric stability	
Wind speeds > 2 m/s	0.3 to 10
Wind speeds < 2 m/s	1 to 100
• Complex terrain or meteorology (e.g., sea breeze regimes)	
Annual average concentrations	0.1 to 10
Short−term releases	0.01 to 100
• Urban releases	
Annual average concentrations	0.25 to 4
≤ 24 h concentrations	0.1 to 10

Table 1.7 is the data derived by the UK National Radiological Protection Board (NRPB; now Health Protection Agency, HPA) (NRPB, 1986). It describes the conditions that must be satisfied to consider the surrounding terrain flat when applying the atmospheric dispersion model. The height criteria for obstacles in the surrounding area are slightly different depending on the atmospheric stability.

Table 1.7. Height criteria for flat terrain assumption (NRPB, 1986)

Atmospheric stability	Criteria
Neutral and unstable	the gradient of the surrounding terrain should be less than about 1 in 10 • for a ridge upwind of the source either $H > 1.5h$ or $x > 20h$ in neutral conditions or $x > 10h$ in very unstable conditions • for an isolated hill upwind of the source either $H > 1.5h$ or $x > 7h$ • for a hill or ridge downwind of the source either $H > h + \sigma_z(x)$ or $\sigma_z(x) > h$
Stable	the gradient of the surrounding terrain should be less than about 1 in 100 • for an obstacle upwind of the source either $H > h$ or $x > 40h$ in slightly stable conditions or $x > 100h$ in very stable conditions • for an obstacle downwind of the source either $H > h + \sigma_z(x)$ or $\sigma_z(x) > h$

where H is the release height (m), h is the obstacle height (m), x is the distance between obstacle and source (m), and $\sigma_z(x)$ is the vertical plume standard deviation (m).

The US Savannah River Laboratory used XOQDOQ to evaluate whether radioactive materials released from the Savannah River site meet regulatory standards. Before that, the XOQDOQ dispersion code was self-evaluated and published as a report (Bauer, 1991). Based on RG 1.111, the calculation formula benchmarking XOQDOQ was written and compared with the results of XOQDOQ for several scenarios. Because the amount of radioactive material emitted from the site was small, comparing the measured and calculated values was not feasible. According to this report, the model's suitability has been verified through experiments in previous studies, and its theoretical basis is also scientifically agreed upon. Therefore, it is mentioned that it is appropriate to apply XOQDOQ to the site evaluation, but the possibility of improving the code needs to be continuously reviewed. In particular, it emphasizes the need for sensitivity analysis for user-specific factors.

The UK HPA (2009) published technical literature on PC-CREAM 08 that summarizes the limitations of Gaussian plume model. Since the formula includes the reciprocal wind speed, it cannot be applied to a calm state or low wind speed conditions. When the wind speed is low, the fluctuations in the speeds and directions become significant, so it does not conform to the fundamental assumption of the plume model. In addition, the model is not suitable when the terrain and weather conditions are not uniform because it uses weather data from a single point. For example, when evaluating a short distance in a coastal area, it may be sufficient to assume flat terrain. Still, a long-distance evaluation or a predicted value for a complex terrain may have a significant error. Also, the closer the atmospheric stability is to the very stable state, the more sensitive the predicted value is to the terrain conditions.

1.3.1. Issues regarding Dispersion Modeling

Domestic nuclear installations that recently applied for construction permits include Shin-Kori Units 5 and 6 and Ki-Jang Research Reactor. KINS (2016, 2018) required the applicants to reassess the suitability of the dispersion coefficient used in both short-term and long-term atmospheric dispersion modeling. The pending issue is whether the model well describes the orographic and meteorological characteristics of the planned sites. The applicant will need to provide the supplementary analysis for the operation permit that supports the continued use of the model.

The issue brought up during the construction permit application for Ki-Jang Research Reactor regards the determination of EAB under elevated release. The planned EAB for the reactor is 160 m, and the applicant only conducted the dose assessment for the short-term and long-term at the boundary distance. The dispersion modeling code ENDOS, developed by KAERI based on XOQDOQ, was used. However, under the elevated release conditions, the maximum dispersion factor was estimated beyond the EAB distance. Therefore, the regulatory body demanded the applicant to reanalyze the modeling results. As a result, the applicant reassessed the dispersion factor between 200 and 590 m to confirm that the maximum dispersion factor was estimated at 300 m to the NW direction from the emission point. In addition, the regulatory body also questioned the suitability of the dispersion coefficient, as they did for Shin-Kori units.

During the examination for the operation permit of Shin-Hanul Unit 1, it was reported that the predicted dose due to atmospheric dispersion nearly reached the regulatory limit. This was due to the redundancy of conservative assumptions that were applied for multi-unit safety analysis. For each reactor and each exposure pathway, the maximum values were summed up at the site boundary. The planned reactors were assigned predicted source terms, while the operating ones were given the maximum amount of liquid and gaseous emissions for the last ten years. As a result, the predicted dose at

the site boundary was 0.227 mSv/year while the dose constraint is 0.25 mSv/year, leaving less than 10 % as a margin of safety.

1.3.2. Previous Studies on Dispersion Model

KAERI or Korea Hydro & Nuclear Power Co. (KHNP) conducted most domestic studies regarding Gaussian plume model for regulatory purposes. In KAERI, the focus of the research was the parametric sensitivity of the model to ensure conservative modeling results. KNHP, on the other hand, concentrated on evaluating the safety margin of the current model compared to other models or tracer experiment results.

The effect of statistical preprocessing of meteorological results, including the number of wind levels, on the dispersion factor, was tested (Hwang et al., 2012). For short-term modeling, PAVAN code was used. The results showed that the change in dispersion factor due to wind levels was minimal compared to the changes due to preprocessing. They confirmed that the fluctuations in the model output were decreased when long-term average weather data were used.

Different approaches in dispersion coefficient parameterization were also evaluated for the short-term dispersion modeling (Hwang et al., 2013). The coefficients defined in (1) NRC, (2) CNSC, and (3) coefficients in MACCS/MACCS2 (Sandia National Lab, United States) were tested. Between (2) and (3), the outputs tend to deviate due to different surface roughness lengths, while NRC dispersion coefficients do not factor in surface roughness.

The dry deposition of Cs-137 and I-131 in the accident scenario was examined (Hwang et al., 2014). Comparing the expected dose at the exclusion area and low population zone boundaries, the doses were decreased when the dry deposition was considered. The authors assumed that it is because the dose due to inhalation exceeds the external dose due to ground deposition for both radionuclides. The wet deposition was also tested, while it is not included in the original XOQDOQ code (황원태 외, 2016). The authors evaluated the

significance of wet deposition in the total deposition factor. In Shin-Kori and Wolsong sites. the wet deposition accounts for 6% and 5% of the total deposition.

According to Jeong et al. (2016), the dispersion factors computed using XOQDOQ depend on the atmospheric stability classification methods. Stability classes can be determined by the temperature lapse rate or standard deviation of wind directions. The tests based on the weather data at Wolsong and Daedeok sites showed greater dispersion factors when the temperature lapse rates were used. However, there was no difference between the two approaches for depositions factors since the relative deposition rate follows a single curve for ground release.

The changes in the annual average dispersion factor due to the definition of the calm state and the different wind speed levels were tested with XOQDOQ (Jeong et al., 2013a). As these parameters can be altered by the applicants, the regulatory body should ensure they are correctly set to avoid underprediction. For example, by subdividing the lower wind speed range, the dispersion factor can increase up to 2.87 times.

The wake effect on the short-term and long-term dispersion factors was evaluated (Jeong et al., 2013b, 2014a). The modeling results from the different Gaussian plume models (ISC3, AERMOD, ARCON96) and the CFD (Computational Fluid Dynamics) calculation are presented. The Wolsong site was used as a modeling domain. As the studies employed different meteorological datasets, a direct comparison was not applicable. Jeong et al. (2014a) mention that by factoring in the wake effect, the long-term dispersion factor tends to increase near the source while decreasing at distances beyond the EAB, which is 914 m.

A tracer experiment was conducted at Wolsong site (Jeong et al., 2014b). The comparisons between observed and predicted were made for 150 receptor points around the emission source. For most measurements, the predicted value exceeded the observed ones. Still, it is difficult to conclude that the conservatism of Gaussian plume model was confirmed. The above tracer experiment was conducted

for 1 hour, while the evaluation during normal operation targets the long-term average value of at least a year.

The studies conducted by the KNHP focused on confirming the conservatism and safety margin of Gaussian plume models. The XOQDOQ modeling results were compared with the observed concentrations of tritium recorded in Wolsong for three years from January 2010 to December 2012 (이갑복 외, 2014a). The predicted values were 10 to 100 times the measured value. The results using XOQDOQ were also compared to the CALPUFF (EPA, USA) modeling results for the locations around the Wolsong site during the above periods (이갑복 외, 2014b; Lee et al., 2017). It was confirmed that XOQDOQ produced a more conservative value while the results from the two models were comparable.

The experimental results from a tracer experiment using SF_6 gas were compared to the predicted values (XOQDOQ and PAVAN) with the emission for 120 minutes (김정미 외 2017, 2018). The predicted values were up to several hundred times higher than the measured ones. Again, further discussion is needed as to whether the conservatism of Gaussian plume model can be confirmed through short-term tracer experiments.

1.3.3. Alternative Models

According to Richter (2016), the Lagrangian particle model may better simulate dispersion under complex terrain conditions than Gaussian plume model. But still, under suitable terrain and meteorological conditions, the differences between the two may not be significant. More importantly, the predictability of the Lagrangian particle model heavily depends on the precisions of input parameters and subordinate modules and functions.

Lutman et al. (2004) compared PLUME, the dispersion module of the PC CREAM code, with the Lagrangian particle model. The differences between the models were relatively small compared to the model uncertainties.

The Lagrangian particle model is suited for long-range transport

modeling. Figure 1.1 is an example of dispersion modeling using HYSPLIT, with Kori site as a source point. Currently, the minimum integration time step in HYSPLIT is one minute. When an average wind speed of 5 m/s is assumed, the time step limit will result in a minimum spatial resolution of about 300 m. Other dispersion models are recommended when the spatial scale is less than 1 km. Dispersion models such as FLEXPART and WRF-CHEM share similar limitations.

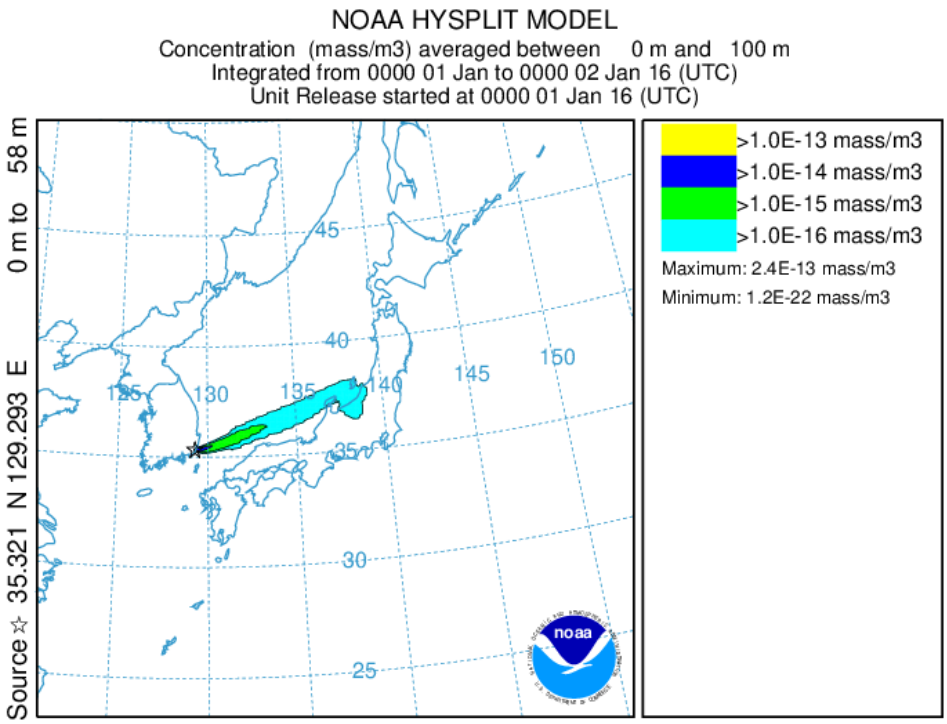

Figure 1.1. Example of dispersion modeling using HYSPLIT

For regulatory purposes, several Lagrangian particle models were made applicable to local dispersion with finer resolution. The NAME model, for instance, was developed by the UK Met Office. While the model was designed initially for incidental release of radionuclides, Nelson et al. (2002) applied the model to assess the impact due to routine discharges from Sellafield nuclear installation.

In Germany, the ARTM code, based on the Lagrangian particle dispersion model AUSTAL2000, was developed for dispersion modeling of radioactive materials under normal operating conditions.

AUSTAL2000 and ARTM require relatively few input parameters such as the surface roughness length, wind measurement height, wind direction and speed, and the stability classes defined by Klug-Manier.

Richter (2016) compared the characteristics of Gaussian and Lagrangian models in terms of regulatory compliance, confirming that the latter better simulates the action of various variables in complex conditions. However, it should be noted that the consistency of Lagrangian model heavily depends on the accuracy of the input variable and sub-models. When Langner and Klemm (2011) evaluated AUSTAL2000 against the observed concentrations, the model displayed poor performance mostly due to simplified handling of the meteorological parameters.

Gaussian puff model can be an alternative to the plume model as well. Choi et al. (2018) compared the modeling results from CALPUFF and PAVAN for Ki-Jang Research Reactor. Within a radius of 1 km from the source, the ratio was close to 0.9, but the difference was widened at 5 km or more. PAVAN tended to underestimate compared to CALPUFF at the close range from the source, and the opposite trend was observed in the long distances.

1.4. Overview of the Contents

In Chapter 2, current atmospheric dispersion modeling for regulatory purposes is analyzed. The effective stack heights, terrain elevation, and correction factors for recirculation and wind speeds are reviewed among the components of Gaussian plume model. The calculation of mixed release conditions and deposition factors are also examined. The newly developed code based on XOQDOQ is introduced.

Chapter 3 examines the preliminary assessment with and without terrain elevation. Other model features, including recirculation factor, mixed release conditions, and wind speed correction, have been tested. As deposition modeling is based on a separately defined relative deposition rate, the current regulatory dispersion model results in maximum deposition factor at the same distance. A more realistic deposition modeling based on deposition velocity is introduced.

AERMOD, which is the dispersion model recommended by the EPA, is implemented in Chapter 4. Since AERMOD requires extra input parameters, a set of codes that can generate meteorological input files for the model is devised. The results from two different models with and without terrain elevation are compared.

In Chapter 5, SO_2 concentrations measured at the air pollution monitors have been employed to generate long-term datasets for model application. The predicted concentration from the models is compared with the observed concentration. Several statistical indicators that evaluate model performance are introduced.

Chapter 2. Model of Choice

2.1. Components of Gaussian Plume Model

As reviewed in Chapter 1, it is conventional to implement the Gaussian plume model for regulatory purposes. The model is particularly useful when dealing with local and long-term dispersion modeling. This chapter focuses on the model components when estimating the annual average dispersion factor for elevated release under normal operating conditions.

2.1.1. Regulatory Guides on Atmospheric Dispersion

KINS RG 1.3 describes the details for implementing the dispersion model for regulatory purposes. It also specifies the proper practice, requirements, and technical details to comply with the relevant regulations. RG 1.3 was first published in 2011 and was revised in 2015.

RG 1.3 states that when assessing the dispersion due to routine releases, the long-term weather data, at least for a year, should be acquired at the location and height that can represent the emission point. The data can be formatted into a joint frequency distribution consisting of wind speed levels, wind directions, and atmospheric stability classes. When applying the joint frequency distribution, it is recommended to subdivide low wind speed ranges to avoid underprediction. Attached Table 3 of RG 1.3 is an example of wind speed levels, divided into 11 levels between 0.5 and 10.0 m/s. When the measured wind speed is lower than the lowest limit of the anemometer, it is categorized as a calm state.

The release types are divided into elevated, ground, and mixed releases. When the release height is less than two times the surrounding buildings, it is assumed as a ground release. And when the release height is more than twice the surrounding structures, i.e., stack emissions, the elevated release is assumed. In the case of

operating conditions, mixed release can be assumed despite the release height criteria. It is also permitted to assume ground release while using the meteorological data at the emission height.

The difference in dispersion factor is small when the receptor point is located sufficiently far from the source. But within short distances from the source point, the dispersion factor varies according to the release type. Under elevated release, the maximum dispersion factor is usually formed outside the exclusion area boundary. On the contrary, when the release height is close to the ground, the estimated concentration decreases as the downwind distance from the source is increased. When modeling elevated releases, one should consider effective plume height. And for ground releases, the wake effect due to surrounding buildings should be accounted for. To assume mixed release, the concentration is estimated by the fractional sum of both release types.

For operating conditions, the annual average dispersion factor for the 80 km radius area should be calculated. The expected dose due to gaseous effluents is estimated for the boundaries of exclusion area, nearest residential area, emergency planned area, and low population zone.

Appendix 1 of the regulatory guide describes the constant mean wind directional model and is a translation of the NRC RG 1.111. RG 1.111 describes the mathematical model for estimating the dispersion of radionuclides emitted from an operating pressurized water reactor. The guideline was first published in 1976 and was revised the next year. In 2014, NRC approved the continued application of the guideline without any modification.

The guideline classifies the regulatory dispersion model as a variable trajectory model, and constant mean wind model. While the former requires temporal and spatial distribution of meteorological data for the domain of interest, the latter assumes that the meteorological condition at the source point can be expanded across the whole domain area. The dispersion model can include removal mechanisms and relevant correction factors to specify the details.

RG 1.111 mainly describes technical details of the constant mean

wind direction model. The standard mathematical description for Gaussian plume model is:

$$\left(\overline{X/Q'}\right)_D = 2.032 \sum_{ij} n_{ij} \left(NXu_i \Sigma_{zj}(X)\right)^{-1} exp\left[-\frac{h_e^2}{2\sigma_{zj}^2(X)}\right] \cdots (\text{eq. } 2.1)$$

Equation 2.1 can be modified for certain release types, removal mechanisms, and other correction factors. The removal mechanism is the process that depletes the radionuclide concentration as it is transported from the source to the receptor. The mechanism includes radioactive decay, dry deposition, and wet deposition.

The model can assume either continuous release or irregular releases, and this research assumes continuous release only. XOQDOQ code, assuming continuous and elevated release, estimates dispersion factor $\overline{X/Q}(x,\ k)$ as:

$$\overline{X/Q}(x,\ k) = \frac{2.032}{x} \cdot RF(x,k) \sum_{i,\ j}^{N,\ 7} \frac{DEPL_{ij}(x,k) \cdot DEC_i(x) \cdot f_{ij}(k)}{\bar{U}_i(x)\sigma_{zj}(x)} \cdot exp\left(\frac{h_e^2}{-2\sigma_{zj}^2(x)}\right) \cdots (eq. 2.2)$$

where $f_{ij}(k)$ is the frequency of weather conditions that corresponds to wind speed level i, direction k, and stability class j. $\bar{U}_i(x)$ is the mean wind speed for level i and the downwind distance x. h_e is the effective stack height, and $\sigma_{zj}(x)$ is the vertical spread of the plume.

Lateral and vertical dispersion coefficients are defined for each atmospheric stability class and downwind distance. Attached Table 2 of the RG 1.3 is the parametrization values for dispersion coefficients applied in XOQDOQ and domestic regulatory guidelines. As a straight-line Gaussian plume model is employed for long-term dispersion modeling, only the vertical dispersion coefficient is necessary.

Equation 2.2 is formulated from Equation 2.1 by incorporating correction factors such as RF, DEC, and $DEPL$. $RF(x,k)$ is the recirculation and stagnation factor due to interaction between terrain

and atmospheric transport. $DEC_i(x)$ is the correction factor for radioactive decay, and $DEPL_{ij}(x,k)$ is the depletion correction factor. Each correction factor can be assumed as default value defined in XOQDOQ code, or site-specific values can be assigned.

In Equation 2.2, the meteorological data are inputted in the form of joint frequency distribution $f_{ij}(k)$. As the straight-line Gaussian plume model assumes that meteorological data at the emission point represents the meteorological conditions for the rest of the domain area, it is necessary to make sure that the weather input represents the domain area. And if the inputted frequency data does not effectively represent the domain of interest, the regulatory body can require the applicant to supplement the modeling results.

2.1.2. Effective Stack Height

Effective stack height h_e is determined from the stack height, plume rise, and terrain elevation as:

$$h_e = h_s + h_{pr} - h_t \ (h_e \geq 0) \cdots (\text{eq. } 2.3)$$

where h_s is the physical stack height, h_{pr} is the plume rise, and h_t is the terrain elevation above the stack base. When elevated release is assumed, precise input and computation for the effective stack height is crucial. For ground release conditions, $h_e = 0$.

XOQDOQ simplifies plume rise for unstable and neutral conditions (A, B, C, D) as:

$$h_{pr} = 1.44(W_0/u)^{2/3} \cdot (x/D)^{1/3} \cdot D - C$$

or

$$h_{pr} = 3\left(\frac{W_0}{u}\right)D$$

where W_0 is the exit velocity of the plume (m/s), u is the wind speed (m/s) at release height, D is the internal stack diameter (m), and $C = 3(1.5 - W_0/u)D$ is the correction for downwash when $W_0 <$

$1.5u$. After comparing the two h_{pr} outputs, the smaller value is used.

For stable conditions (E, F, G), two more equations are added:

$$h_{pr} = 4(F_m/S)^{1/4}$$

or

$$h_{pr} = 1.5(F_m/u)^{1/3} \cdot S^{-1/6}$$

where $F_m = (W_0 D/2)^2$ is the momentum flux parameter (m^4/s^2), g is the acceleration of gravity (m/s^2), T is the ambient air temperature (K), and $S = 8.7 \times 10^{-4}$, 1.75×10^{-3}, 2.45×10^{-3} for stabilities E, F, and G. The smallest value for h_{pr} among the four equations is employed.

2.1.3. Terrain Elevation

When the effective stack height is computed as in above section, the terrain elevation h_t is subtracted directly from the sum of stack height and plume rise. The plume centerline moves closer to the ground surface for receptor points where the terrain height is greater than the stack base. In other words, it is assumed that the plume centerline remains horizontal as the plume is transported above the terrain. The effective stack height becomes zero when the terrain elevation is higher than the combined height of stack and plume rise.

Instead of assuming that terrain does not influence the plume centerline height, simple methods for terrain adjustment can be applied. For instance, the half-height approach or plume path coefficient adjustment method is adopted in dispersion models such as CALPUFF and AUSPLUME (Scire et al., 2000; Bluett et al., 2004). This approach assumes that plume or puff centerline can sometimes follow the terrain elevation. When the atmosphere is unstable, the tendency of plumes or puffs to flow over the terrain can be intensified. And when the atmosphere is stable, the lifting of plumes or puffs becomes less significant.

The terrain adjustment coefficients used in CALPUFF (Scire et al., 2000) are defined as $C = 0.5$ for unstable and neutral stability

conditions, and $C = 0.35$ for stable ones. The effective plume height at the receptor location can be adjusted as:

For $h_t \geq h_s + h_{pr}$,

$$h_e = (h_s + h_{pr}) \cdot C$$

For $h_t < h_s + h_{pr}$,

$$h_e = (h_s + h_{pr}) - h_t \cdot (1 - C)$$

where h_t is the terrain elevation above the base of the stack. Figure 2.1 is the graphical representation of the above method. In Chapter 3, the computed results for dispersion and deposition factor based on different terrain adjusting approaches are compared.

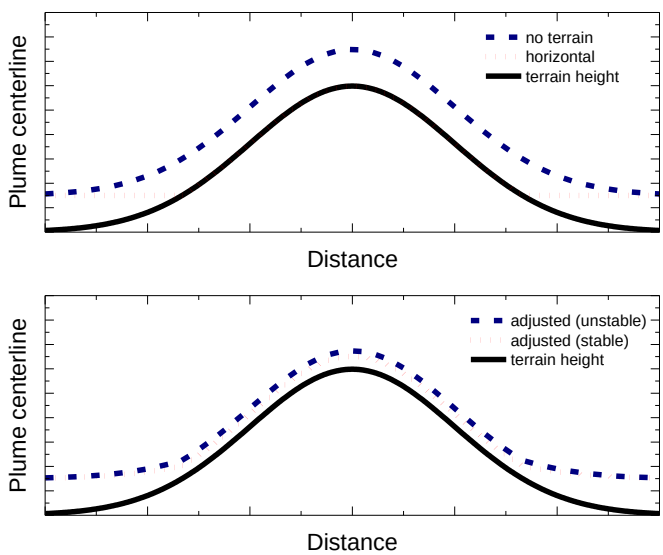

Figure 2.1. Schematic Comparison of Terrain Adjusting Methods

2.1.4. Correction Factors: Wind speed, Recirculation

In the case of elevated release, wind speed measured at the height of emission should be inputted. For ground release, it is customary to apply wind data measured at 10 m height. The emission height can be changed due to adjustments in design or mitigation purposes. Then the measured wind speed can be extrapolated to match the new height. Here, the default correction method used in XOQDOQ is applied:

$$COR = (SL/PL)^{EX} \cdots (\text{eq. } 2.4)$$

where COR is the correction factor applied to the measured wind speeds; PL is the original wind height; SL is the adjusted wind height; EX is 0.25, for unstable or neutral atmospheric conditions; and 0.50, for stable atmospheres.

The recirculation factor is the correction factor for site-specific terrain and meteorological characteristics. The default recirculation factor can increase the dispersion factor up to four times for receptor points close to the source. The recirculation factor is elaborated in Chapter 3.

2.1.5. Ground and Mixed Releases

The dispersion coefficients need to be corrected for wake effects to expand Gaussian plume model defined for elevated releases to the ground and mixed releases. According to KINS RG 1.3, the ground release is assumed when the emission height is less than twice the surrounding building structures. In the case of ground release, the wake effect and plume meandering due to surrounding buildings should be accounted for. On the contrary, the elevated release type can be assumed when the emission height is greater than twice the surrounding buildings (e.g., stack release). Still, it is permitted to assume ground or mixed release despite the height criteria when long-term and normal operating conditions are evaluated.

Mixed release can be applied to stack releases where the stack height is less than twice the surrounding heights. The ratio between plume exit velocity W_0 and the mean wind speed $\bar{u}$ is the determinant of the release type. When $W_0/\bar{u} \geq 5.0$, elevated release is assumed and when $W_0/\bar{u} \leq 1.0$, ground release should be assumed. For $1 < W_0/\bar{u} \leq 1.5$, the fraction of ground release E_t is computed as:

$$E_t = 2.58 - 1.58(W_0/\bar{u})$$

and for $1.5 < W_0/\bar{u} \leq 5.0$,

$$E_t = 0.3 - 0.06(W_0/\bar{u})$$

The total concentration due to mixed release is estimated as a fractional sum of ground and elevated releases.

For ground releases, the wake effect due to surrounding buildings is reflected by adjusting the dispersion coefficient as below. As the effective stack height h_e becomes zero, the last exponential term in Equation 2.1 can be ignored. The adjusted dispersion coefficient is calculated as:

$$\text{If } \left(\sigma_{zj}^2(X) + 0.5D_z^2/\pi\right)^{\frac{1}{2}} \leq \sqrt{3}\sigma_{zj}(X),\ \Sigma_{zj}(X) = \left(\sigma_{zj}^2(X) + 0.5D_z^2/\pi\right)^{\frac{1}{2}}$$

$$\text{Else if } \left(\sigma_{zj}^2(X) + 0.5D_z^2/\pi\right)^{\frac{1}{2}} > \sqrt{3}\sigma_{zj}(X),\ \Sigma_{zj}(X) = \sqrt{3}\sigma_{zj}(X)$$

where D_z is the surrounding building height (m).

2.1.6. Deposition Factor

Deposition factor is the amount of materials deposited per unit area. XOQDOQ calculates the deposition factor $\overline{D/Q}(x,k)$ (m^{-2}) as:

$$\overline{D/Q}(x,k) = \frac{RF(x,k)\sum_{i,j}^{N,7} D_{ij}f_{ij}(k)}{(2\pi/16)x} \cdots \text{(eq. 2.5)}$$

where D_{ij} is the relative deposition rate (m) from Figures 7 through 10 of RG 1.111. Here, the relative deposition rate is written as a function of wind speed because the effective stack height is dependent on the wind speed.

Parameterization coefficients for the relative deposition rate D_{ij} can be found in NRC RG 1.111 and XOQDOQ manual (Sagendorf et al., 1982). For site-specific meteorological or terrain conditions to be considered, it is recommended to modify relative deposition rate accordingly.

Another approach to calculate deposition factor is by applying deposition velocity (EPA, 2004; Sportisse, 2007). The dry deposition flux can be calculated as the dry deposition flux F_d is calculated as:

$$F_d = X_d \cdot V_d \cdots (\text{eq. } 2.6)$$

where F_d is dry deposition flux (ug/m^2/s), X_d is concentration (ug/m^3) calculated at reference height, and V_d is deposition velocity (m/s). By replacing $\overline{X/Q}$ instead of X_d in the above equation, deposition factor $\overline{D/Q}$ can be calculated.

For particles, the deposition velocity is defined with a resistance scheme, where the settling of particle is expressed in terms of electrical resistance (EPA, 2004). The particle deposition velocity V_{dp} can be estimated as:

$$V_{dp} = \frac{1}{R_a + R_P + R_a R_p V_g} + V_g \cdots (\text{eq. } 2.7)$$

where R_a is the aerodynamic resistance, R_p is the quasi-laminar sublayer resistance, and V_g is the gravitational settling velocity for particles.

The aerodynamic resistance is calculated as:

For stable and neutral conditions $(L > 0)$,

$$R_a = \frac{1}{k u_*}\left[ln\left(\frac{z_r}{z_0}\right) + \frac{5 z_r}{L}\right]$$

and for unstable conditions $(L < 0)$,

$$R_a = \frac{1}{ku_*}\left[ln\frac{\left(\sqrt{1-16\frac{z_r}{L}}-1\right)\left(\sqrt{1-16\frac{z_0}{L}}+1\right)}{\left(\sqrt{1-16\frac{z_r}{L}}+1\right)\left(\sqrt{1-16\frac{z_0}{L}}-1\right)}\right]$$

where k is von Karman constant $(= 0.4)$, u_* is the friction velocity, and L is the Monin−Obukhov length. The definition and derivation of these meteorological parameters are elaborated in Chapter 4.

When the size distribution of particle is known, the quasi−laminar sublayer resistance is parameterized as:

$$R_p = \frac{1}{(Sc^{-2/3}+10^{-3/St})(1+0.24w_*^2/u_*^2)u_*}$$

where $Sc = v/D_B$ is Schmidt number, v is the kinematic viscosity of air (m^2/s) corrected based on hourly ambient air temperature and pressure, D_B is Brownian diffusivity (cm^2/s) of the pollutant in the air, $St = (V_g/g)(u_*^2/v)$ is Stokes number, g is the acceleration due to gravity (m/s^2), and w_* is the convective velocity scale (m/s). The Brownian diffusivity can be estimated as:

$$D_B = 8.09 \cdot 10^{-10} \cdot [T_a S_{CF}/d_p]$$

where d_p is the particle diameter (μm), and S_{CF} is the slip correction factor which is computed as:

$$S_{CF} = 1 + \frac{2x_2(a_1 + a_2 e^{-(a_3 d_p/x_2)})}{10^{-4} \cdot d_p}$$

where $x_2 = 6.5 \cdot 10^{-6}$, $a_1 = 1.257$, $a_2 = 0.4$, $a_3 = 0.55 \cdot 10^{-4}$ are constants.

If the particle characteristics are known, the gravitational settling velocity is calculated as:

$$V_g = \frac{(\rho - \rho_{air})g \cdot d_p^2 \cdot c_2}{18\mu} S_{CF}$$

where ρ is the density of particle (g/cm^3) and $\rho_{air} = 1.2 \cdot 10^{-3}$ is the density of air (g/cm^3), $\mu = 1.81 \cdot 10^{-4}$ is the absolute viscosity of air (g/cm/s), and $c_2 = 1.0 \cdot 10^{-8}$ is the unit conversion constant ($cm^2/\mu m^2$).

When the size distribution of particles is not well known and a small fraction is in particles with a diameter of 10 μm or larger, the quasi-laminar sublayer resistance can be parameterized based on observations of sulfate dry deposition:

For stable and neutral conditions $(L > 0)$,

$$R_p = \frac{500}{u_*}$$

and for unstable conditions $(L < 0)$,

$$R_p = \frac{500}{u_* \left(1 - \frac{300}{L}\right)}$$

By determining R_a and R_p for each stability condition, the deposition velocity can now be determined. The deposition velocity is calculated as a fractional sum of velocities for fine particles and coarse particles as:

$$V_d = fV_{df} + (1 - f)V_{dc}$$

where V_d is overall deposition velocity of the particles, f is a fraction of particulate substance that is fine mode (smaller than 2.5 um in diameter), V_{df} is deposition velocity of fine particulate substance, and V_{dc} is deposition velocity of coarse particulate

substance. From Equation 2.7, V_{df} and V_{dc} are calculated by assuming $V_g = 0$, and $V_g = 0.002$ (m/s).

The fine particle fraction f can be input by the user with reference to Appendix B of Wesely et al. (2001). Among the particle size information for selected hazardous air pollutants, $f = 0.8$ defined for radionuclides was applied. The derivation of deposition velocities and results based on domestic meteorological data are elaborated in Chapter 3 and Chapter 4.

2.2. Code Implementation

US NRC recommends XOQDOQ as a standard code for regulatory dispersion modeling. The code calculates annual average values of dispersion and deposition factors according to the methodologies specified in RG 1.111. The code is now under the NRC Radiation Protection Computer Code Analysis and Maintenance Program (RAMP) management. The NRCDose3 software, which includes XOQDOQ as a module, is available instead of a stand-alone code.

Using the XOQDOQ as provided by RAMP for further modeling processes has several limitations. The subsidiary functions that define the model details cannot be modified, and it is difficult to break down the calculated results into short distances. Iterating calculations for parametric analysis are unavailable as well.

Thus, a new dispersion model based on XOQDOQ was developed. Specifically, the ANNUAL module of the original code, which acts as the main script that manages various subroutines, was reproduced. Related modules and functions were also included. Python (version 3.8.1) was used as a programming language.

Subroutines linked to the ANNUAL module include calculating dispersion factors, plume rise, corrected wind speeds, relative deposition rates, ground release fractions for mixed releases, recirculation factors, etc. These subroutines were all written as user-defined functions so that they can be modified when necessary.

In XOQDOQ, plume depletion includes only dry depletion. The depletion correction factor is determined by wind speed, atmospheric

stability, downwind distance, and wind direction. The radioactive decay correction factor depends on the decay constant for each radionuclide, wind speed, and downwind distance. As the research focused on the conservative approach for regulatory purposes, subroutines for plume depletion and radioactive decay were not included in this version.

2.2.1. Test Cases for Benchmarking

Two test cases were inputted to compare the newly developed code with the original one. Test case (1) assumed elevated release from a 72 m stack without adjacent building structures. Maximum wind speeds for each level were 0.5, 1, 1.5, 2, 3, 4, 5, 6, 8, 10, and 30 m/s, and the speed distribution was assumed to be uniform. Single wind direction was assumed for each atmospheric stability class from A to G. Stack diameter and plume exit velocity were set as 2 m and 10 m/s, respectively.

Test case (2) assumed mixed release from a 72 m stack with an adjacent building height of 60 m. Other input parameters were set the same as a test case (1).

Figures 2.2 and 2.3 are the test results for cases (1) and (2), respectively. When dispersion factors were in the order of 10^{-7}, approximately four significant figures accuracy was obtained.

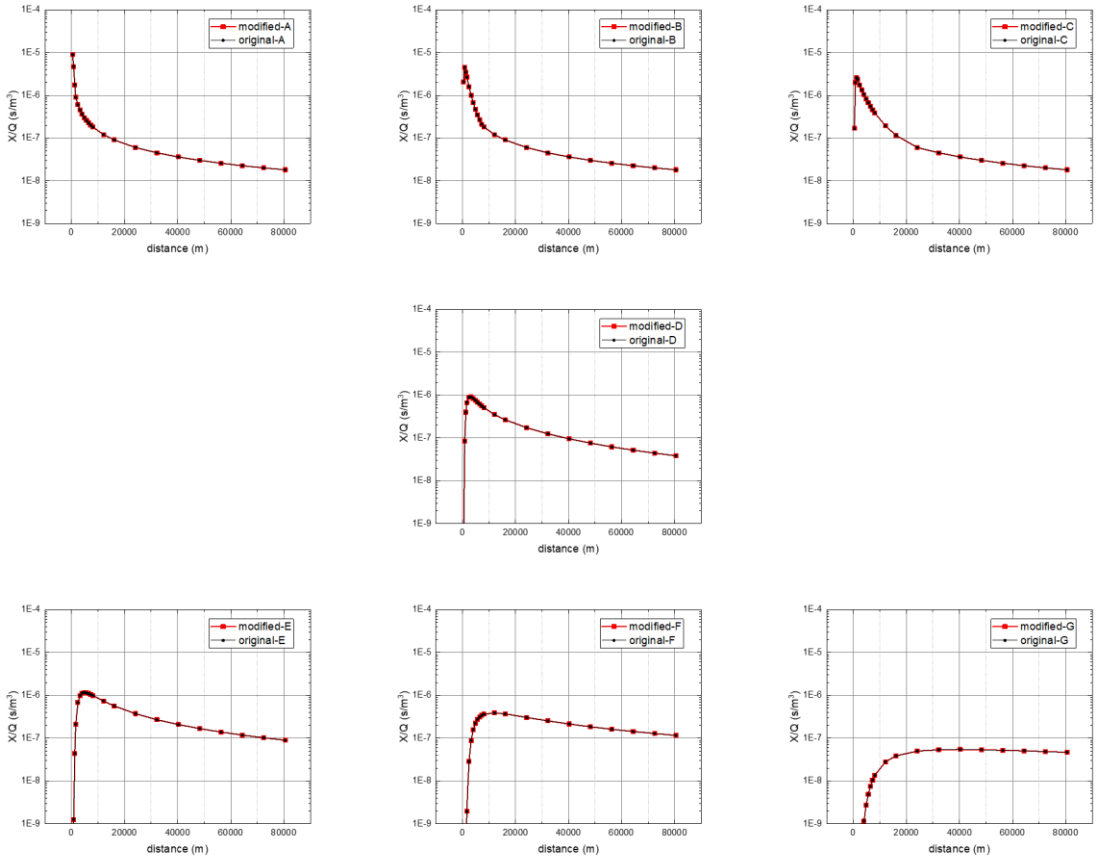

Figure 2.2. Comparison with the original XOQDOQ code – Test Case (1)

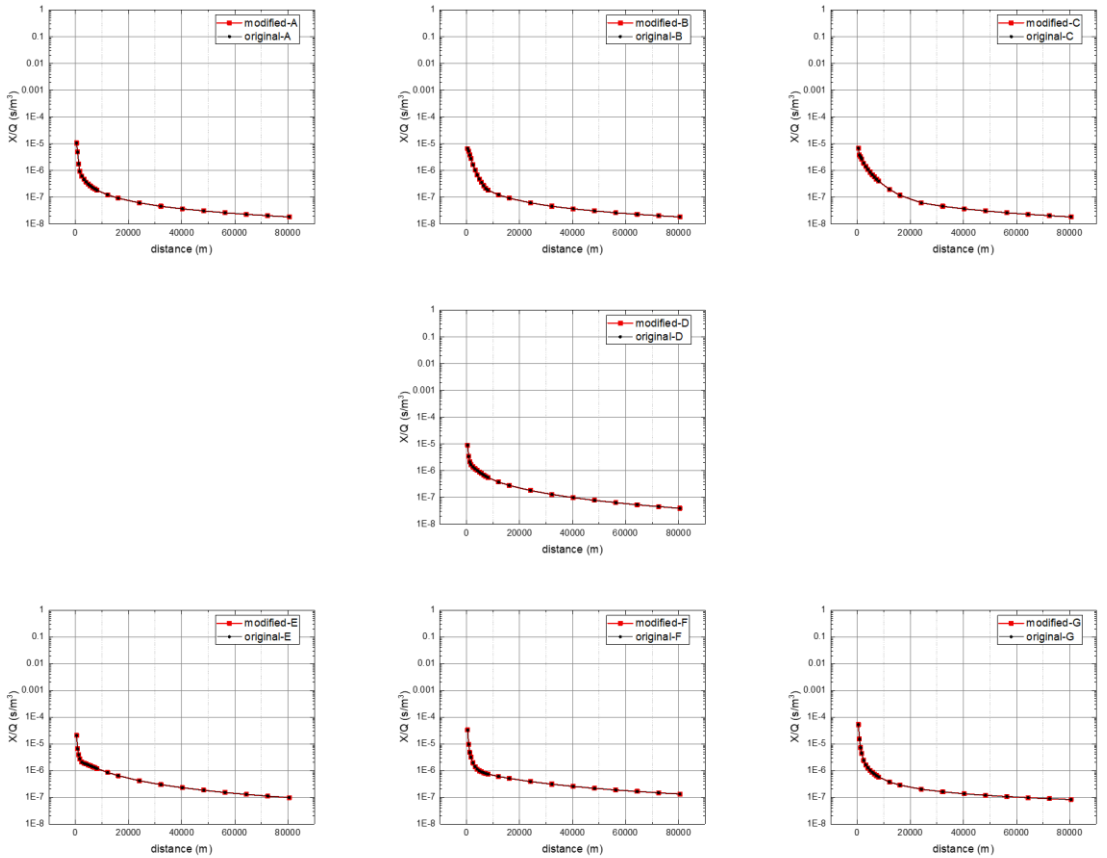

Figure 2.3. Comparison with the original XOQDOQ code – Test Case (2)

2.2.2. New Features included in the Code

Several advancements were made in the new version of code based on XOQDOQ. First, the adjusted plume height approach is added to assume the terrain-following plume for dispersion factor calculation. The coefficients were set depending on the atmospheric stability, as described in Section 2.1.2.

Second, the deposition factor can also be calculated using the deposition velocity approach. As the deposition factor is computed from the dispersion factor, the maximum location for both factors coincide. The details of these new features were elaborated in Section 2.1.5.

Handling meteorological and orographic data has become more convenient. Instead of filling in the frequency distribution, the measured wind speed, direction, and atmospheric stability can now be inputted as it is. The measured data are converted into the frequency format, following the user-defined wind speed levels. Terrain height for each distance and direction can also be entered in the form of a table. The sub-grid values are interpolated when necessary.

2.2.3. Parametric Sensitivity

The model proposed in this study modified the effective stack height estimation scheme in the original code. The sensitivity of the dispersion factor according to the terrain height was compared with the original and modified models. When the terrain height is increased by 80 m, the dispersion factor increased by ~180 times in the original model and 4.6 times in the modified model.

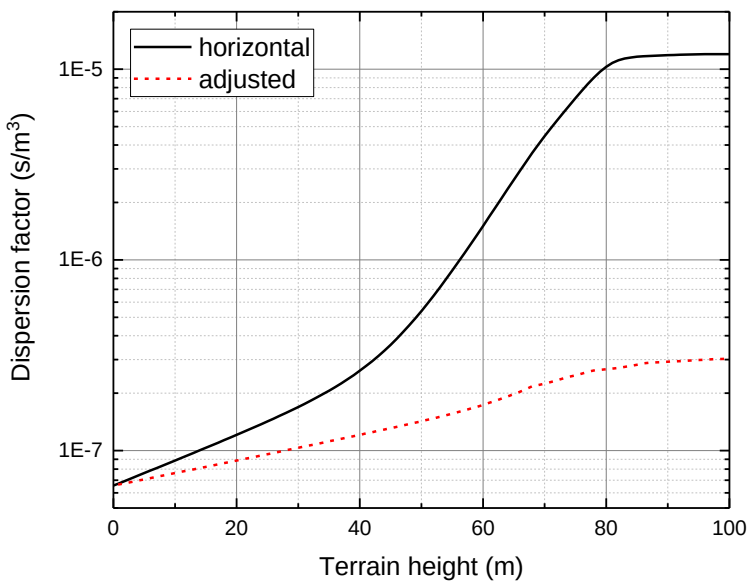

Figure 2.4. Sensitivity of dispersion factor due to terrain height

Other parameters related to effective stack height are stack diameter, stack height, and plume exit velocity. The sensitivity ratio of the modified model for the stack parameters did not deviate from the original model. Among the parameters, sensitivity due to stack height was the greatest for both original and modified models.

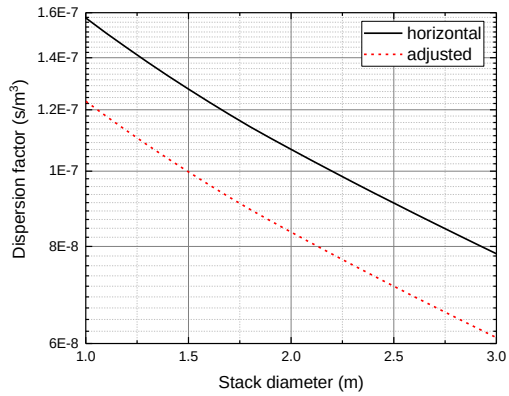

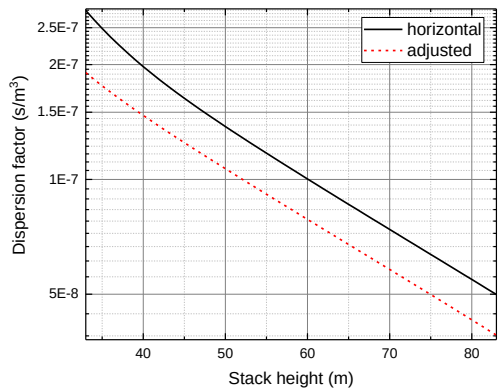

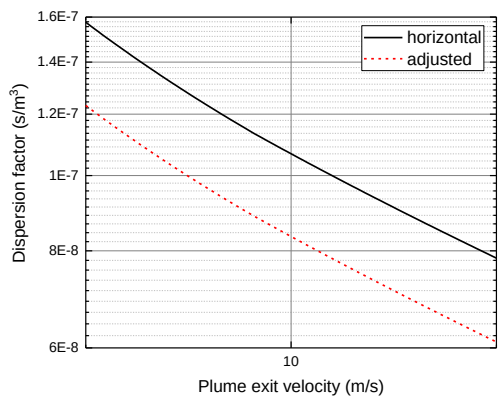

Figure 2.5. Sensitivity of dispersion factor due to stack parameters

Chapter 3. Preliminary Assessment

3.1. Dispersion excluding Terrain Elevation

3.1.1. Areas of Interest

The target areas for preliminary dispersion assessment are Wolsong and Kori nuclear power plant sites. As in Figure 3.1, both sites are in the southeast region of the Korean peninsula. The nuclear power plants at both sites are in the coastal area, close to the East Sea.

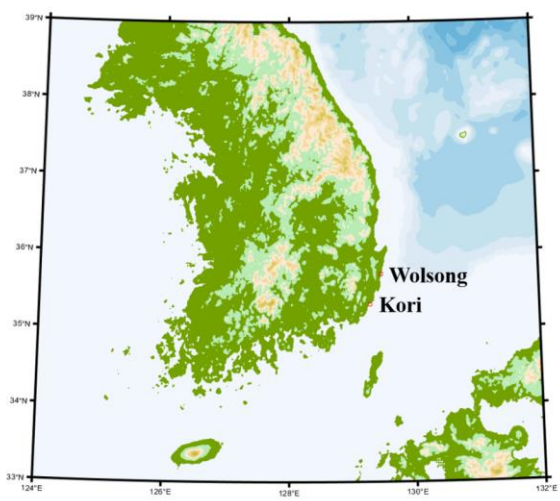

Figure 3.1. Location of Wolsong and Kori sites

Wolsong site has four CANDU reactors. The reactor Unit 1 is in the terminal shutdown phase as of 2021. The Kori site has four PWR nuclear reactors, where the reactor Unit 1 is also in the terminal shutdown phase. As in Table 1.4, regulatory dispersion modeling for these reactors assumed ground releases. In this preliminary assessment, however, elevated releases with 58 m stack height were assumed.

3.1.2. Meteorological Data and Stability Criteria

The measurement data acquired from Wolsong and Kori nuclear power plant sites from 2016 to 2018 were used. The measurement data include ten-minute average values for wind speeds, directions, and temperatures, measured at 10 m and 58 m from the ground. In Wolsong, the atmospheric stability was categorized according to the temperature lapse rate and standard deviations in 10 m and 58 m wind directions. For Kori site, the categorization is based on temperature lapse rate only.

Gaussian plume model simplifies the vertical and lateral turbulence by categorizing atmospheric stability. XOQDOQ is based on Pasquill stability, and the dispersion coefficients are determined by the seven degrees of stability from extremely unstable (A) to strongly stable (G). According to KINS RG 1.3, the atmospheric stability can be determined using one of three indices: temperature lapse rate, standard deviations in wind direction, and bulk Richardson number. Table 3.1 summarizes the criteria for each.

Table 3.1. Criteria for atmospheric stability classification

Description	Pasquill Class	Temperature lapse rate ($\Delta T/\Delta z$: $^{\circ}C/100\,m$)	Directional standard deviation (σ_θ)	Bulk Richardson Number (R_b)
Extremely unstable	A	$\Delta T/\Delta z \leqq -1.9$	$22.5 \leqq \sigma_\theta$	$R_b \leqq -0.35$
Moderately unstable	B	$-1.9 < \Delta T/\Delta z \leqq -1.7$	$17.5 \leqq \sigma_\theta < 22.5$	$-0.35 < R_b \leqq -0.18$
Weakly unstable	C	$-1.7 < \Delta T/\Delta z \leqq -1.5$	$12.5 \leqq \sigma_\theta < 17.5$	$-0.18 < R_b \leqq -0.04$
Neutral	D	$-1.5 < \Delta T/\Delta z \leqq -0.5$	$7.5 \leqq \sigma_\theta < 12.5$	$-0.04 < R_b \leqq 0.01$
Weakly stable	E	$-0.5 < \Delta T/\Delta z \leqq 1.5$	$3.8 \leqq \sigma_\theta < 7.5$	$0.01 < R_b \leqq 0.07$
Moderately stable	F	$1.5 < \Delta T/\Delta z \leqq 4.0$	$2.1 \leqq \sigma_\theta < 3.8$	$0.07 < R_b \leqq 0.13$
Strongly stable	G	$4.0 < \Delta T/\Delta z$	$\sigma_\theta < 2.1$	$0.13 < R_b$

To maintain conservative prediction, it is recommended to apply a temperature lapse rate. And when using alternative methods, the representativeness of the categorization should be justified. It is conventional to calculate the temperature lapse rate between 10 m from the ground and the emission height.

Table 3.2 is the stability classification system suggested by Pasquill (1961), as cited in Kahl and Chapman (2018). It should be

noted that the unstable periods and stable periods are assigned exclusively for daytime and nighttime. The criteria for solar insolation (daytime) and cloud cover (nighttime) are based on eye measurement.

Table 3.2. Pasquill stability classification scheme (Kahl and Chapman, 2018)

Surface (10 m) wind speed (m/s)	Daytime insolation			Nighttime cloud cover	
	Strong	Moderate	Slight	Thinly overcast or > 4/8 low cloud	<3/8 cloud
< 2	A	A-B	B	-	-
2-3	A-B	B	C	E	F
3-5	B	B-C	C	D	E
5-6	C	C-D	D	D	D
> 6	C	D	D	D	D

According to Kahl and Chapman (2018), the stability classes were introduced solely for simplified dispersion modeling. Thus, modelers should take extra care for the determination of atmospheric stability and its limitations. Mohan and Siddiqui (1998) also pointed out that different stability classification schemes lead to different patterns of stability distribution.

Figure 3.2 shows the annual atmospheric stability at Wolsong site. When temperature lapse rate had been applied, stability class E was the most frequent throughout the year, while stability class D was the most frequent for the standard deviation of wind direction. And with temperature lapse rate as determination criteria, the frequency of stability class A in 2016 was notably higher than those of the following years.

Based on the standard deviation of wind directions, the frequency of the most unstable conditions was relatively uniform for the years monitored. Overall, the temperature lapse rate criteria were inclined towards stable, and the standard deviation of wind direction criteria

were inclined toward unstable conditions.

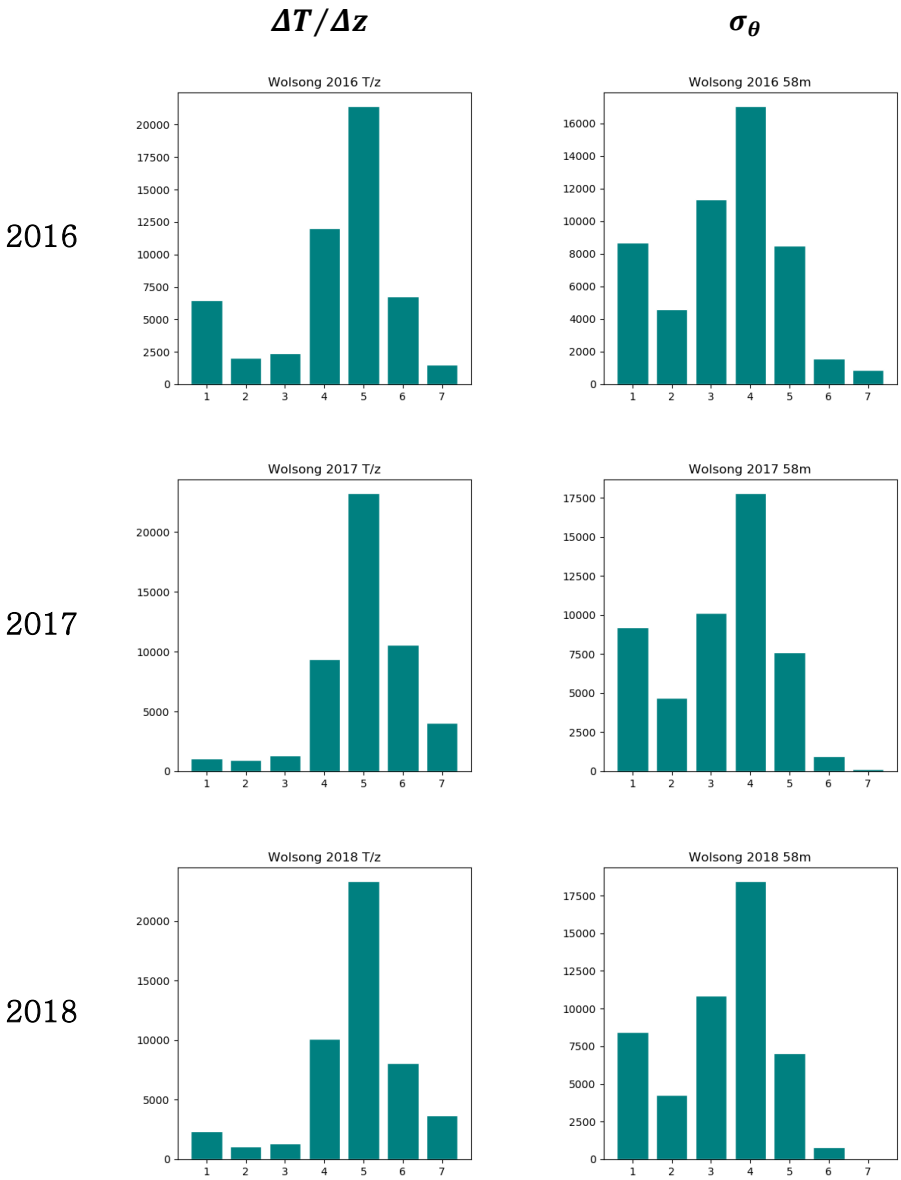

Figure 3.2. Atmospheric stability distribution in Wolsong based on different methods

In Figures 3.3 and 3.4, the temporal and seasonal variations of atmospheric stability are analyzed. Based on the temperature lapse, the unstable conditions occurred more frequently during the daytime, while the standard deviation of wind direction resulted in little temporal difference. While the seasonal variations were not significant for the former, the unstable classes based on the directional deviations showed notably higher frequency for the winter seasons.

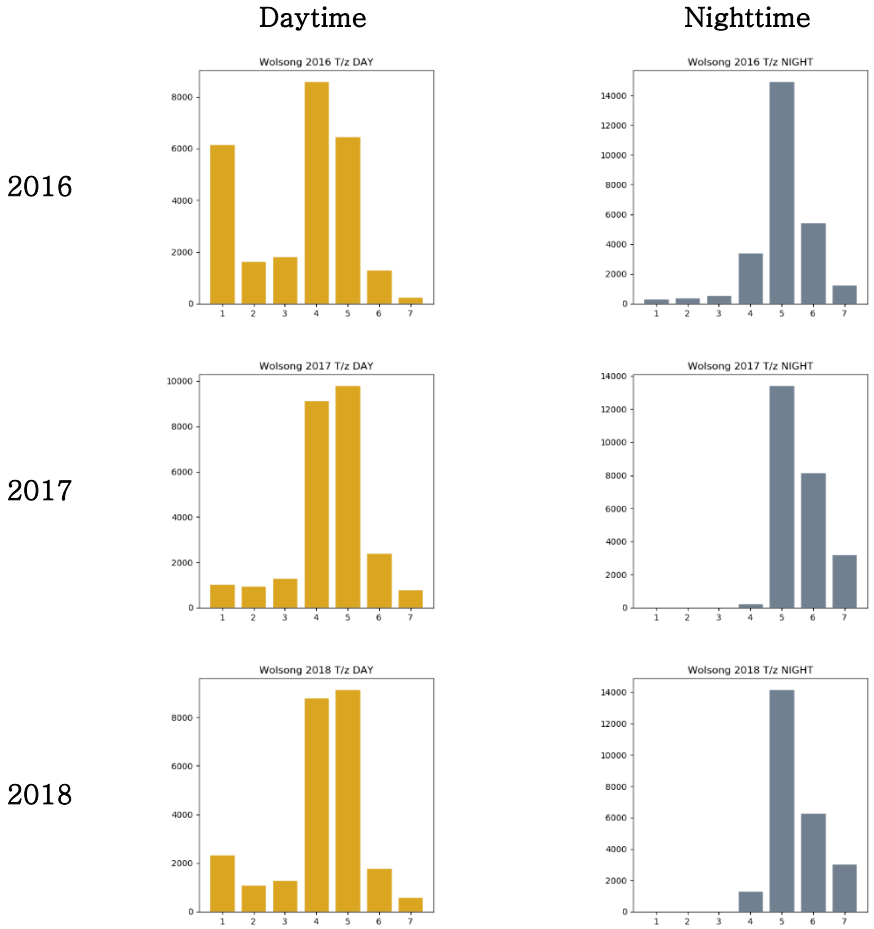

Figure 3.3. Temporal variation of stability class based on temperature lapse rate in Wolsong

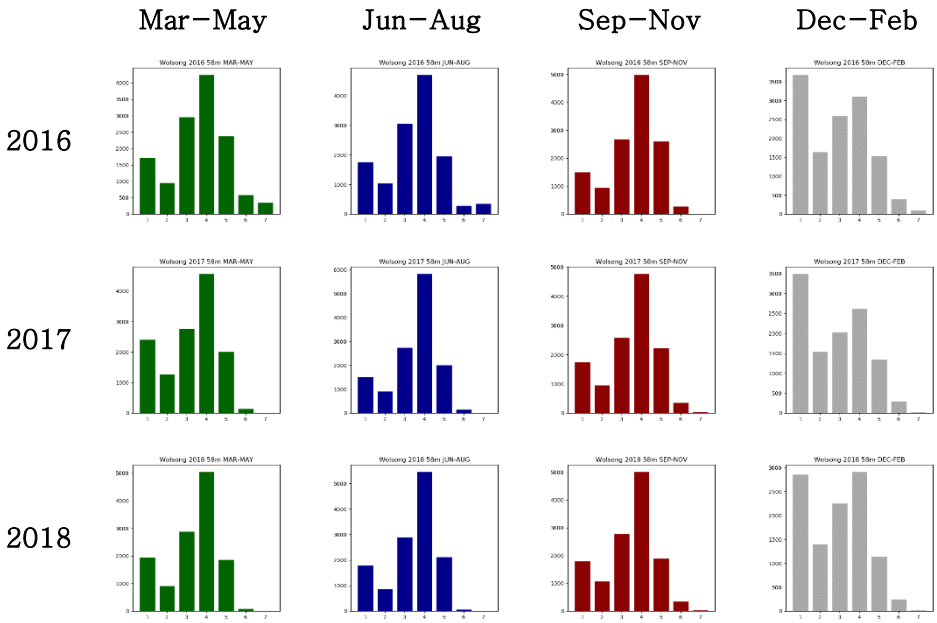

Figure 3.4. Seasonal variations in stability class based on standard deviation of wind directions in Wolsong

On-site measurement data for Kori site includes atmospheric stability based on temperature lapse rate only. As in Figure 3.5, the temporal characteristics of the stability class were observed. Throughout the year, the most frequent stability class was D (neutral), and the unstable conditions tended to occur more frequently than in Wolsong.

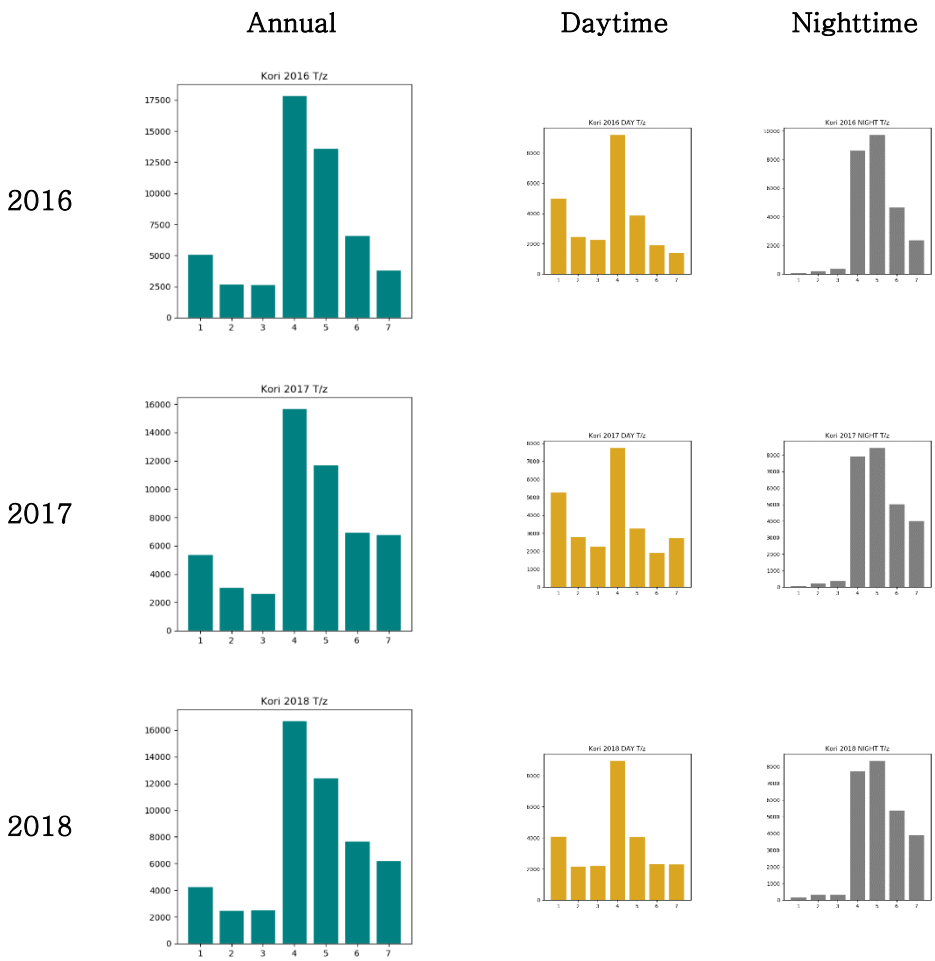

Figure 3.5. Annual and temporal variation of stability class based on temperature lapse rate in Kori

Figures 3.6 and 3.7 are the annual distributions of wind directions and speeds measured in Wolsong and Kori. The prevailing wind throughout the year was NW in Wolsong. The seasonal characteristics were also significant, with high frequencies of NW wind during winter. In Kori, the prevailing wind direction was N, particularly dominant during autumn.

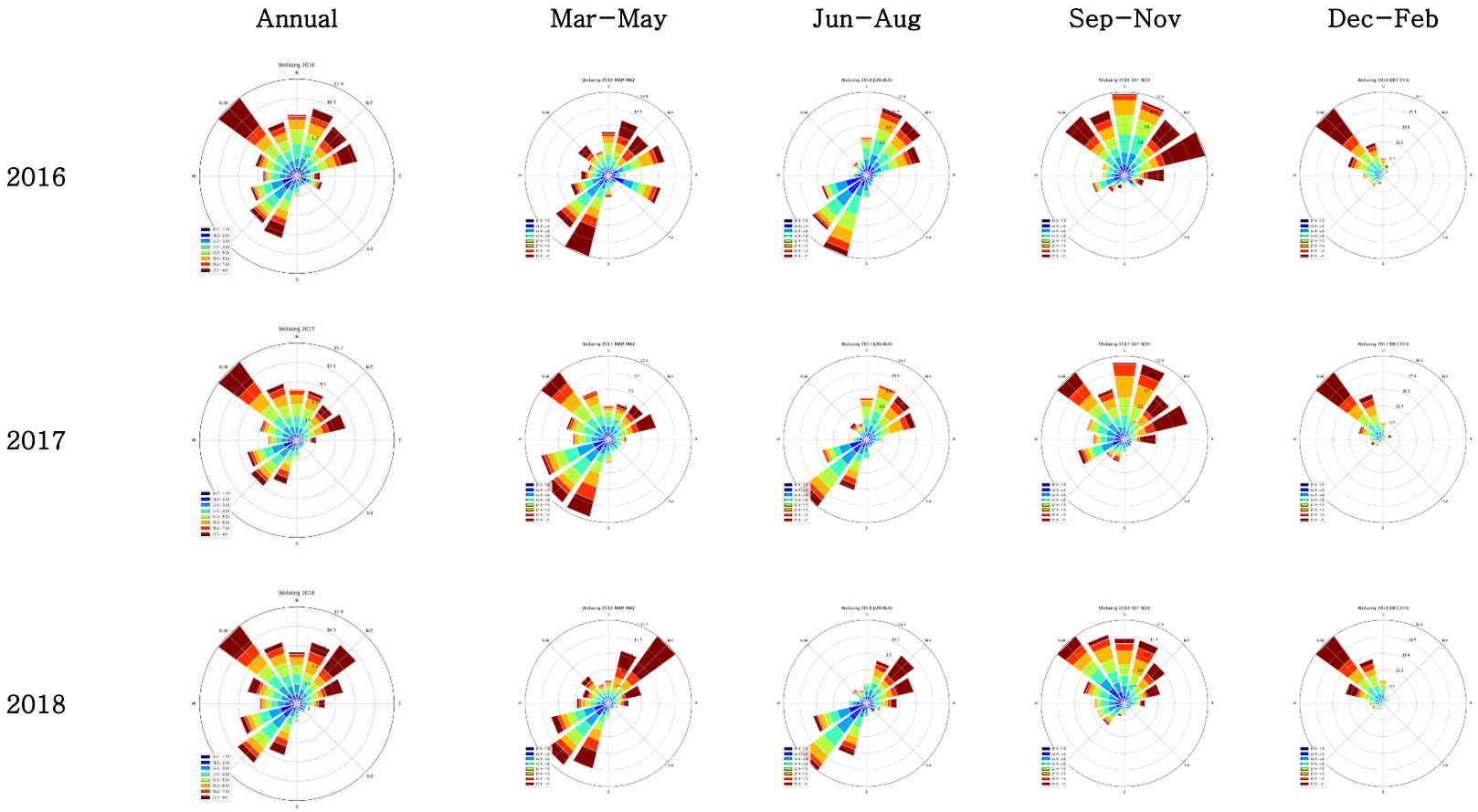

Figure 3.6. Annual and seasonal distribution of wind speed and direction in Wolsong

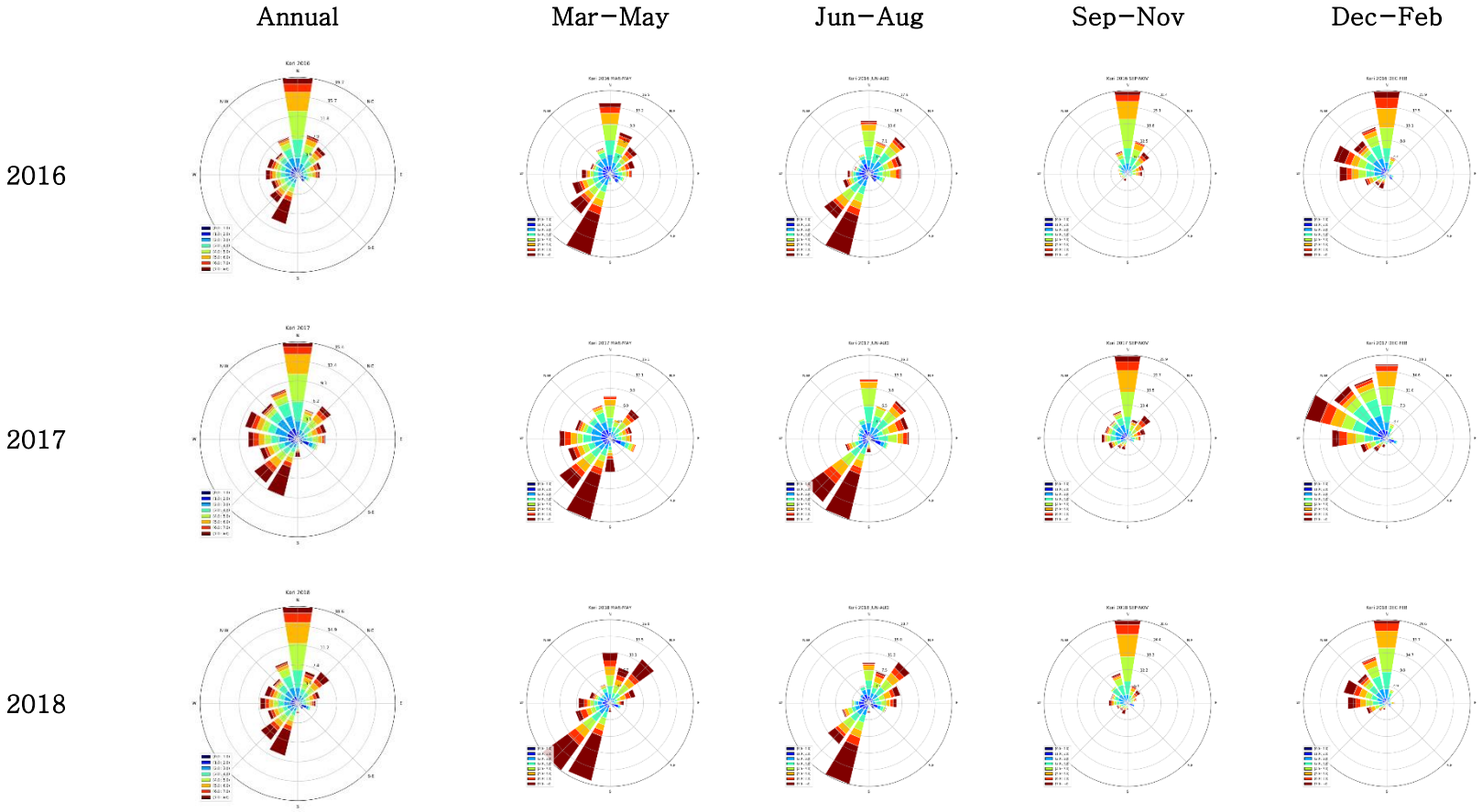

Figure 3.7. Annual and seasonal distribution of wind speed and direction in Kori

3.1.3. Base Scenario

Annual average dispersion factors for Wolsong and Kori sites between 2016 and 2018 were calculated. Elevated release at 58 m was assumed. Maximum wind speeds for each level were 1, 2, 4, 8, 16, and 32 m/s. On-site measurement weather data contains wind speed and direction measured at 58 m height. Other parameters were set the same as in Section 2.2.1, test case (1).

Dispersion factors were calculated for a 10 km radius with a 10 m resolution. The atmospheric stability class based on temperature lapse rate was applied. Tables 3.3 and 3.4 are the maximum dispersion factor values and their locations. Figures 3.8-3.10 show the contour plots of the estimated dispersion factors.

For Wolsong site, an additional stability class based on the standard deviation of 58 m wind direction is available. Compared with the temperature lapse rate, the new stability class increased the maximum dispersion factors, while the distances to the maximum points became farther from the source. Also, the maximum dispersion factor was formed in the SE direction because the unstable atmospheric conditions were the most frequent during the winter season, and the prevailing wind direction during winter was NW.

For Kori site, the prevailing north wind resulted in long-range transport, and the maximum values were formed near the source point, primarily due to the east wind.

Table 3.3. Maximum X/Q values and locations
(base scenario, Wolsong)

Year	$\Delta T/\Delta z$		σ_θ	
	Maximum (s/m^3)	Location	Maximum (s/m^3)	Location
2016	2.80E−07	330 m, WSW	4.10E−07	410 m, SE
2017	1.08E−07	2400 m, SE	5.42E−07	390 m, SE
2018	1.04E−07	330 m, NNE	4.87E−07	410 m, SE

Table 3.4. Maximum X/Q values and locations (base scenario, Kori)

Year	Maximum (s/m^3)	Location
2016	2.38E−07	330 m, W
2017	2.04E−07	340 m, W
2018	1.88E−07	1990 m, S

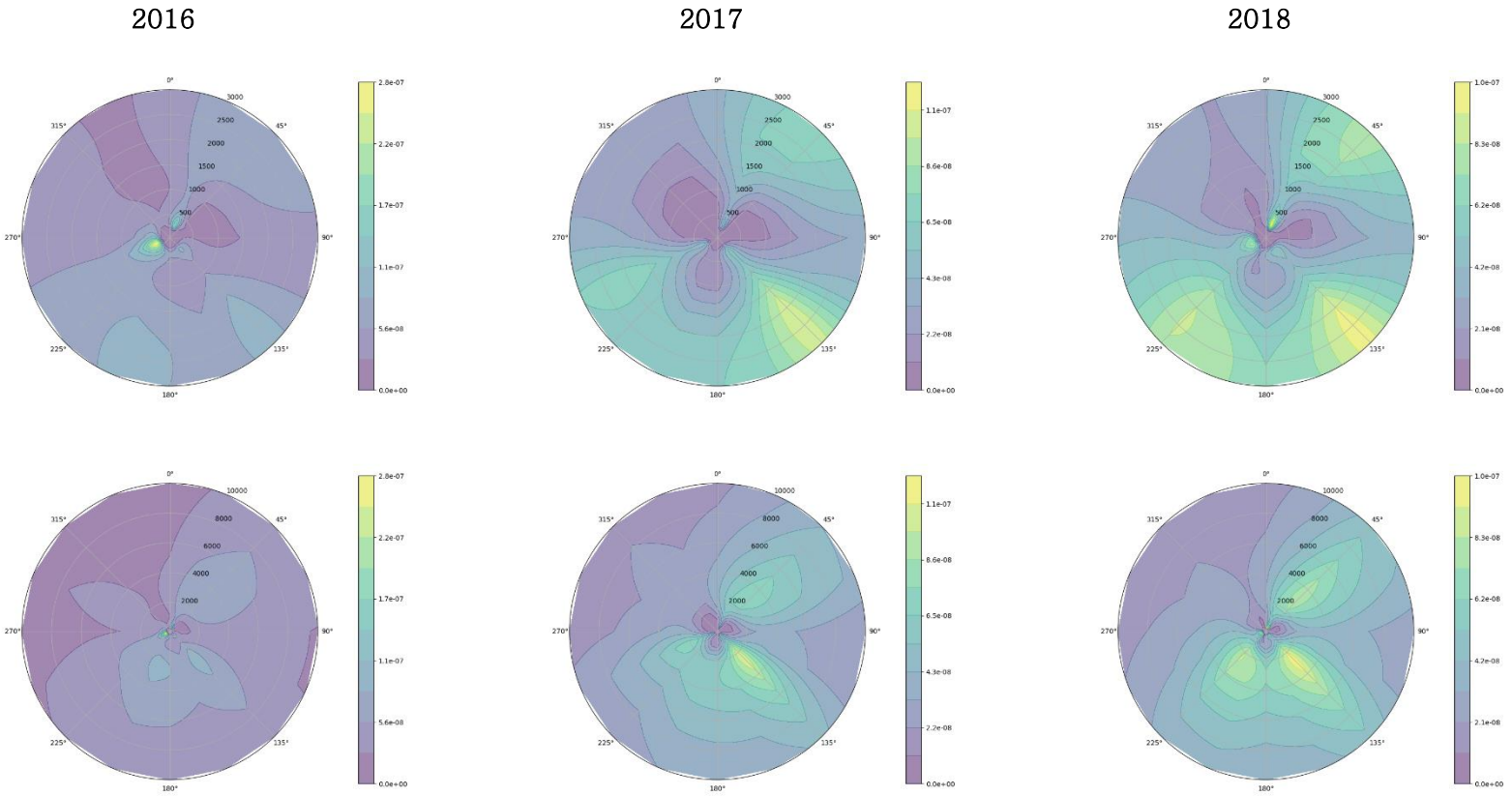

Figure 3.8. Dispersion factors in 2016−2018 (Wolsong, base scenario, $\Delta T/\Delta z$)
Top: 3 km, Bottom: 10 km radius

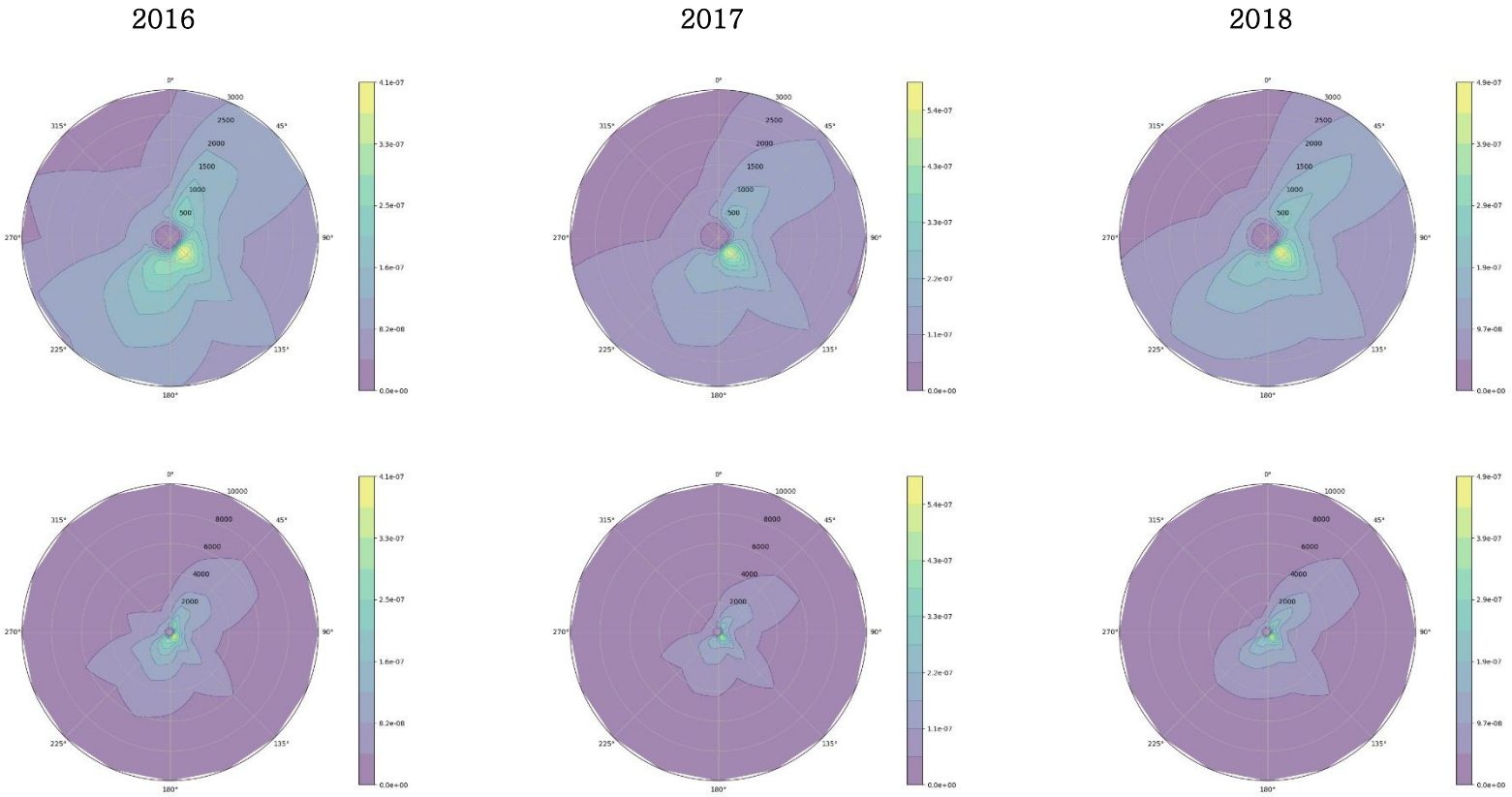

Figure 3.9. Dispersion factors in 2016−2018 (Wolsong, base scenario, σ_θ)
Top: 3 km, Bottom: 10 km radius

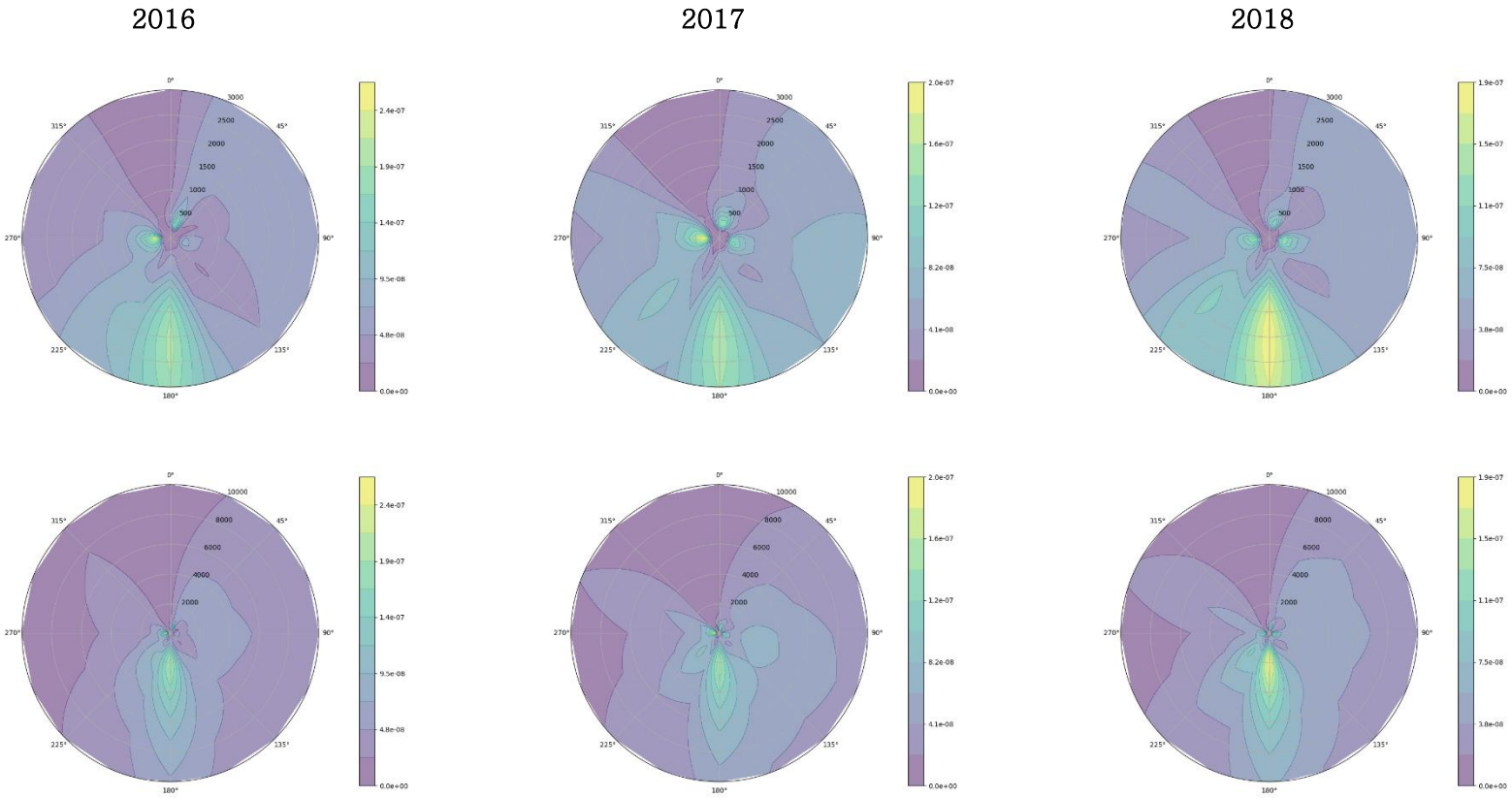

Figure 3.10. Dispersion factors in 2016−2018 (Kori, base scenario)
Top: 3 km, Bottom: 10 km radius

3.1.4. Recirculation and Stagnation

Meteorological data is the crucial input parameter for the atmospheric dispersion model. Since Gaussian plume model uses the meteorological data measured at a single location in the form of a joint frequency distribution, it cannot reflect the effects of weather over time or terrain. Some correction factors can be applied to the basic equation of the model to prevent the dispersion factor from being underestimated.

In XOQDOQ, the recirculation factor is multiplied at the final step of calculating the atmospheric dispersion factor and is defined according to the distance and wind direction. By default, the maximum value of the factor is 4 up to a radius of about 1 km from the source. After that, the factor decreases exponentially between 1 and 10 km. The recirculation factor can increase the dispersion factor and the deposition factor near the emission source.

NRC RG 1.111 states that the recirculation factor should be based on measured data or relevant study results. The recirculation factor value provided by XOQDOQ is based on previous experimental studies on open terrain, and it reflects the increase in concentration due to stagnation and recirculation.

The frequency of air stagnation and recirculation phenomena should be inferred from the weather conditions measured at a single point to determine whether to apply the recirculation factor. Allwine and Whiteman (1994) provided methods to quantify the degree of atmospheric stagnation, recirculation, and ventilation through a series of meteorological data analyses.

The integral quantities such as wind run and transport distance are defined, and the recirculation factor can be derived from the ratio of the two qualities (Allwine and Whiteman, 1994). The wind run, the sum of wind vectors for each time interval, is a measure of stagnation, and a small wind run indicates the stagnated atmosphere. If the transport distance is much smaller than the wind run, it means that the pollutant has been recirculating near the point of emission. The criteria to determine the level of recirculation and stagnation are also

provided. Still, they are based on site-specific values derived from the measurements in the Grand Canyon region, which cannot be directly compared with other regions.

Kim et al. (2007) applied the method for domestic nuclear installations. As they compared the analysis results with the above criteria, the sites (Kori, Wolsong, Yeonggwang, and Uljin) did not show significant recirculation or stagnation characteristics.

Reviewing the regulatory details and previous studies regarding the recirculation factor it could be confirmed that the default recirculation factor, as in XOQDOQ, is the conservative correction factor that prevents underestimation due to recirculation and stagnation in the typical open terrain. The exact correction factor for site-specific meteorological patterns would require a long-term tracer experiment. For now, the use of the default recirculation factor can be acceptable since it can guarantee a certain level of safety margin in modeling.

Table 3.5 and Figures 3.11 and 3.12 are the results of dispersion modeling for Wolsong and Kori sites. The XOQDOQ default recirculation factor was applied for both sites. Compared to the base scenario, there were several noticeable changes in the dispersion pattern. First, from Wolsong's (2016, 2018) and Kori's (2016, 2017) base scenario, the maximum dispersion factors were already formed in distances less than a 1 km radius from the source. Thus, the maximum locations were not changed after they had been corrected with the recirculation factor. For the rest cases, the distances to the maximum locations were changed for the points beyond the 1 km radius. The maximum dispersion factor was increased to 2.85-4.00 times the base scenario.

Table 3.5. Maximum X/Q values and locations (recirculation)

Year	Wolsong		Kori	
	Maximum (s/m^3)	Location	Maximum (s/m^3)	Location
2016	1.12E−06	330 m, WSW	9.54E−07	330 m, W
2017	3.08E−07	1220 m, SE	8.16E−07	340 m, W
2018	4.16E−07	330 m, NNE	6.18E−07	1120 m, S

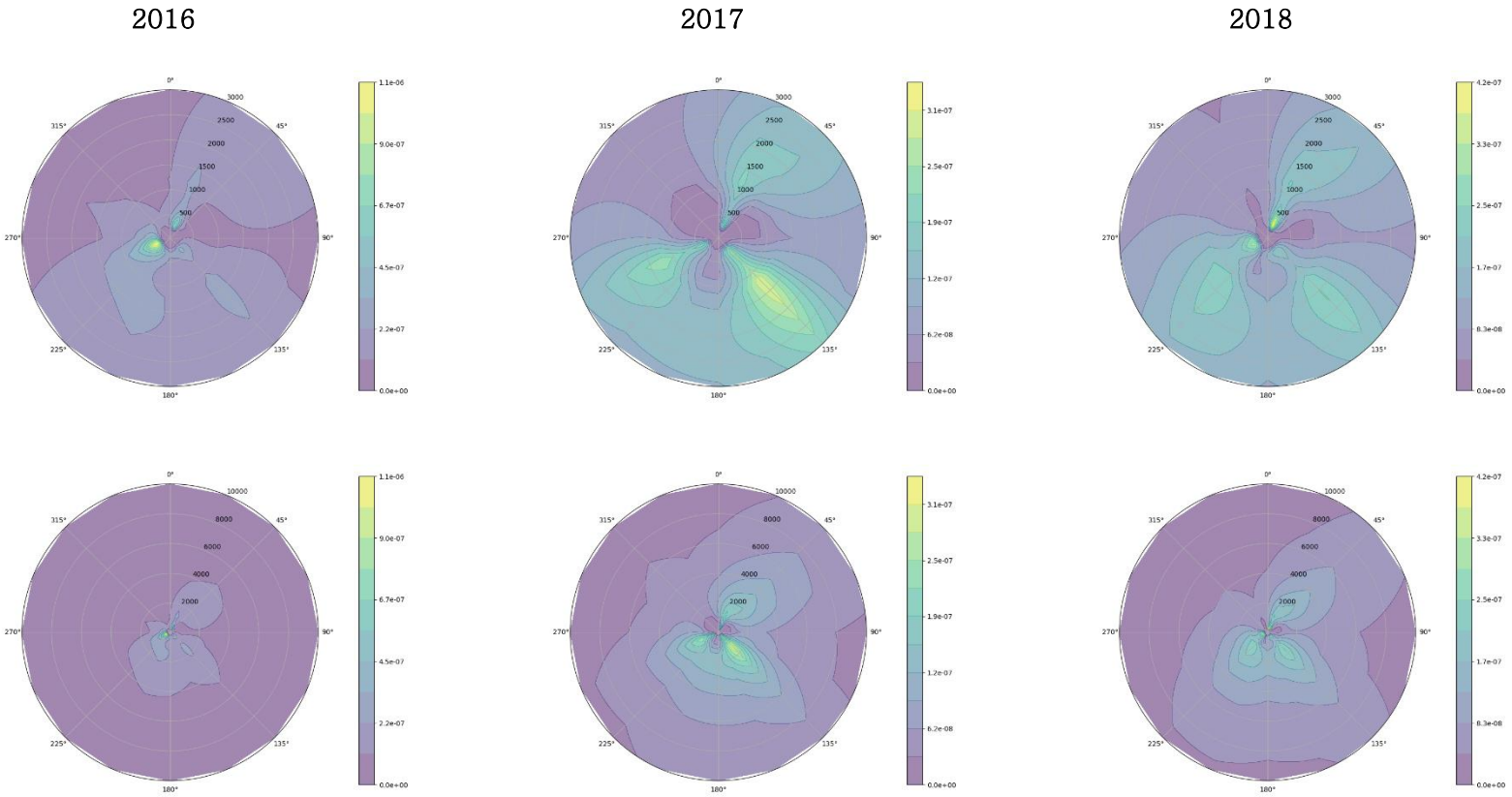

Figure 3.11. Dispersion factors in 2016–2018 (Wolsong, recirculation)
Top: 3 km, Bottom: 10 km radius

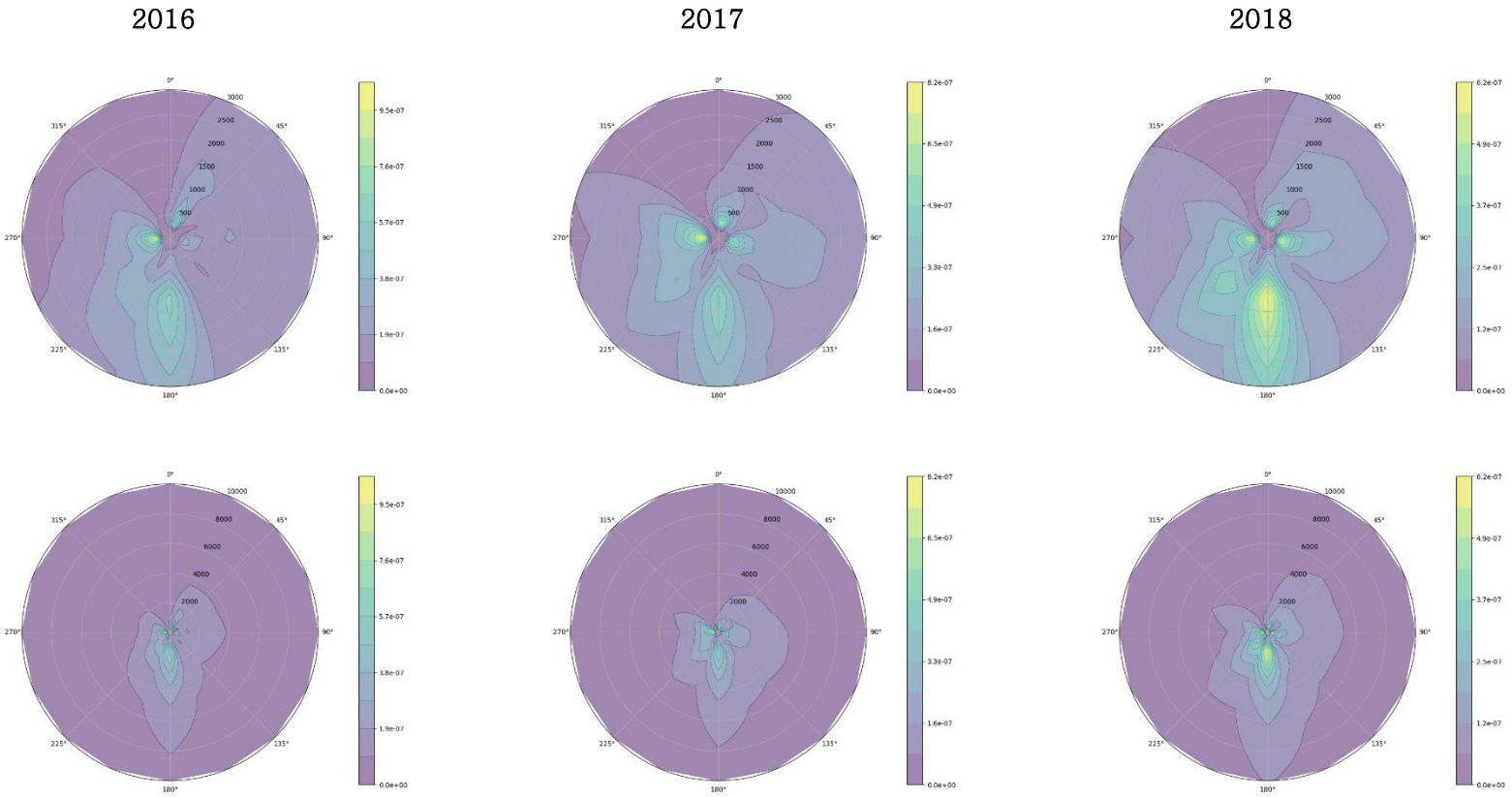

Figure 3.12. Dispersion factors in 2016−2018 (Kori, recirculation)
Top: 3 km, Bottom: 10 km radius

3.1.5. Mixed Release

When the mixed release is assumed, E_t is the fraction of ground release of the total. E_t is determined by the ratio of the plume exit velocity W_0 to the mean wind speed $\bar{u}$. As the ratio $W_0/\bar{u}$ increases, the fraction of ground release E_t decreases.

When the ground release is assumed, the effective plume height h_e is zero. As the exponential term in the Equation 2.1 can be ignored, the total dispersion factor for mixed release near the source tends to increase as the fraction E_t increases.

Table 3.6 and Figure 3.13 are the modeling results for mixed release in Wolsong and Kori. The stack height of 58 m and the adjacent building height of 50 m were assumed. As the dispersion factor decreases with the increasing distance from the source, the EAB distance of 300 m was adopted and the dispersion factor at the EAB was calculated. The maximum dispersion factors were formed in SE (Wolsong) and NNE (Kori) directions for all three years.

The mixed release led to the increase in dispersion factor to 19.6–60.1 times the base scenario. It was anticipated that mixed release is primarily affected by its ground dispersion fraction unless there is a significant increase in the ratio $W_0/\bar{u}$.

Table 3.6. Maximum X/Q values for mixed release at EAB = 300 m

Year	Wolsong		Kori	
	Maximum (s/m^3)	Direction	Maximum (s/m^3)	Direction
2016	5.49E-06	SE	6.35E-06	NNE
2017	6.49E-06	SE	8.23E-06	NNE
2018	5.18E-06	SE	9.20E-06	NNE

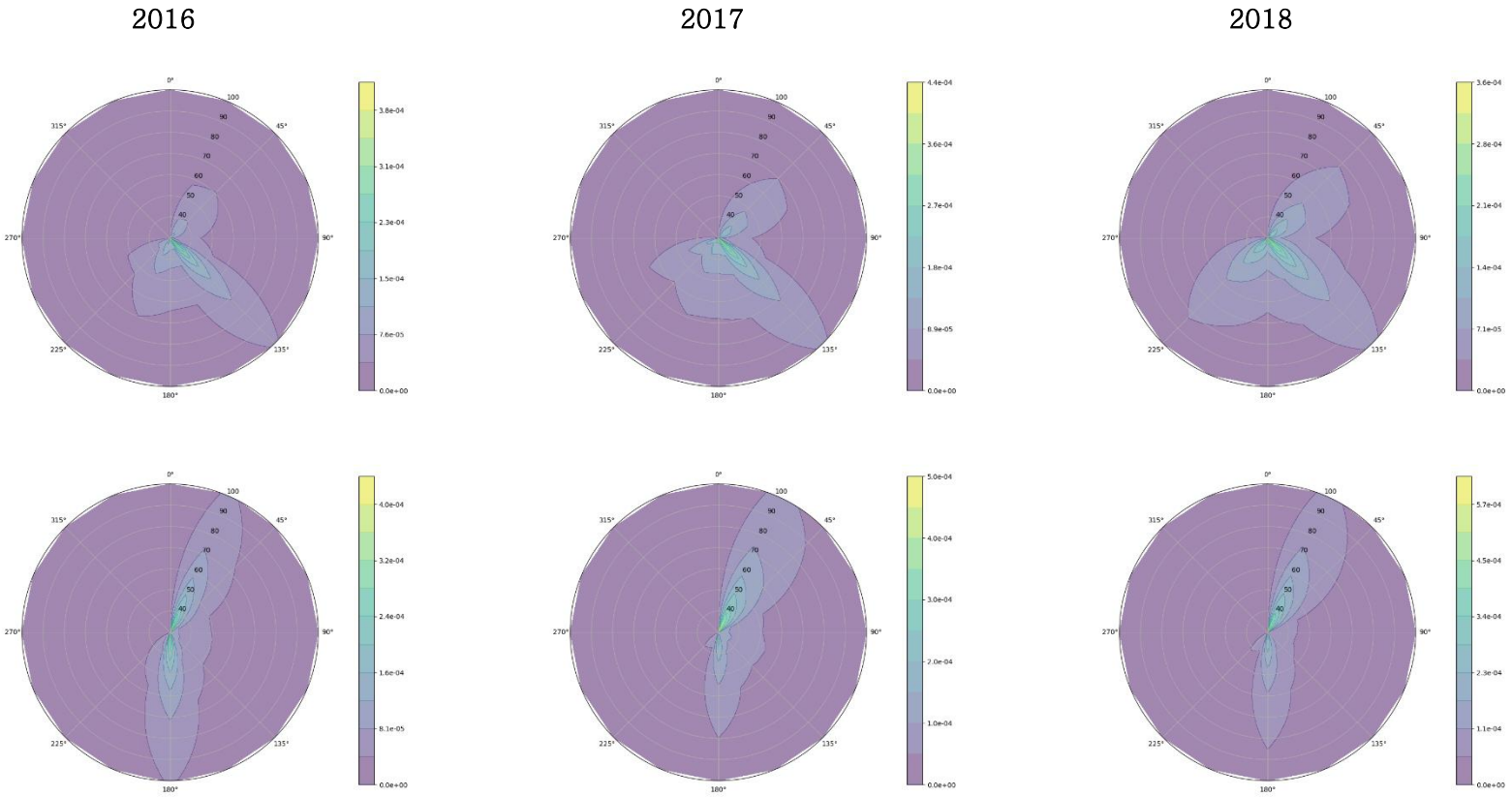

Figure 3.13. Dispersion factors in 2016–2018 (mixed release)
Top: Wolsong, Bottom: Kori

3.1.6. Wind Speed Correction

In case of elevated release, the wind speed at the height of emission is required. However, when the measured height is different from the actual emission height, the wind speed can be corrected as in Section 2.1.4. To examine the effects of wind speed correction, a dispersion modeling was performed with measured wind height at 48 m, while the desired height is 58 m.

Table 3.7 and Figure 3.14 show the dispersion factor with corrected wind speed. The maximum dispersion factors were slightly decreased to 0.94−0.97 times compared to the base scenario. The distances to the maximum points were reduced for Wolsong (2017) and Kori (2018).

Table 3.7. Maximum X/Q values and locations (wind correction)

Year	Wolsong		Kori	
	Maximum (s/m^3)	Location	Maximum (s/m^3)	Location
2016	2.71E−07	330 m, WSW	2.31E−07	330 m, W
2017	1.02E−07	2340 m, SE	1.98E−07	340 m, W
2018	1.01E−07	330 m, NNE	1.82E−07	1940 m, S

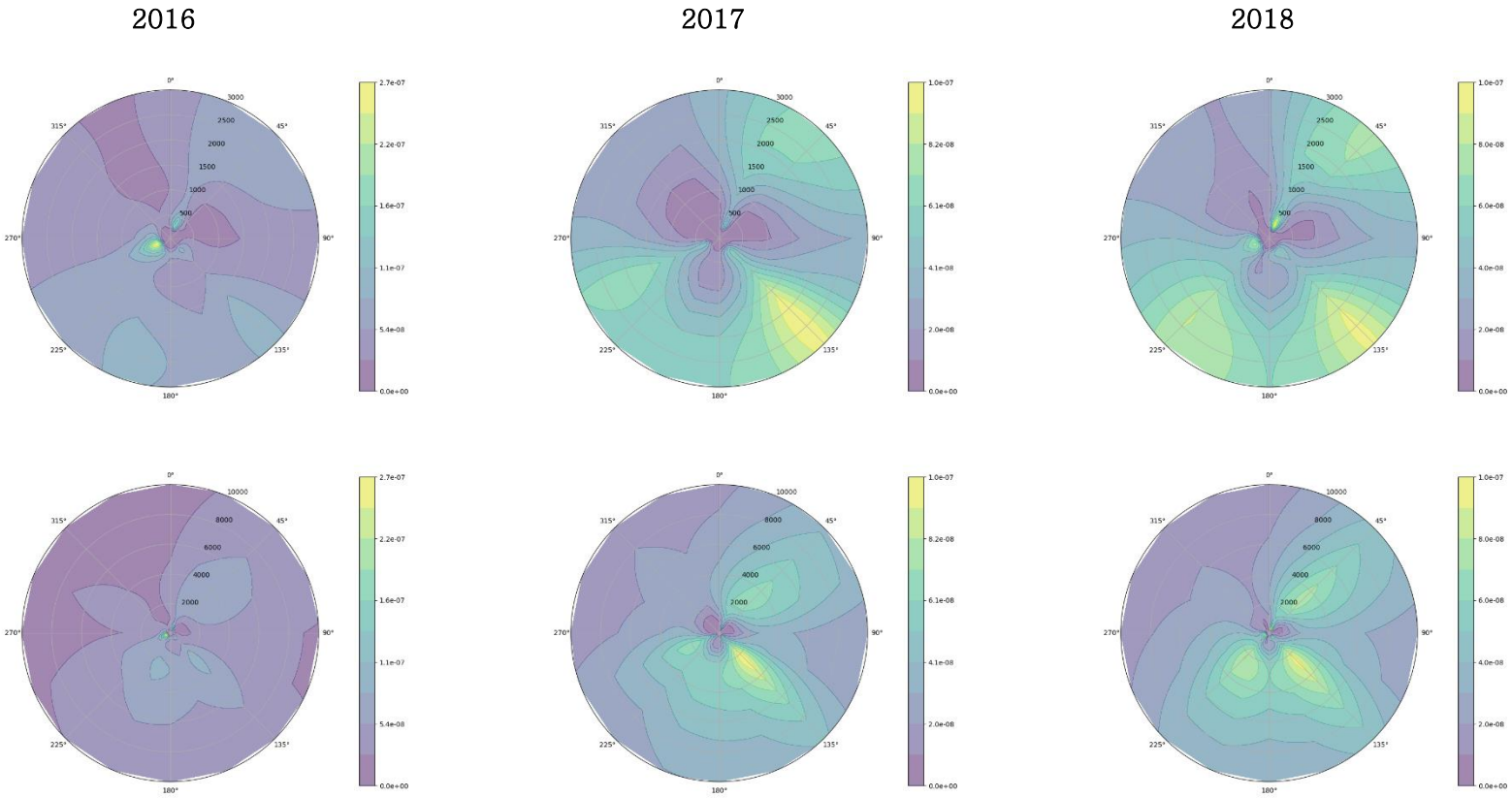

Figure 3.14. Dispersion factors in 2016–2018 (Wolsong, corrected wind speeds)
Top: 3 km, Bottom: 10 km radius

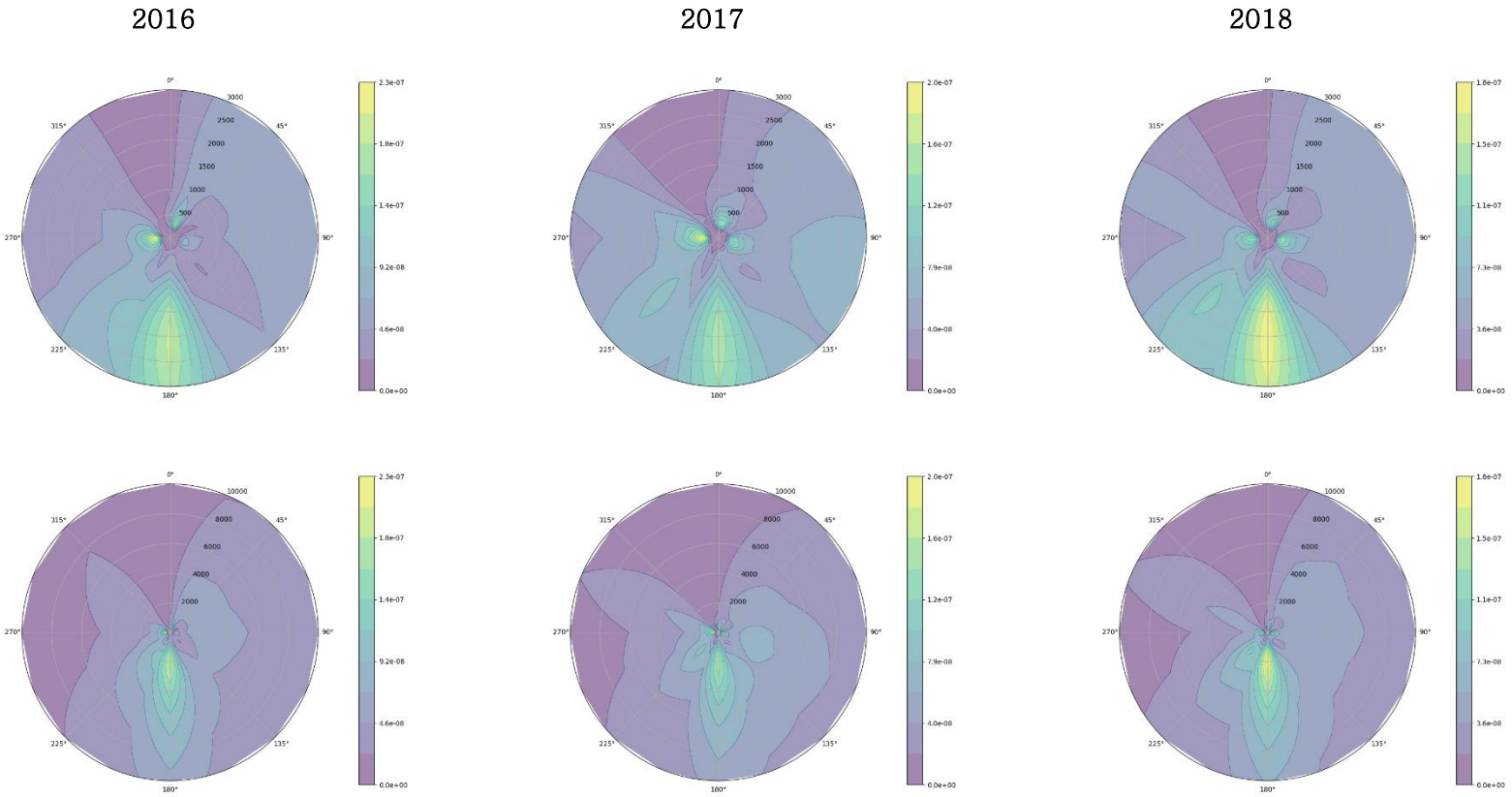

Figure 3.15. Dispersion factors in 2016–2018 (Kori, corrected wind speeds)
Top: 3 km, Bottom: 10 km radius

3.2. Dispersion including Terrain Elevation

3.2.1. Terrain Data Acquisition

Digital Elevation Model is a file containing terrain elevation values in a raster format. DEM files in GeoTIFF format can be retrieved from the Application for Extracting and Exploring Analysis Ready Samples (AppEEARS) of the US Geological Survey (USGS). For the regions of interest in this research, the finest resolution is 30 m (1 arc-second). Among the several options, the USGS-ASTER DEM was employed. The elevation values were extracted with Python-Geospatial Data Abstraction Library (GDAL) version 3.2.1. The terrain handling function for the modified XOQDOQ code can interpolate terrain data for the sub-grid points.

The 30 m and 90 m resolution data were compared for dispersion factor calculation to test the sensitivity due to the terrain resolution.

The 90 m terrain elevation data were generated from the 30 m data with two distinctive downgrading approaches as in Figure 3.16. In the first method, the average value of the adjacent 30 m terrain data was calculated. While in the second method, the maximum elevations among the neighboring 30 m data were selected as 90 m data.

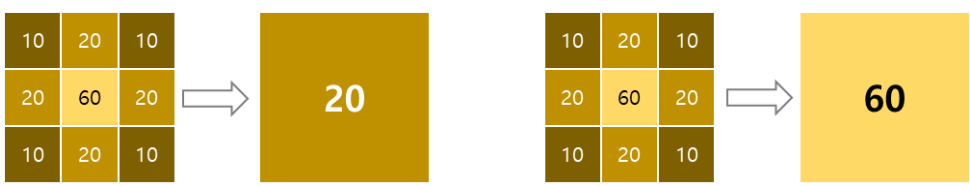

Figure 3.16. Two approaches for resolution downgrading

Table 3.8 contains the maximum dispersion factors computed with terrain heights having different resolutions. As anticipated, the max-height approach led to more conservative values than the mean-height approach. The result showed that when the resolution of terrain elevation is coarse, it is vital to ensure that the peak terrain elevations in the domain are well-represented in the data.

Table 3.8. Dispersion factors with different terrain resolutions

	No Terrain	30 m	Mean-height (90 m)	Max-height (90 m)
Maximum X/Q (s/m^3)	1.04E-07	5.18E-07	4.68E-07	5.13E-07
Location	329 m, NNE	1710 m, NW	1836 m, NW	1736 m, NW

3.2.2. Results and Discussion

The dispersion factors for Wolsong and Kori sites were calculated between 2016 and 2018 using terrain elevation data. Model parameters other than terrain heights were the same as in the base scenario. The terrain height at the stack base was set as zero, and the receptor heights lower than the stack base were also set to zero. Thus, underprediction due to lower terrains could be avoided in the model calculation.

Tables 3.9 and 3.10 are the maximum dispersion factors calculated for each site. Figures 3.17 and 3.18 show the pattern of dispersion with terrain heights. By inputting terrain height information, both maximum value and location were changed compared to the base scenario.

The two assumptions on plume heights, horizontal and adjusted plume, led to different modeling results. Under the horizontal plume assumption, the dispersion factors were increased to 8.3-27.3 times the base scenario without terrains. On the other hand, the adjusted plume assumption resulted in gradual increases less than 4.3 times

the base scenario. The distances to the maximum points were farther in the adjusted plume cases and different directions for Wolsong (2017, 2018).

Table 3.9. Maximum X/Q values and locations (with terrain elevation, Wolsong)

Year	Horizontal plume		Adjusted plume	
	Maximum (s/m^3)	Location	Maximum (s/m^3)	Location
2016	2.33E−06	750 m, WNW	5.06E−07	900 m, WNW
2017	2.13E−06	840 m, NW	4.32E−07	1170 m, N
2018	1.68E−06	840 m, NW	4.49E−07	2250 m, SW

Table 3.10. Maximum X/Q values and locations (with terrain elevation, Kori)

Year	Horizontal plume		Adjusted plume	
	Maximum (s/m^3)	Location	Maximum (s/m^3)	Location
2016	3.90E−06	630 m, NNE	6.06E−07	870 m, NNE
2017	4.46E−06	630 m, NNE	4.37E−07	870 m, NNE
2018	5.14E−06	640 m, NNE	5.79E−07	870 m, NNE

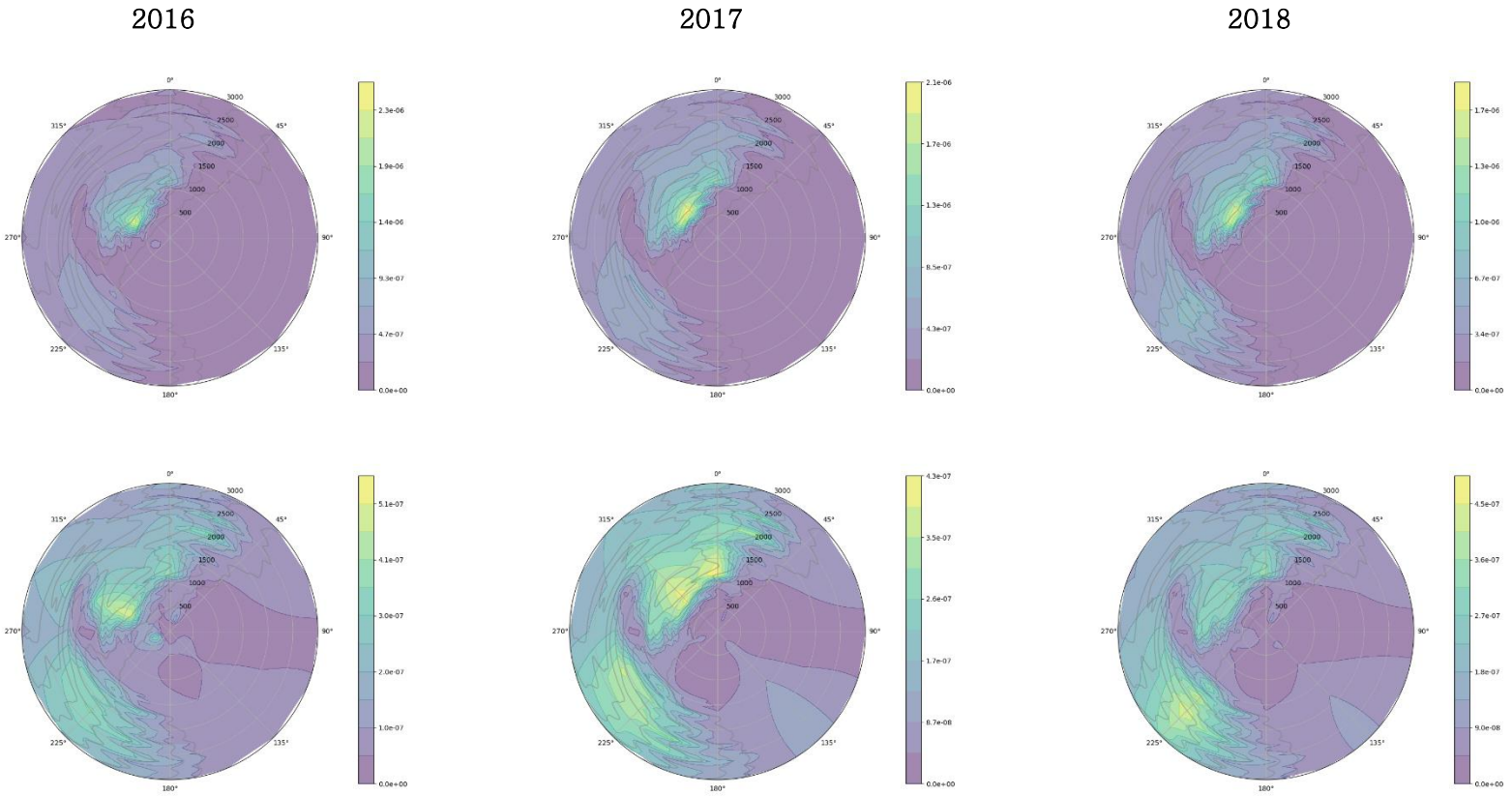

Figure 3.17. Dispersion factors in 2016−2018 (Wolsong)
Top: horizontal plume, Bottom: adjusted plume

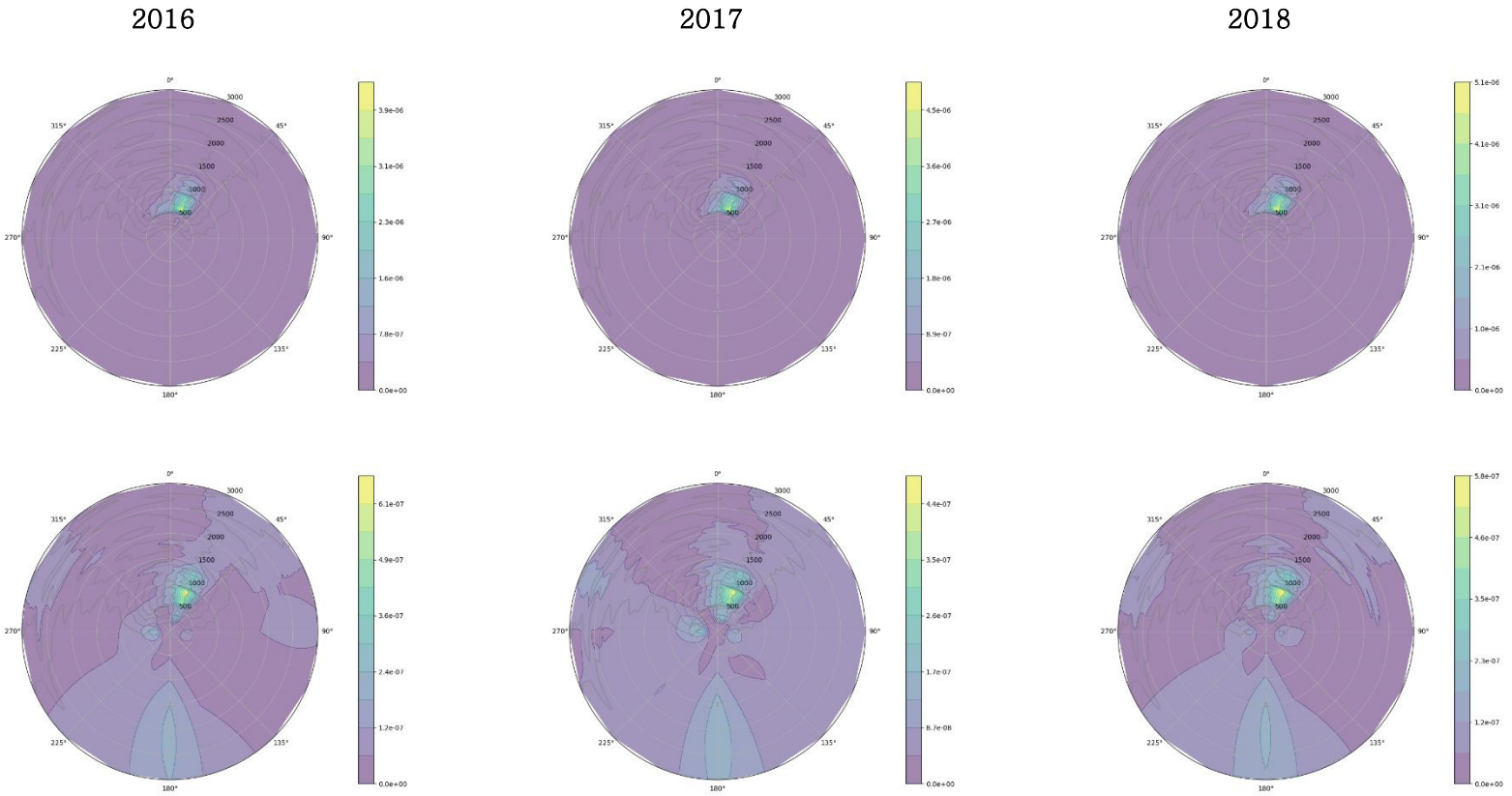

Figure 3.18. Dispersion Factors in 2016−2018 (Kori)
Top: horizontal plume, Bottom: adjusted plume

3.3. Deposition

The deposition factor is a significant input in dose estimation. Deposited radionuclides can cause radiation exposure either directly or indirectly through ingestion (Leelossy et al., 2018). For example, Jones et al. (2013) assessed the possible radiological impact of routine discharges from nuclear power plants in England and Wales. Among the predicted individual doses from atmospheric releases, more than 60% was due to the ingestion of terrestrial foodstuffs containing radionuclides. In comparison, inhalation of radionuclides in the plume was expected to be around 30% of the total dose.

As reviewed in the previous chapter, there are two different approaches to estimating deposition factors. XOQDOQ applies separate functions for relative deposition rate, while other models calculate deposition flux from the dispersion factor.

Tables 3.11 and 3.12, and Figures 3.19 and 3.20 are the deposition factors in Wolsong and Kori. They were computed with default XOQDOQ relative deposition rate functions.

The results indicated that based on separate deposition rates, the distances to the maximum points could be the same (390 m) when terrain elevation was not inputted. For atmospheric stability A, B, C, and the stack height between 45 and 80 m, the deposition rate follows a single function of downwind distance. Therefore, the maximum point for the relative deposition rate function, which is ~400 m, became the maximum distance for the estimated deposition factors.

When terrain heights were factored in, the maximum points for dispersion factors were changed except for Wolsong (2016, 2017). As the exponential term containing the effective stack height was not included (see eq. 2.5), the difference due to adjusted plume heights was negligible.

Table 3.11. Maximum D/Q values and locations
(without terrain elevation)

Year	Wolsong		Kori	
	Maximum (s/m^3)	Location	Maximum (s/m^3)	Location
2016	1.17E−08	390 m, WSW	8.43E−09	390 m, W
2017	4.01E−09	390 m, WSW	8.20E−09	390 m, W
2018	5.14E−09	390 m, NNE	6.04E−09	390 m, E

Table 3.12. Maximum D/Q values and locations
(with terrain elevation, horizontal plume)

Year	Wolsong		Kori	
	Maximum (s/m^3)	Location	Maximum (s/m^3)	Location
2016	1.17E−08	390 m, WSW	3.03E−08	590 m, NNE
2017	4.01E−09	390 m, WSW	2.78E−08	590 m, NNE
2018	6.15E−09	520 m, W	3.08E−08	590 m, NNE

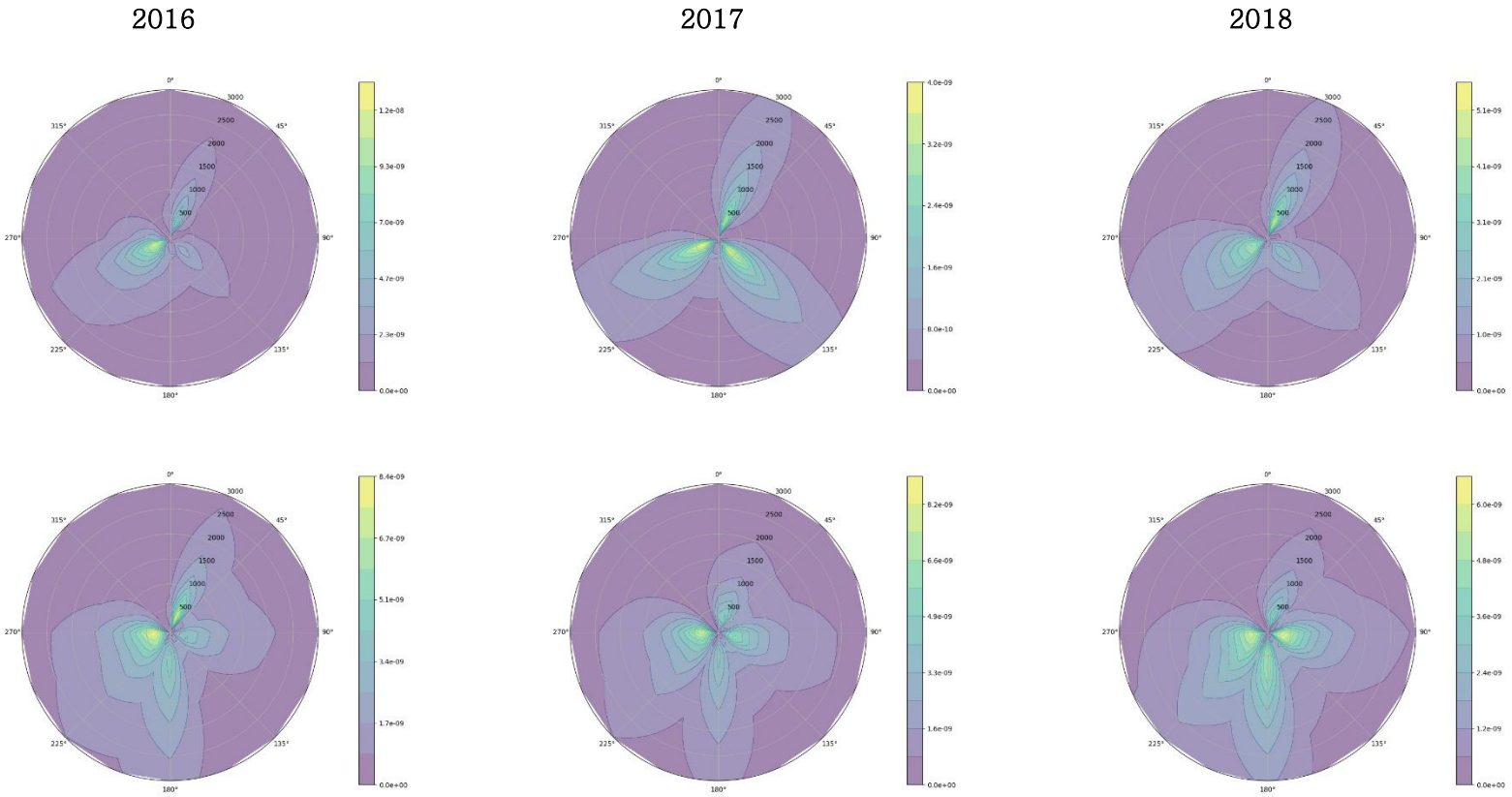

Figure 3.19. Deposition Factors in 2016−2018 (without terrain elevation)
Top: Wolsong, Bottom: Kori

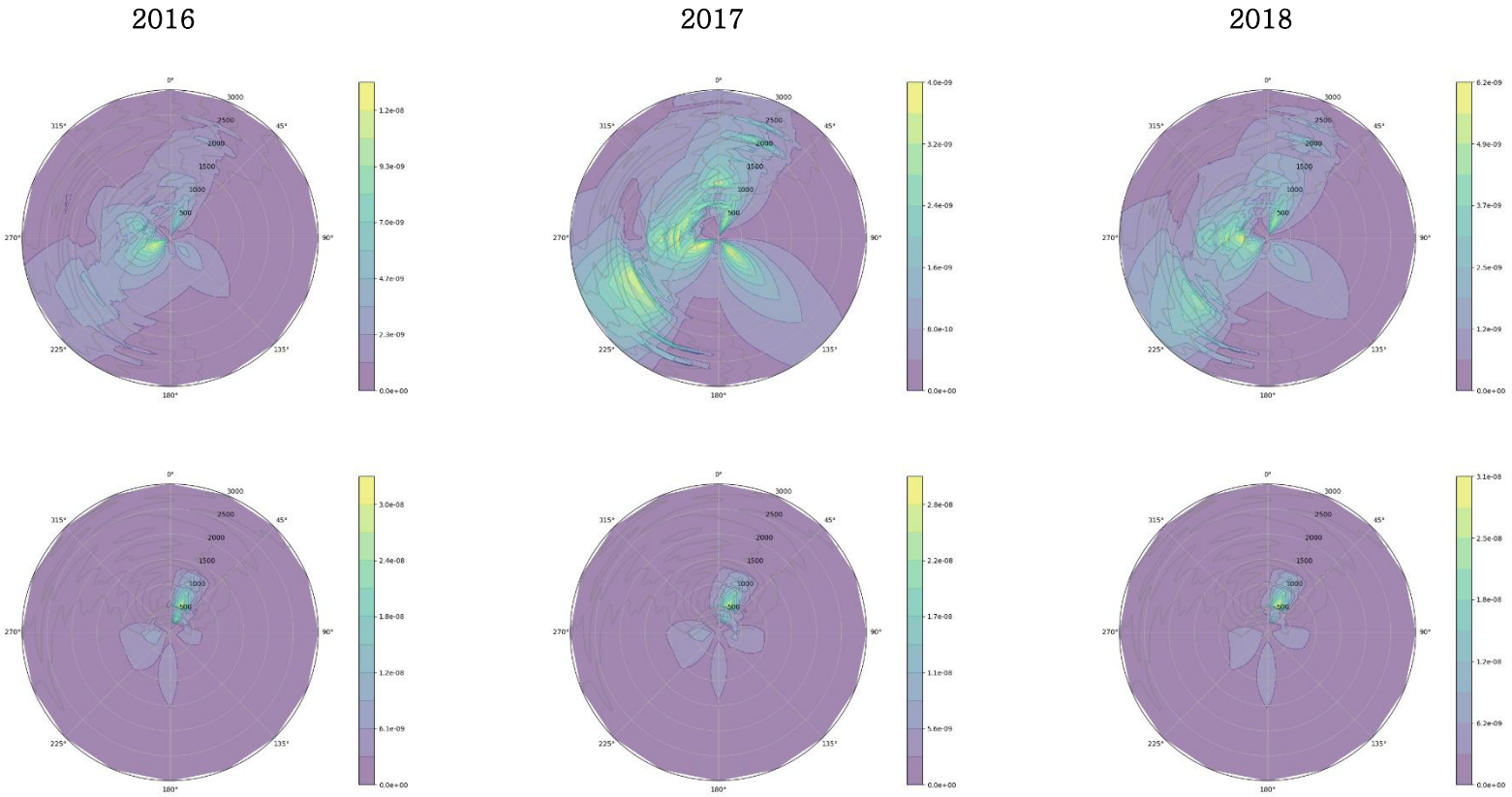

Figure 3.20. Deposition Factors in 2016–2018 (with terrain elevation)
Top: Wolsong, Bottom: Kori

The deposition modeling based on particle deposition velocity (see Section 2.1.6) was reviewed. To compare with the default deposition factor computed from XOQDOQ, the meteorological parameters in Wolsong and Kori were analyzed. The derivation processes for friction velocity and Monin-Obukhov length are elaborated in Chapter 4.

The overall deposition velocities assuming f=0.8 are 0.0033 m/s in Wolsong and 0.0042 m/s in Kori. The velocities were comparable to the range of dry deposition velocities reviewed by Sportisse (2007).

Tables 3.13-3.15 and Figures 3.21-3.23 are the modeling results for dispersion factors computed with site-specific deposition velocities. The factors displayed a percentage difference between -93 and -87% compared to the default case (without terrain) by implementing the velocity-based deposition modeling. With terrain elevation, the range of difference was between -46 and 76% for horizontal plumes and between -93 and -64% for adjusted plumes.

Table 3.13. Maximum D/Q values and locations
(without terrain elevation)

Year	Wolsong		Kori	
	Maximum (s/m^3)	Location	Maximum (s/m^3)	Location
2016	9.25E−10	330 m, WSW	1.00E−09	330 m, W
2017	3.55E−10	2400 m, SE	8.57E−10	340 m, W
2018	3.43E−10	330 m, NNE	7.91E−10	1990 m, S

Table 3.14. Maximum D/Q values and locations
(with terrain elevation, Wolsong)

Year	Horizontal plume		Adjusted plume	
	Maximum (s/m^3)	Location	Maximum (s/m^3)	Location
2016	7.70E−09	750 m, WNW	1.67E−09	900 m, WNW
2017	7.04E−09	840 m, NW	1.43E−09	1170 m, N
2018	5.55E−09	840 m, NW	1.48E−09	2250 m, SW

Table 3.15. Maximum D/Q values and locations
(with terrain elevation, Kori)

Year	Horizontal plume		Adjusted plume	
	Maximum (s/m^3)	Location	Maximum (s/m^3)	Location
2016	1.64E−08	630 m, NNE	2.55E−09	870 m, NNE
2017	1.87E−08	630 m, NNE	1.83E−09	870 m, NNE
2018	2.16E−08	640 m, NNE	2.43E−09	870 m, NNE

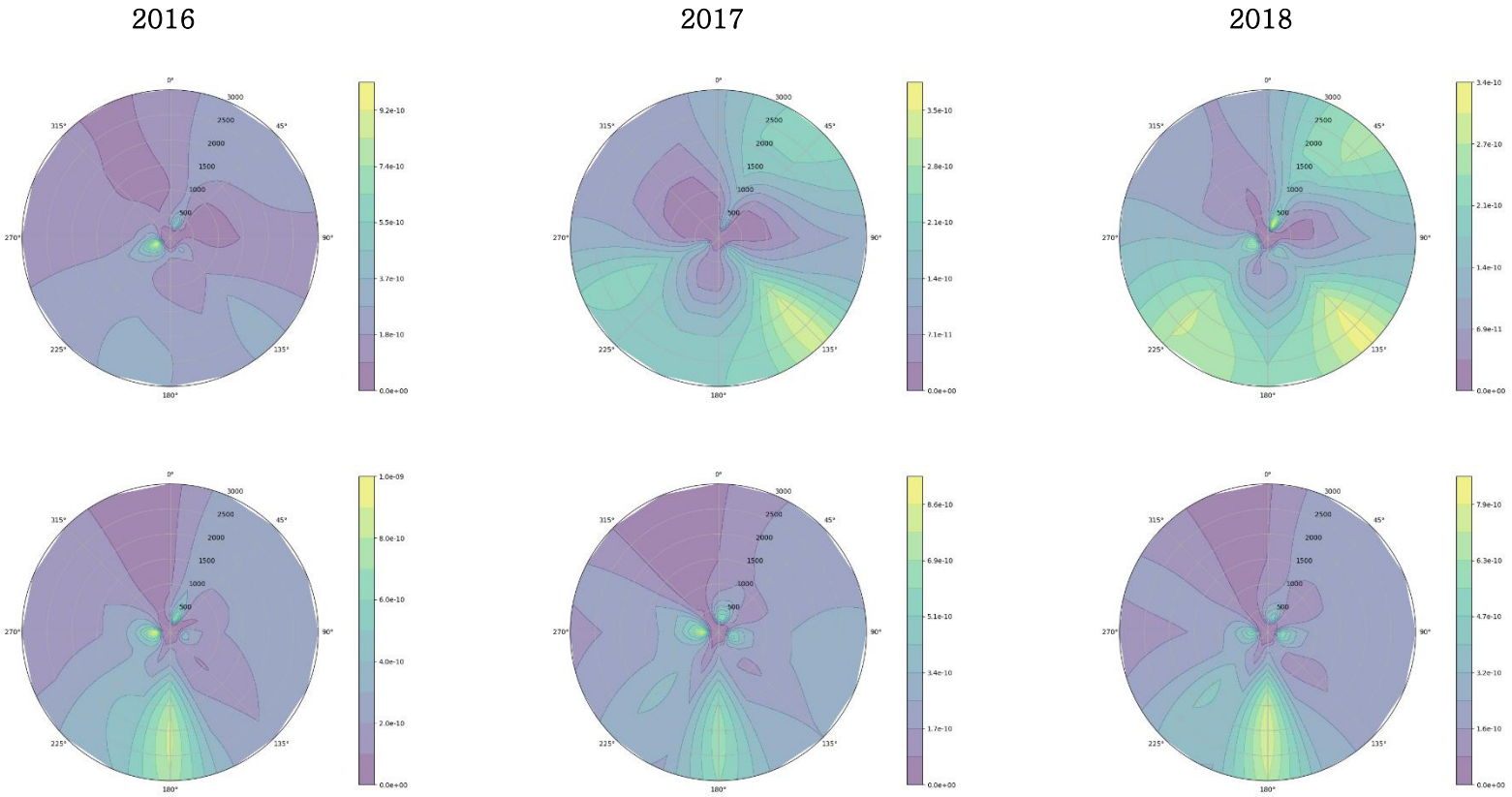

Figure 3.21. Deposition Factors in 2016–2018 (new deposition, without terrain elevation)
Top: Wolsong, Bottom: Kori

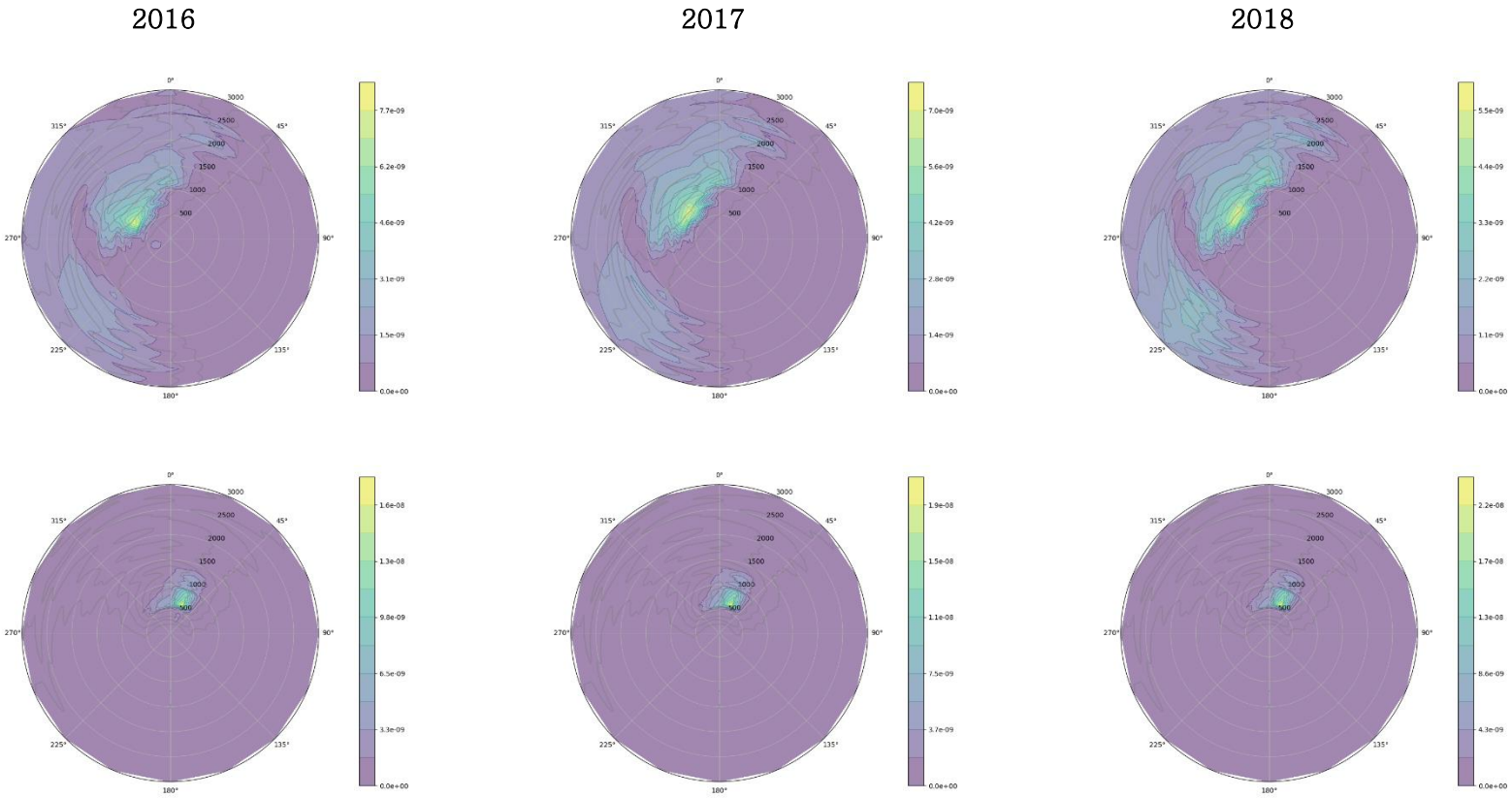

Figure 3.22. Deposition Factors in 2016−2018 (new deposition, with horizontal plume)
Top: Wolsong, Bottom: Kori

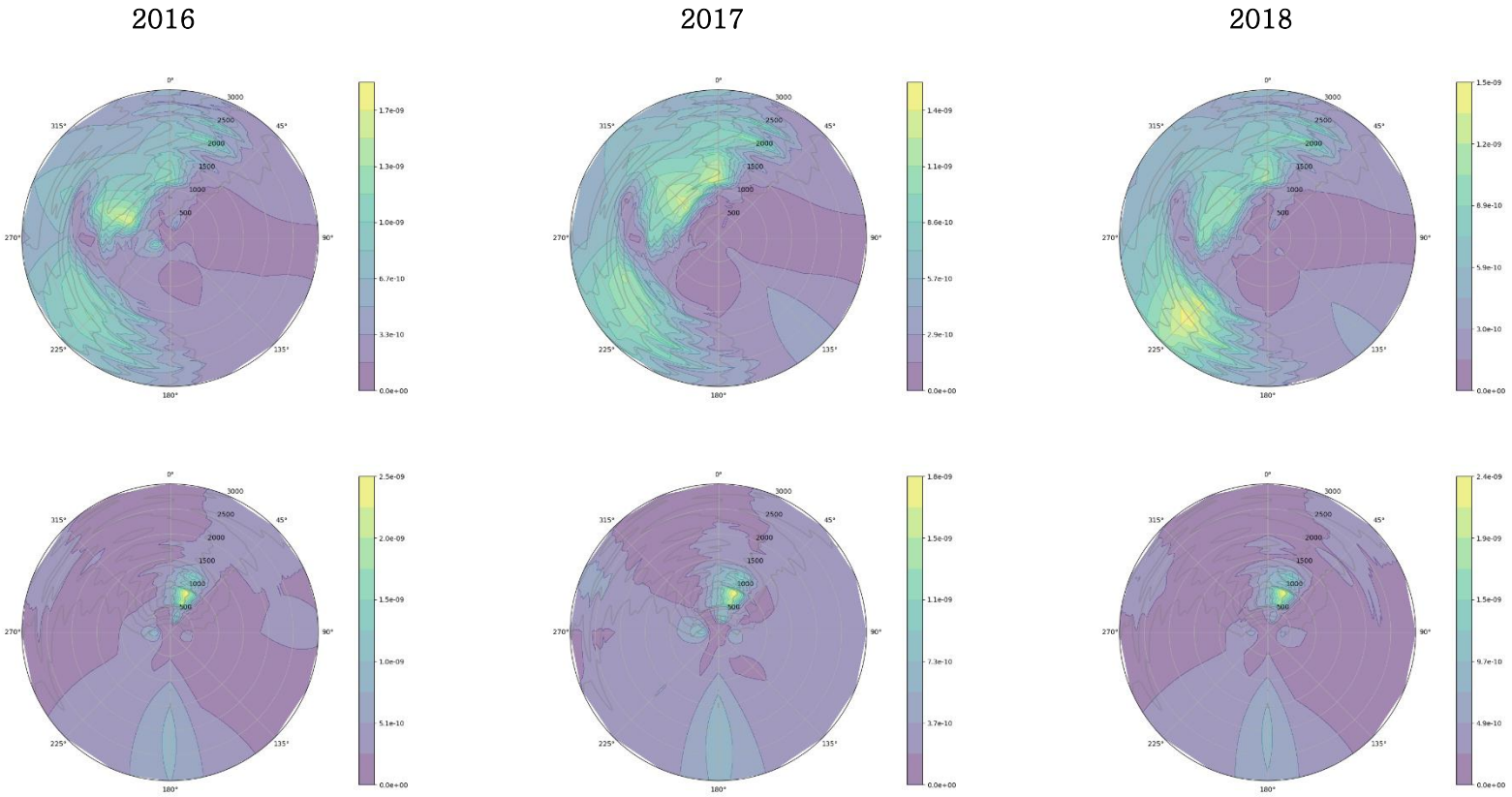

Figure 3.23. Deposition Factors in 2016–2018 (new deposition, with adjusted plume)
Top: Wolsong, Bottom: Kori

3.4. Dose Assessment

For the Wolsong and Kori sites, dose assessment was performed at the EAB (Kori: 700 m, Wolsong 914 m) and nearest residential areas (Kori: 1.1 km, Wolsong: 1.46 km). The dispersion and deposition factors were calculated as described in the previous sections. Mixed release, elevated release excluding terrain elevation (base case), elevated release with horizontal plume assumption (horizontal model), and elevated release with adjusted plume assumption (adjusted model) was compared. The dose assessment followed the default settings of the NRC's GASPAR code.

At the EAB, the maximum dispersion and deposition factor among the 16 directions were inputted to the dose assessment model. In the case of elevated release conditions, the maximum locations were the receptor points with high terrain elevation. Mixed release and horizontal model resulted in comparatively high dose. The dose assessed with the adjusted model was higher than the base case but lower than the mixed release case and horizontal model.

As the residential areas have low terrain elevations, the horizontal and adjusted model displayed similar dose levels. In the case of mixed release, the dispersion and deposition factors were decreased with distance. Thus, the estimated dose showed a slight difference with the elevated release cases.

Among the pathways considered, the ingestion accounted for most of the total dose. Thus, the relative percentage to dose constraint is the largest in the case of internal exposure. On the other hand, other pathways were below 1% of the dose constraints.

Table 3.16. Estimated dose at the EAB (Wolsong, 2016)

(Unit: mSv/y)

	Mixed release	Base case	Horizontal	Adjusted
External dose due to plume	3.62E−04	1.54E−05	3.30E−04	9.07E−05
External dose due to ground deposition	3.08E−07	2.24E−07	2.24E−07	6.79E−08
Ingestion	**4.60E−02**	**1.96E−03**	**4.53E−02**	**1.15E−02**
Inhalation	2.83E−03	1.21E−04	2.79E−03	7.10E−04

Table 3.17. Estimated dose at the residential area (Wolsong, 2016)

(Unit: mSv/y)

	Mixed release	Base case	Horizontal	Adjusted
External dose due to plume	5.09E−05	1.35E−05	5.75E−05	5.45E−05
External dose due to ground deposition	9.89E−08	5.86E−08	9.89E−08	4.07E−08
Ingestion	**6.46E−03**	**1.71E−03**	**7.31E−03**	**6.93E−03**
Inhalation	3.99E−04	1.06E−04	4.50E−04	4.27E−04

Table 3.18. Percentage of estimated dose to dose constraint at the EAB (Wolsong, 2016)

	Mixed release	Base case	Horizontal	Adjusted
Air dose (beta)	0.34%	0.01%	0.33%	0.08%
Air dose (gamma)	0.34%	0.01%	0.34%	0.09%
Effective dose (whole body)	0.72%	0.03%	0.71%	0.18%
Equivalent dose (skin)	0.59%	0.03%	0.58%	0.15%
Internal dose	**33%**	**1%**	**32%**	**8%**

Table 3.19. Percentage of estimated dose to dose constraint at the residential area (Wolsong, 2016)

	Mixed release	Base case	Horizontal	Adjusted
Air dose (beta)	0.05%	0.01%	0.05%	0.05%
Air dose (gamma)	0.05%	0.01%	0.05%	0.05%
Effective dose (whole body)	0.10%	0.03%	0.12%	0.11%
Equivalent dose (skin)	0.08%	0.02%	0.09%	0.09%
Internal dose	**5%**	**1%**	**5%**	**5%**

3.5. Summary and Conclusion

Dispersion and deposition factors for Wolsong and Kori sites between 2016 and 2018 were assessed. Effects of recirculation, mixed release, and wind speed correction were tested, excluding terrain elevation. It was confirmed that the dispersion factor under mixed release exceeded the values assuming elevated releases.

Both original and modified versions of the XOQDOQ model were applied for dispersion modeling, including terrain elevation. The original model based on horizontal plume state modeling resulted in a higher dispersion factor than the modified model based on adjusted plume state modeling. Dispersion factors, including terrain heights, were still below mixed release cases.

The original model calculated the deposition factor with the relative deposition rate function, which is predetermined for several effective stack height ranges. In this case, maximum deposition factors could be formed at the same distances. In the modified model, the velocity-based deposition modeling, where the deposition pattern becomes dependent on the dispersion, was implemented. The deposition factors calculated from the modified model were decreased compared to the original model.

The dose at the EAB and the nearest residential area was assessed based on the dispersion and deposition modeling results. Among the pathways considered, the ingestion of radionuclides accounted for most of the total dose. Both mixed release and horizontal models displayed a significant difference in dose estimated at the EAB and the residential area. In contrast, the difference was minimal in the case of the adjusted model.

Chapter 4. Model Intercomparison

4.1. AERMOD Modeling System

AERMOD was developed as a conjoined project of EPA and the American Meteorological Society (AMS) (Cimorelli et al., 2005). AERMOD is one of the preferred and recommended models of EPA for air quality dispersion modeling. Korea Environment Institute (KEI) also recommended potential license applicants to implement AERMOD for environmental impact assessment (KEI, 2005).

According to the Clean Air Act, the dispersion models recommended for evaluating the concentration of air pollutants are referred to as "preferred models" by the EPA. They are listed in "Appendix W: Guideline on Air Quality Models (the Guideline)" of 40 CFR Part 51. Since 2005, AERMOD has been recommended by the Guideline as an atmospheric dispersion model applicable to short ranges (within ~50 km). Several significant modifications to the AERMOD model formulations were proposed to mitigate the overprediction tendency under conditions such as a stable atmosphere combined with low wind speeds.

Currently, three models are recommended by the EPA as "Preferred and Recommended Model" based on the Guideline: AERMOD, CTDMPLUS (Complex Terrain Dispersion Model Plus Algorithms for Unstable Situations), and OCD (Offshore and Coastal Dispersion Model Version 5). CTDMPLUS can be used when complex terrain is the primary concern in dispersion modeling, and it can provide higher resolution than AERMOD. OCD is a model for simulating the dispersion in the ocean or coastal region. It should be noted that AERMOD is a comprehensive model that can also be applied to elevated releases under complex terrain and has been validated by an extensive set of experimental data. Therefore, in this study, AERMOD was chosen for model comparison.

Both AERMOD and XOQDOQ are based on the steady-state Gaussian plume model. Nevertheless, AERMOD derives turbulent spreads by directly modeling the planetary boundary layer properties,

while XOQDOQ follows simplified dispersion coefficients defined by Pasquill stability criteria. The stability scheme only provides a surrogate for the turbulent intensity through the stability classes (Turner, 1996).

AERMOD uses meteorological inputs to model turbulence characteristics such as vertical profiles of wind speed, lateral and vertical turbulence, and potential temperature. Thus, AERMOD requires far more detailed input parameters than XOQDOQ. Figure 4.1 summarizes the data flow for meteorological and terrain data input in AERMOD.

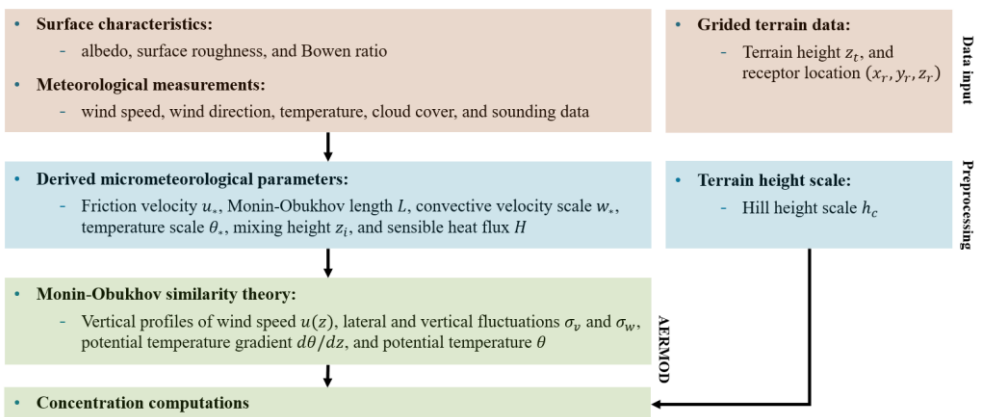

Figure 4.1. Meteorological and terrain data flow in AERMOD (modified from EPA, 2019a)

AERMOD requires surface characteristics such as albedo, Bowen ratio, and surface roughness length. These are categorized as site-specific constant parameters, but in some cases, users can set them as variables dependent on time and location. Wind speed and direction, ambient temperature, cloud cover, and early morning sounding data comprise the measured weather data. Both surface characteristics and measured data are preprocessed to derive planetary boundary layer parameters such as friction velocity, Monin-Obukhov length, convective velocity scale, temperature scale, mixing height, and sensible heat flux. These derived parameters combined with input data are passed on to the dispersion modeling stage.

AERMET is a meteorological preprocessor for AERMOD. Data

files with specific formats can be inputted into AERMET and automatically preprocessed into the input files. Surface weather data formats such as CD-144, SAMSON, HUSWO, ISHD, or TD-3280 are compatible, and TD-6201 or FSL for upper air sounding data. When site-specific data are used, they should be first converted into readable ASCII format.

To perform AERMOD modeling with incomplete weather data, Carbonell et al. (2010) have developed a set of codes that can generate surface and profile input files with a minimum required information. On the other hand, Lim and Bae (2015) developed a software package that translates domestic meteorological data files into the US format that can be inputted into AERMET.

For this research, however, it is necessary to concatenate several measurement data into a single input. For instance, it was required to combine site-specific and ASOS measurements into AERMOD input. Therefore, a set of preprocessing codes was devised that generates necessary input files for AERMOD from user-input information. The codes were written in MATLAB (Mathworks, version: R2021a) and can be used for further studies.

Terrain data input follows a separate procedure. For each receptor marked in AERMOD input, both terrain elevation height and hill height scale are required. The details of meteorological and terrain data preprocessing are elaborated in the following sections.

4.2. Derivation of Meteorological Parameters

Minimum meteorological information needed for AERMOD can be summarized as in Table 4.1 (EPA, 2019a). Meteorological data are categorized into surface information and profile information, and they are formatted into two separate files for AERMOD input.

Sensible heat flux, surface friction velocity, convective velocity scale, Monin-Obukhov length, and mixing heights are derived parameters. These derived parameters are calculated during the preprocessing phase. The detailed derivation process follows EPA (2019a, 2019b) and Cimorelli et al. (2005). In addition, alternative derivations were applied for some parameters, such as sensible heat flux and convective mixing heights, and the results were compared.

The rest are measurement data. Measurement data are subdivided into two groups. The first group includes wind speed, direction, and temperature for all the heights measured. These are included in the on-site measurement data. However, other information such as precipitation, relative humidity, station pressure, and cloud cover should be retrieved from different sources since they are not included in the on-site data. Instead, they are available in the ASOS (Automated Synoptic Observing System) measurements, provided by the Open MET Data Portal of Korean Meteorological Administration (KMA).

Table 4.1. Minimum meteorological information for AERMOD input

Meteorological data	Unit	Note
Surface information		
Sensible heat flux	W/m^2	Derived parameter
Surface friction velocity	m/s	
Convective velocity scale	m/s	
Convectively driven mixing height	m	
Mechanistically driven mixing height	m	
Monin-Obukhov length	m	
Wind speed	m/s	On-site measurement
Wind direction	degrees	
Anemometer height	m	
Temperature	K	
Measurement height	m	
Precipitation code		ASOS measurement
Precipitation amount		
Relative humidity	%	
Station pressure	Mbar	
Cloud cover	Tenth	
Profile information		
Measurement height	m	On-site measurement
Wind direction	degrees	
Wind speed	m/s	
Temperature	℃	
Directional standard deviation		
Vertical standard deviation		

4.2.1. Sensible Heat Flux

In AERMOD, sensible heat flux H determines the atmospheric stability of the planetary boundary layer. The fluxes can be measured with various methods, but when such measurements are not available, they can be parameterized using other model parameters (Holstag and Ulden, 1983).

The boundary layer is treated as convective when $H > 0$ and stable when $H < 0$. From the definition of net radiation R_n (W/m^2):

$$R_n = H + \lambda E + G$$

where H is the sensible heat flux (W/m^2), λE is the latent heat flux (W/m^2) for λ is the specific latent heat of evaporation (J/kg) and E is the evaporation rate (kg·m^{-2}·s^{-1}). As $0.1R_n$ is substituted for ground heat flux, G:

$$H = \frac{0.9R_n}{(1 + 1/B_0)} \cdots \text{(eq. 4.1)}$$

where $B_0 = H/\lambda E$ is Bowen ratio.

AERMET estimates net radiation as:

$$R_n = \frac{\big(1 - r(\varphi)\big)R + c_1 T^6 - \sigma_{SB} T^4 - c_2 n}{(1 + c_3)}$$

where ambient temperature T, and fractional cloud cover n are required as input. $r(\varphi)$ is the albedo under the solar elevation angle of φ.

The value of albedo usually depends on the solar elevation. But in this study, a representative value of r was used for simplicity. The coefficients in the above equation are $c_1 = 5.31 \times 10^{-13}$ (W·m^{-2}·K^{-6}), c_2 = 60 (W/m^2), and c_3 = 0.12. $\sigma_{SB} = 5.67 \times 10^{-8}$ (W·m^{-2}·K^{-4}) is the Stefan–Boltzmann constant. The ambient temperature and the fractional cloud cover measured from the ASOS station were used.

The solar insolation R can be estimated as:

$$R = R_0\left(1 + b_1 n^{b_2}\right)$$

where $R_0 = a_1(\sin\varphi) + a_2$ is the clear sky insolation, with $a_1 = 990$ (W/m^2), $a_2 = -30$ (W/m^2) and. The coefficients are $b_1 = -0.75$, and $b_2 = 3.4$.

As information such as surface temperature and solar insolation along with the duration hours are available from the ASOS, another method could be applied to compute the sensible heat flux (An et al., 2017):

$$R_n = (1 - r)R_{si} - L\uparrow + L\downarrow$$

where $L\uparrow = \varepsilon_s \sigma_{SB} T_s^4$, and $L\downarrow = \varepsilon_a \sigma_{SB} T_a^4$ are net long wave radiations from the surface and from the sky, respectively. R_{si} is the solar radiation (W/m^2), and r is the soil surface albedo. R_{si} is computed as the hourly insolation (MJ/m^2) divided by the duration (hours) from the ASOS measurement data.

For long wave radiations, ε_s is the soil emissivity with a typical range between 0.9 and 0.98, and T_s is the surface temperature (K). $\varepsilon_a = 0.7 + 5.95 \times 10^{-4} e_a \exp(1500/T_a)$ is the air emissivity, $e_a = (RH/100)e_s$ is the vapor pressure (kPa) where RH is the relative humidity (%), T_a is the air temperature (K), and $e_s = 0.6107 \exp(17.269(T_a - 273.15)/T_a)$ is the saturated vapor pressure at the temperature T_a.

Figure 4.2 compares the sensible heat fluxes estimated as in AERMET (with cloud cover) and directly computed with insolation measured at ASOS stations. The raw data show irregular peaks due to short insolation hours combined with nonzero insolation values. For the following model calculations, the AERMET method was used.

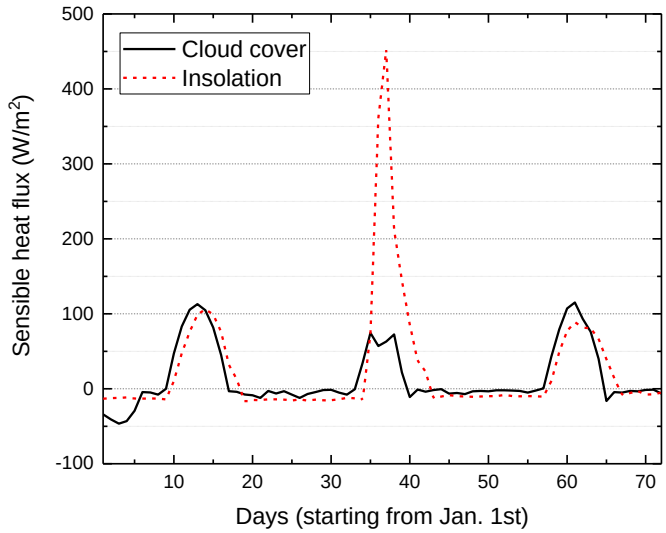

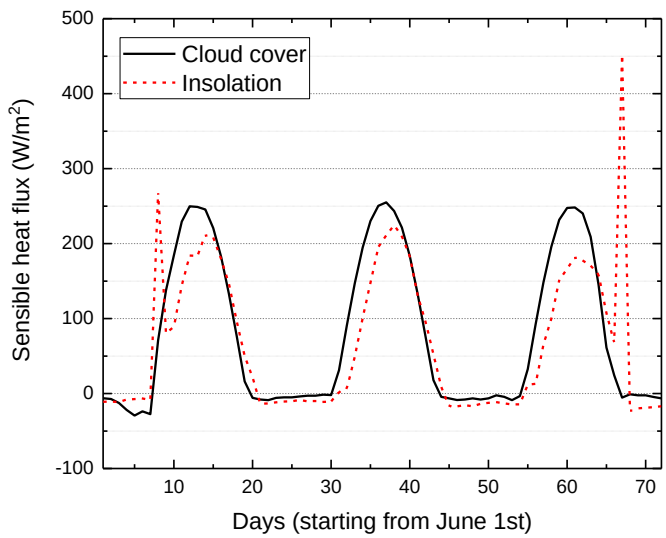

Figure 4.2. Sensible heat fluxes estimated with different approaches

4.2.2. Convective Parameters

Convective parameters include friction velocity u_* (m·s^{-1}), and Monin−Obukhov length L (m). In the absence of measurements, u* and L are derived from the available parameters, with the use of Monin−Obukhov theory. AERMET calculates each parameter as:

$$u_* = \frac{ku}{\ln\left(\frac{z_{ref}}{z_0}\right) - \psi_m\left(\frac{z_{ref}}{L}\right) + \psi_m\left(\frac{z_0}{L}\right)} \cdots \text{(eq. 4.2)}$$

$$L = \frac{-\rho c_p T u_*^3}{kgH} \cdots \text{(eq. 4.3)}$$

where k is the von Karman constant (= 0.4), u is the wind speed at reference height (m/s), z_{ref} is the reference height for wind speed and direction (m), z_0 is the surface roughness length (m), ρ is the density of air (kg·m^{-3}), c_p is the specific heat capacity of air (J·kg^{-1}·K^{-1}), and g is the acceleration due to gravity.

ψ_m is the stability function defined as:

$$\psi_m\left(\frac{z}{L}\right) = 2\ln\left(\frac{1+\mu}{2}\right) + \ln\left(\frac{1+\mu^2}{2}\right) - 2\tan^{-1}\mu + \frac{\pi}{2}$$

where $\mu = (1 - 16z/L)^{1/4}$. As u_* and L are reciprocally defined, two parameters are estimated through iterative process. To initialize u_*, it is assumed that $\psi_m = 0$ for neutral condition ($L = \infty$). Then u_* and L are calculated by iteration, until the values of L differ by 1% or less.

4.2.3. Convective Mixing Height

The mixing layer is an atmospheric boundary layer that covers the earth surface during daytime (Lee et al., 2014). Convective mixing layer determines the maximum height below which the turbulent mixing occurs. In AERMET system, convective mixing height z_{ic} (m), is formulated based on the methods of Carson (1973):

$$z_{ic}\theta(z_{ic}) - \int_0^{z_{ic}} \theta(z)dz = (1+2A)\int_0^t \frac{H(t')}{\rho c_p}dt \cdots (\text{eq. } 4.3)$$

where $\theta(z)$ is the initial potential temperature distribution from the morning sounding data. The righthand side represents the cumulative heat flux input at $z = 0$, and $A = 0.2$. Note that AERMET restricts the maximum height of convective mixing layer to 4000 m.

Sounding data are available for several locations in Korea. Rawinsonde measures pressure, temperature, and height as it descends from the upper air. The measurements are made twice a day, at 00:00 and 12:00 UTC. The daily measurements at 00:00 UTC from Pohang site were used, which is approximately 9:00 am, local time.

One of the more conventional approaches to estimate convective mixing height is the parcel method. The method follows a surface temperature up to its intersection with the temperature profile of the most recent sounding data (Seibert et al., 2000). With the same early morning sounding data, the parcel method was applied to see the difference. Figure 4.3 compares the convective mixing heights derived using two distinctive methods.

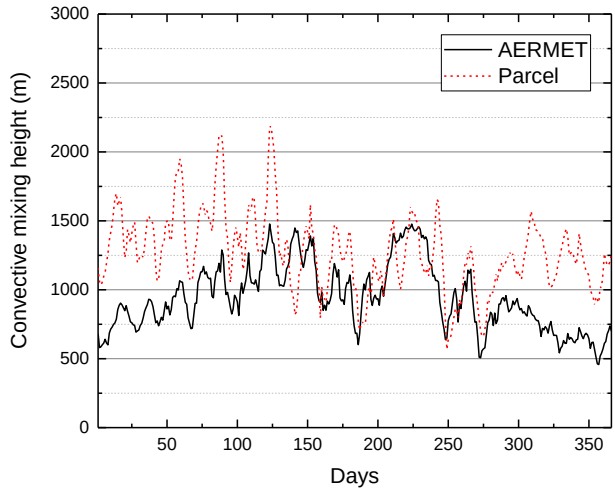

Figure 4.3. Convective mixing height based on two different methods

For mixing heights in a convective boundary layer $(L < 0)$, z_{ic} is compared with the mechanical mixing height z_{im}, and the higher value is selected.

Finally, turbulent velocity scale w_* is computed from sensible heat flux and convective mixing height:

$$w_* = \left(\frac{gHz_{ic}}{\rho c_p T}\right)^{1/3} \cdots \text{(eq. 4.4)}$$

4.2.4. Stable Parameters

For stable boundary layer, friction velocity u_* is computed as:

$$u_* = \left(\frac{C_D u}{2}\right)\left(1 + \left(1 - \left(\frac{2u_0}{C_D^{1/2} u}\right)^2\right)^{1/2}\right) \cdots \text{(eq. 4.5)}$$

where $C_D = k/\ln(z_{ref}/z_0)$ is the neutral drag coefficient, $u_0 = \left((\beta_m z_{ref} g\theta_*)/T\right)^{1/2}$, and $\beta_m = 4.7$. Potential temperature scale θ_*, is estimated with cloud cover n as:

$$\theta_* = 0.09(1 - 0.05n^2)$$

To obtain real-valued solution for u_*, the following inequality should be satisfied:

$$\frac{4u_0^2}{C_D^2 u^2} \leq 1$$

and critical wind speed u_{cr} is derived from the above inequality as:

$$u_{cr} = \left(\frac{4\beta_m z_{ref} g\theta_*}{TC_D}\right)^{\frac{1}{2}}$$

and

$$u_{*cr} = \frac{C_D u_{cr}}{2}$$

For wind speeds less than u_{cr}:

$$u_* = u_{*cr}\left(\frac{u}{u_{cr}}\right)$$

and

$$\theta_* = \theta_{*cr}\left(\frac{u_*}{u_{*cr}}\right)$$

Due to the restriction in heat flux, the product of θ_* and u_* is limited below 0.05 ($m \cdot s^{-1}K$). When $\theta_* u_* > 0.05$, u_* is recalculated with θ_* substituted by $0.05/u_*$ in Equation 4.5.

For stable boundary layer, sensible heat flux and Monin-Obukhov length are estimated after u_* and θ_* were obtained:

$$H = -\rho c_p u_* \theta_* \cdots (\text{eq. } 4.6)$$

$$L = \frac{-\rho c_p T u_*^3}{kgH} \cdots (\text{eq. } 4.7)$$

Mechanical mixing height z_{im}, which is the mixing height under stable conditions can be simply computed as:

$$z_{im} = 2300u_*^{3/2} \cdots (\text{eq. } 4.8)$$

4.2.5. Wind Direction Adjustment

For XOQDOQ, wind speed and direction measured at one level (release height = 58 m) are used as input. However, for AERMOD, wind speed and direction at multiple levels (in this case, 10 and 58 m) can be inputted and are interpolated between the reference heights.

To effectively compare the modeling results with XOQDOQ, wind directions for AERMOD were pre-processed into sixteen directions. Removing directional variations would lead to overprediction in AERMOD, which is inherent in XOQDOQ.

4.3. Terrain Data Preprocessing

Terrain data also needs preprocessing procedure. Hill height scale h_c along with terrain elevation at the receptor location are specified in the source pathway of AERMOD input.

Figure 4.4 describes the method AERMOD uses to consider the effect of terrain elevation. The dispersion calculation was divided into two extreme plume states: (1) horizontal plume and (2) terrain-responding plume.

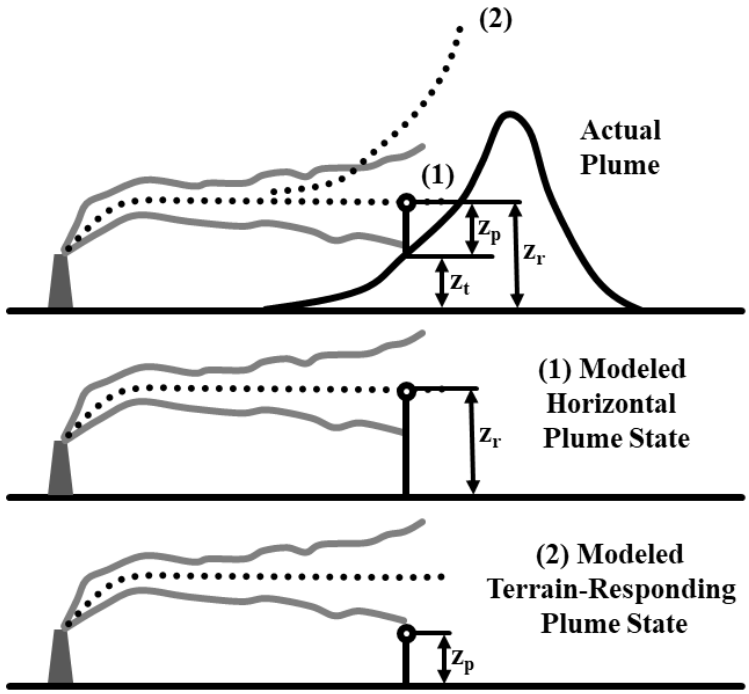

Figure 4.4. Effect of terrain elevation in AERMOD
(modified from Cimorelli et al., 2005)

For very stable atmospheric conditions, the plume centerline tends to remain horizontal regardless of the terrain. On the contrary, for very unstable conditions, the plume tends to follow the terrain. As the plume centerline is elevated responding to the terrain elevation, it can be assumed that the terrain effect is neglected. The actual plume state can be modeled as the fractional sum of the two cases as:

$$C_T\{x_r, y_r, z_r\} = fC_{C,S}\{x_r, y_r, z_r\} + (1-f)C_{C,S}\{x_r, y_r, z_p\} \cdots \text{(eq. 4.9)}$$

where $C_T\{x_r, y_r, z_r\}$ is the total concentration, $C_{C,S}\{x_r, y_r, z_r\}$ is the contribution from the horizontal plume, $C_{C,S}\{x_r, y_r, z_p\}$ is the contribution from the terrain-responding plume, f is the weighting factor. The subscripts C and S indicates that both convective and stable conditions are considered (Cimorelli et al., 2005).

The weighting factor f depends on the amount of mass residing in each state. This mass partitioning is based on the relationship

between the critical dividing streamline height H_c and the vertical concentration distribution at a receptor. The fraction of the plume mass below H_c is computed as:

$$\varphi_p = \frac{\int_0^{H_c} C_S\{x_r, y_r, z_r\}dz}{\int_0^{\infty} C_S\{x_r, y_r, z_r\}dz}$$

For convective conditions, $H_c = 0$, and $\varphi_p = 0$. The weighting factor is given by $f = 0.5(1 - \varphi_p)$. It can be inferred from the above equation that for the plume heights entirely below H_c, the concentration is determined by the horizontal plume only. On the other hand, when the plume is entirely above the H_c or when the boundary layer is convective, $\varphi_p = 0$ and $f = 0.5$.

H_c can be calculated using a receptor−specific hill height h_c that represents the height of a single isolated hill, which would act to affect the flow at the receptor in a manner similar to the real terrain (Perry, 1992).

$$\frac{1}{2}u^2(H_c) = \int_{H_c}^{h_c} N^2(z)(h_c - z)dz$$

where $u(H_c)$ is the wind speed at the height H_c, $N = [(g/\theta)\partial\theta/\partial z]^{1/2}$ is the Brunt−Vaisala frequency, θ is the potential temperature, and h_c is the hill height scale. The above equation can be solved for H_c iteratively, by using the temperature gradient and wind speed at the hilltop (h_c) as initial value and then moving down to the height where the equation is satisfied.

As the solution for H_c and weighting factor determination is included in AERMOD, only terrain elevation and hill height scale are needed. The hill height scale can be estimated with following procedure of EPA (2018):

1. For each receptor, use the receptor elevation height as the initial controlling hill height scale.
2. Search for the controlling hill height in the DEM file in which

the receptor is located. This is done by calculating the slope between the receptor and each node based on the respective distance and elevation difference.

3. If the slope is 10% or greater, the DEM node elevation is compared to the controlling hill height scale. If higher, the controlling hill height scale is replaced by the node elevation value as the new controlling hill height scale.
4. All the nodes within the DEM file that are within the domain are searched.

For this study, the grid data with resolution of 1-arc second were used and sizes larger than 10×10 km^2 were considered as a single domain. When dealing with larger or finer terrain data, the calculation process for hill height scale can be time-consuming. One may enhance the computing efficiency by restricting the domain size for each receptor.

4.4. Results and Discussions

Meteorological data were generated as described in the above section. The data are divided into surface and profile files and used as external input files for the AERMOD modeling. The elevation and hill height scale for each receptor is directly included in the AERMOD input file.

AERMOD requires three land-use parameters, which are site-specific: albedo, Bowen ratio, and surface roughness length. While albedo and Bowen ratios are only used during the preprocessing stage, surface roughness is also a parameter in the dispersion modeling. The sensitivities of maximum concentration predicted by AERMOD to these land use parameters are elaborated in the following section.

For model options, the regulatory default option (DFAULT), which can override other non-default options in the input file, was selected. Stack parameters in AERMOD include stack diameter, height, plume exit velocity, and exit temperature. Stack diameter, height, and exit velocity were set the same as in XOQDOQ. The exit temperature was set to 425 K.

4.4.1. Comparison with XOQDOQ

Tables 4.2-4.3 and Figures 4.5-4.6 are the results from AERMOD dispersion modeling. Without terrain elevation, the percentage difference of AERMOD to XOQDOQ dispersion factors was between -54 and 26%. For Wolsong site, the maximum dispersion factors of AERMOD were greater than those of XOQDOQ, except for 2016. In Kori, XOQDOQ overpredicted the dispersion factors compared to AERMOD results. The maximum locations for AERMOD were formed around 460-480 m (Wolsong) and 610-650 m (Kori), both in NNE directions. XOQDOQ resulted in the maximum locations in various directions with shorter distances (330-340 m), but under certain meteorological conditions, the maximum location was formed relatively far from the source.

The results from AERMOD with terrain elevation were compared with the XOQDOQ results assuming horizontal or adjusted plume heights. Compared to horizontal plume heights, the AERMOD results showed a percentage difference between −92 and −81%. The maximum locations for AERMOD were formed in farther distances and different directions (2017−2018, Wolsong). Comparing the AERMOD results with the adjusted plume heights, the percentage difference was decreased to between −51 and −14%, nearly in the factor of 2 range. Also, the maximum locations became coherent in the two models.

Table 4.2. Maximum X/Q values and locations (without terrain)

Year	Wolsong		Kori	
	Maximum (s/m^3)	Location	Maximum (s/m^3)	Location
2016	1.30E−07	480 m, NNE	1.24E−07	630 m, NNE
2017	1.35E−07	480 m, NNE	1.32E−07	610 m, NNE
2018	1.31E−07	460 m, NNE	1.21E−07	650 m, NNE

Table 4.3. Maximum X/Q values and locations (with terrain)

Year	Wolsong		Kori	
	Maximum (s/m^3)	Location	Maximum (s/m^3)	Location
2016	4.36E−07	1050 m, WNW	3.84E−07	870 m, NNE
2017	2.12E−07	1260 m, N	3.68E−07	870 m, NNE
2018	2.43E−07	2680 m, SW	4.54E−07	870 m, NNE

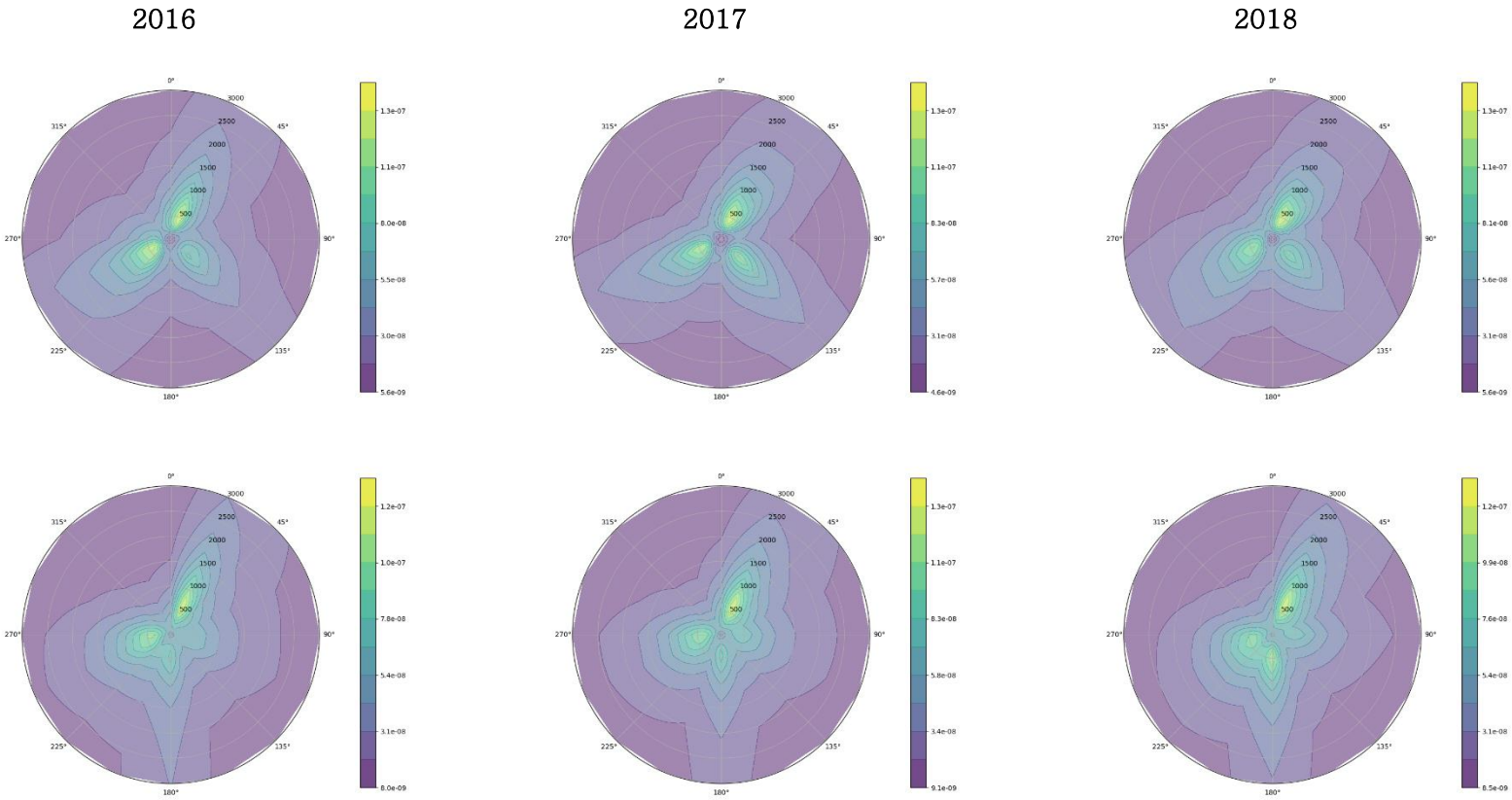

Figure 4.5. Dispersion factors in 2016−2018 (without terrain, AERMOD)
Top: Wolsong, Bottom: Kori

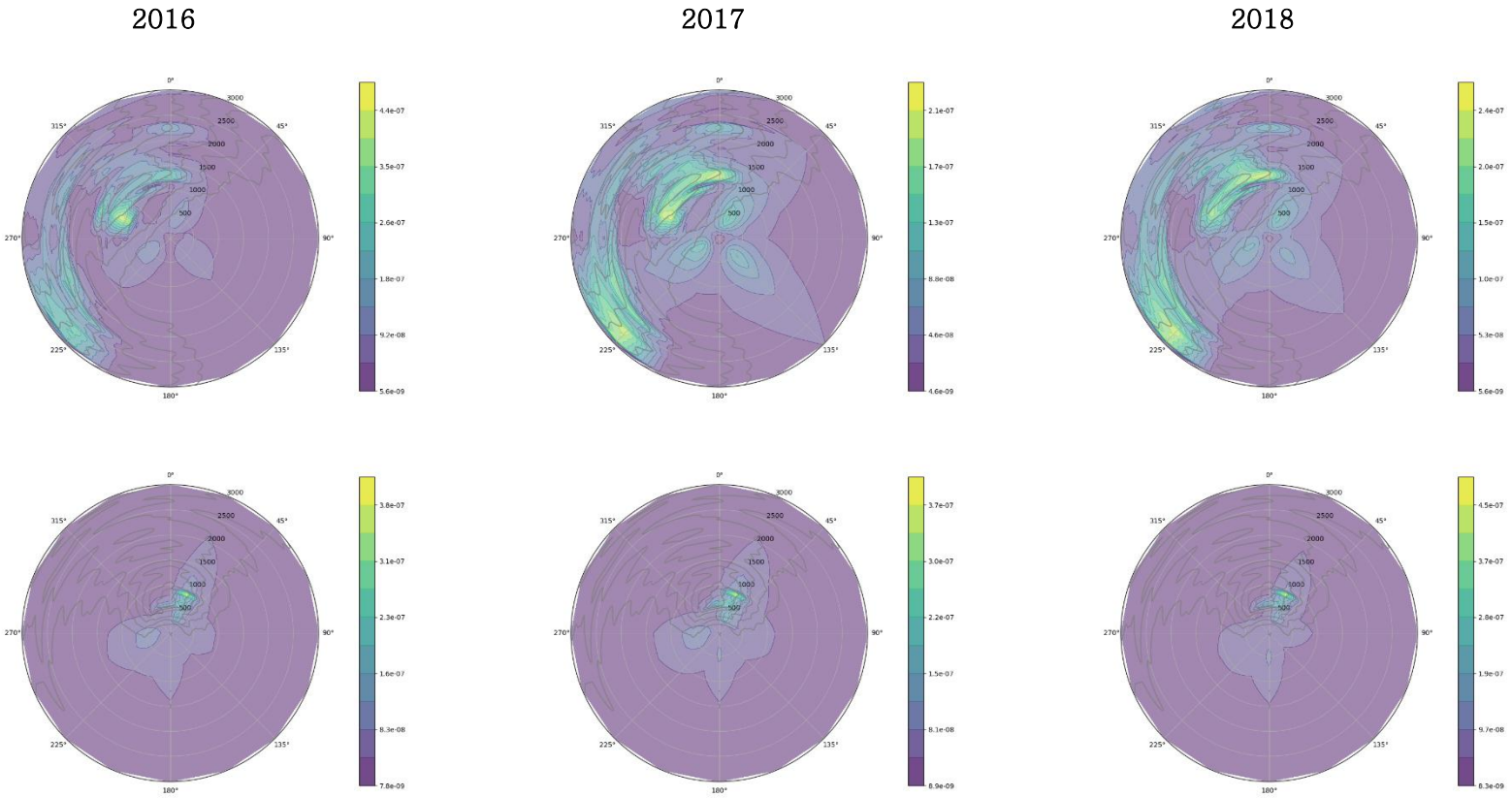

Figure 4.6. Dispersion factors in 2016−2018 (with terrain, AERMOD)
Top: Wolsong, Bottom: Kori

4.4.2. Uncertainties due to Land Use Parameters

Land use parameters inputted to AERMOD are albedo, Bowen ratio, and surface roughness length. As these parameters affect the model output, they should be representative of the site characteristics. Gibson et al. (2005) reviewed the ranges of the parameters for specific terrain characteristics.

Grosch and Lee (1999) analyzed the sensitivity of AERMOD to the selection of land use parameters. Based on the ranges of land use parameter values suggested by the EPA, they categorized the cases as in Table 4.4. The below scenarios were applied to the AERMOD calculation. The receptor location for each scenario was set the same as the maximum location of the base case.

Table 4.4. Land use parameters for sensitivity analysis (Grosch and Lee, 1999)

Scenario	Albedo	Bowen ratio	Roughness length
Base case	0.2	1.0	0.1
Low albedo	0.1	1.0	0.1
High albedo	0.45	1.0	0.1
Low Bowen ratio	0.2	0.1	0.1
High Bowen ratio	0.2	10.0	0.1
Low roughness length	0.2	1.0	0.0001
High roughness length	0.2	1.0	1.3

The cases were analyzed for Wolsong and Kori in 2016. Figures 4.7 and 4.8 show the maximum dispersion factor for the base case and its sensitivities due to variations in land use parameters. It should be noted that the predicted concentrations for each parameter showed opposite sensitivities, depending on whether terrain elevation was considered or not. Long et al. (2004) also analyzed the sensitivity of AERMOD to input parameters and confirmed the opposite response for ground and elevated sources.

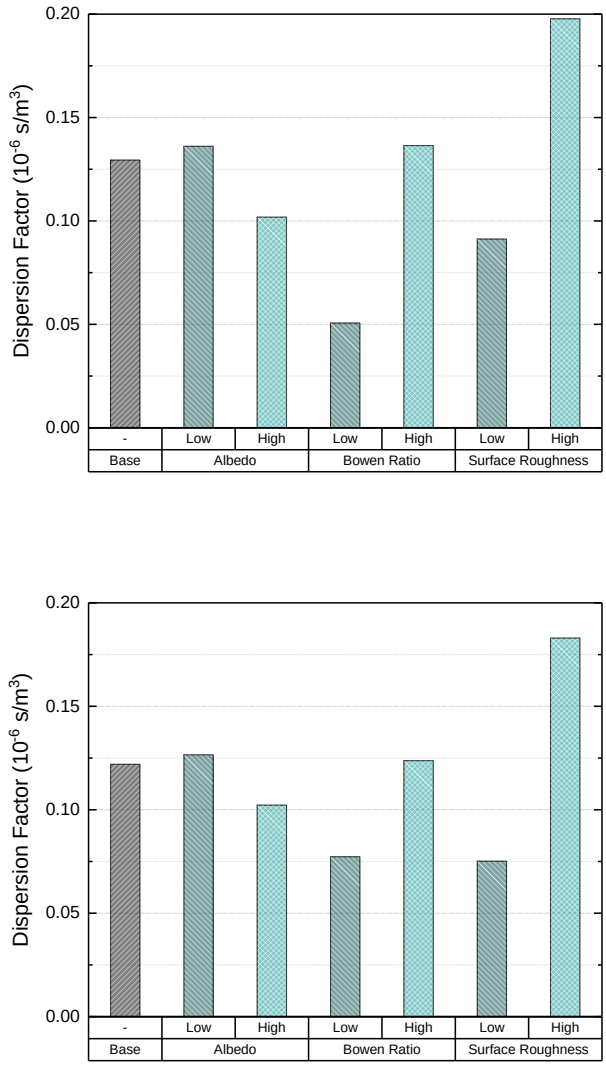

Figure 4.7. Sensitivities of maximum dispersion factor value due to land use parameters without terrain data (Top: Wolsong, Bottom: Kori)

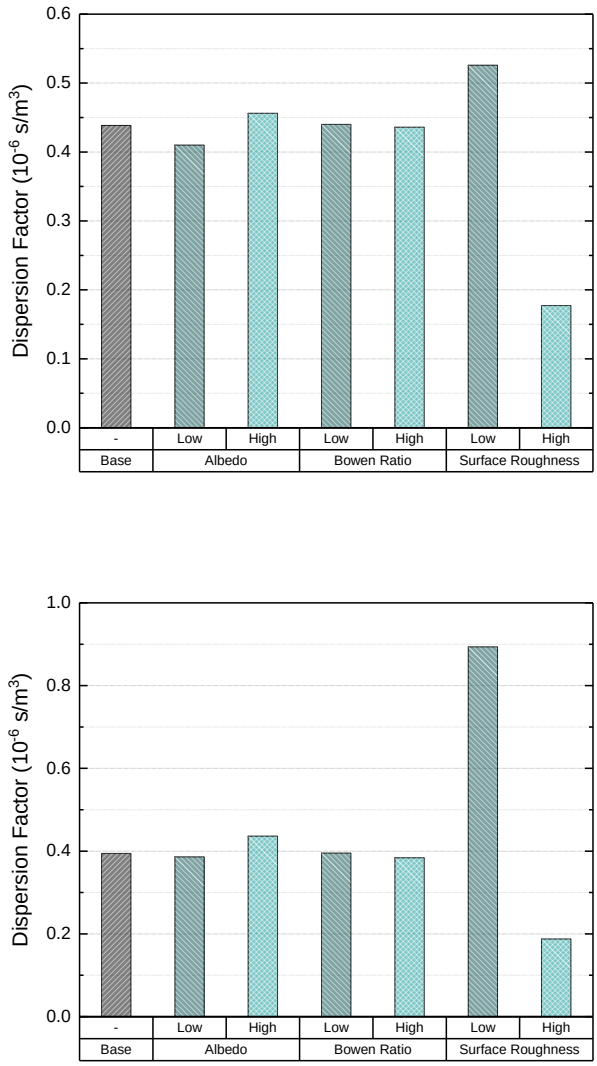

Figure 4.8. Sensitivities of maximum dispersion factor value due to land use parameters with terrain data (Top: Wolsong, Bottom: Kori)

The increase in albedo led to a decrease in net radiation and thus the decrease in sensible heat flux (see Section 4.2.1). On the contrary, the increase in Bowen ratio increased sensible heat flux. As sensible heat flux is proportional to the turbulent velocity scale (see Equation 4.4), the vertical turbulence can be enhanced for low albedo and high Bowen ratio scenarios. The increase in surface roughness length can lead to an increase in u_*, and thus an increase in vertical turbulence (Barnes et al., 2014).

Without terrain elevation, the increase in vertical turbulence under elevated release results in an increase in predicted concentration at the ground surface. Thus, the concentrations were increased for low albedo, high Bowen ratio, and high surface roughness length scenarios.

When terrain elevation is considered, the corresponding receptor heights are 106 m (Wolsong) and 85 m (Kori). In these cases, the increase in vertical turbulence leads to a decrease in predicted concentrations since the receptor heights are close to the plume centerlines. Thus, the changes in land use parameters showed opposite sensitivities when compared to the no terrain cases.

4.5. Summary and Conclusion

When terrain elevation was not factored in, the discrepancies between the XOQDOQ and AERMOD results were mainly due to the different approaches in turbulence modeling. Excluding the terrain elevation, dispersion factors from the models were approximately in the factor of 2 range.

Including terrain elevation, however, XOQDOQ increased by 8.3 to 27.3 times, while AERMOD only increased by 1.6 to 3.8 times compared to the base scenario. The overprediction in the original XOQDOQ compared to AERMOD was due to the horizontal plume state assumption. Applying the adjusted plume height approach, the discrepancy with the AERMOD results was mitigated, while the dispersion factors were maintained as more conservative. The locations of the maximum dispersion also showed better agreement with AERMOD when the adjusted model was used.

As the AERMOD modeling system is recommended by EPA as a regulatory dispersion model, the regulatory body can also consider employing it as a regulatory model for nuclear installations. But it should be noted that the model has far more meteorological inputs, derived parameters, and land use inputs that require preprocessing.

Chapter 5. Model Application to Air Pollutant

5.1. Case Descriptions

For atmospheric dispersion models, validation against measured values has been an important issue. Although most models for regulatory purposes already passed the validation process at the stage of development, it is still important to verify the model under specific meteorological and terrain conditions.

As mentioned in Chapter 1, a tracer experiment was conducted to validate the current regulatory dispersion model for domestic nuclear power plants (Jeong et al.,2014b; 김정미 외, 2017, 2018). As the Pasquill stability scheme is mainly based on the Prairie Grass experiment, it has been repeatedly pointed out that the model should not be applied to complex terrain conditions. However, since most nuclear power plants in Korea have been using the methods based on the Pasquill stability, it was essential to confirm that the current model guarantees a sufficient safety margin.

For regulatory dispersion modeling, a collection of field datasets such as the model validation kit (Olesen and Chang, 2010) can be applied as a reference for model performance evaluation. However, since most field experiments applicable for validation are short-term dispersion experiments that took place for few hours to several days, the datasets to validate long-term average concentrations are still limited in number.

Crawford et al. (2020) suggested using air pollution monitoring data combined with meteorological and emission data to generate a long-term dataset. They applied the obtained datasets to evaluate the predictability and evolutionary improvement of the model.

Several studies also compared the predicted concentrations from modeling with the observed concentrations from air pollution monitors for long-term analysis. For example, Gibson et al. (2013)

applied AERMOD to evaluate the dispersion of particulate matter ($PM_{2.5}$), NO_x, and SO_2 from point and primary line sources in Nova Scotia, Canada. The AERMOD model evaluation showed a good agreement between the modeled and observed SO_2 concentrations for the annual and monthly averages.

Lee et al. (2014) also evaluated the concentrations and source contribution of PM_{10} and SO_2 emitted from the industrial complexes in Ulsan, Korea. They also found that values predicted using the dispersion model were below the observed values due to the background concentrations not included (i.e., regional baseline pollutant levels, uncertain emission sources, air pollutants transported from the sources outside the study area).

5.1.1. Target Areas and Emission Data

The long-term datasets of SO_2 dispersion were generated from Pohang, Donghae, and Boryeong, all of which are in the coastal region. The major facilities with continuous SO_2 emission were set as a point source in Pohang and Donghae. In Boryeong, the dispersion originating from two point-sources was modeled. Air pollution monitors located within a 20 km radius from the source point were considered receptors.

Emission data can be retrieved from the TMS (Tele-Monitoring System). For each stack in major emitters, a monitoring device is attached to record the amount of gaseous effluents in real-time. The measured TMS data are confirmed and disclosed for the total amount emitted per year from each emitter.

As in previous studies, severe uncertainties in the input parameters are presumed to be the major source of error (Tartakovsky et al., 2013). The uncertainties include source parameters such as the location, diameter and height of the stack, stack exit velocity, and temperature.

5.1.2. SO_2 Background Subtraction

According to the National Research Council (1975), about 98% of the SO_x emitted from anthropogenic sources is SO_2. The remaining fraction is typically composed of sulfur trioxide (SO_3) and its derivatives. The primary natural sources of SO_2 are volcanoes and wildfires, but in industrialized regions, the anthropogenic emissions of SO_2 are much greater than the natural sources.

According to EPA (2009) review, most man-made SO_2 emissions are originated from point sources such as fuel combustion and other industrial facilities. SO_2 has a spatial variability relatively higher than other pollutants such as PM and ozone (O_3) (EPA, 2017). This is partly due to the point source nature of SO_2. Another contributing factor is the dispersion and oxidation of SO_2 in the atmosphere that decrease SO_2 concentrations with increasing distance from the source. Lee (2018) performed a backward trajectory analysis on the SO_2 levels in Ulsan, Korea. Based on CALPUFF results, it was suggested that the most crucial factor for the SO_2 level was point sources in the local industrial area.

The lifetime of SO_2 emitted from a point source can vary depending on the meteorological conditions. In dispersion modeling, the decrease in SO_2 concentration due to chemical reactions can be parameterized. For example, when the “urban” option is selected in the AERMOD input file, the 4-hour decay function for SO_2 is automatically employed. As the “rural” option was selected for this research, the decay function was not in effect.

There are several methods to subtract the background SO_2 concentrations from the observed concentrations. First, measured background values can be subtracted. For example, Ju et al. (2018) measured the long-term trend of major air pollutants over regions in Korea using observation data and modeling. However, these average values were not intended as background concentrations and the measurements for the years of interest in this study are not available. Several monitoring stations are dedicated to measuring national

backgrounds, but they are in distant locations from the regions of interest.

Instead, the method suggested by Dresser and Huizer (2011) was adopted. The lowest hourly concentration reported at any monitor in the nearby region was set as the hourly background concentration.

5.1.3. Statistical Analysis

Since the Air Quality Directive (AQD 2008), the European Commission has strengthened the regulation regarding ambient air quality. Many air quality models for the assessment and forecast of pollutant concentrations are being developed. Therefore, the evaluation of their performance has become an important issue. Thunis et al. (2012) proposed the Root Mean Square Error redefined based on the observation Uncertainty ($RMSE_U$) as a key index for the model performance criteria.

When the observed concentration is O_i and the predicted concentration is M_i, the root mean square error can be calculated as:

$$RMSE = \sqrt{\frac{1}{N}\sum(O_i - M_i)^2}$$

where the subscript i indicates the time step, and N is the total number of time intervals. Thunis et al. (2012) suggested normalizing the above index with the observation uncertainty. Thus, the performance of the model results compared to the observation uncertainty can be evaluated as:

$$RMSE_U = \frac{\sqrt{\frac{1}{N}\sum(O_i - M_i)^2}}{2U}$$

where the observation uncertainty U is defined as:

$$U = \sqrt{\frac{1}{N}\sum(U_r(O_i) \times O_i)^2}$$

where $U_r(O_i)$ is the relative uncertainty when the observed concentration is O_i. If the relative uncertainty is not available, it can be assumed to be independent of the concentration. For instance, $U_r = 0.15$, as the Data Quality Objective defined in AQD 2008 is 15% for SO_2.

The range of $RMSE_U$ is categorized as below. By normalizing the $RMSE$ with U, model results are required to have a similar margin of tolerance as observations (Thunis et al., 2012):

1. $RMSE_U \leq 0.5$; the difference between observation and prediction is less than the observation uncertainty.

2. $0.5 < RMSE_U \leq 1.0$; the difference between observation and prediction is greater than the observation uncertainty. Still, the model result might be closer to the "true value" than the observation.

3. $RMSE_U > 1.0$; the prediction is further away from the "true value" than the observation.

Other statistical indicators are fractional bias (FB), normalized mean square error ($NMSE$) and factor of 2 ($FAC2$).

Fractional bias measures the systemic bias of the model, and the negative value indicates the overprediction. Normalized mean square error measures the random error of the model in terms of its scatter from the observed value. Each index is defined as:

$$FB = 2((\bar{O} - \bar{M})/(\bar{O} + \bar{M}))$$

$$NMSE = \overline{(O - M)^2}/(\bar{O} \cdot \bar{M})$$

The factor of 2 is the fraction of data which the ratio of observed and predicted concentration is in the factor of 2:

$$0.5 \leq M/O \leq 2.0$$

$RMSE_U = FB = NMSE = 0$, and $FAC2 = 1$ indicate a perfect model. Hanna and Chang (2012) suggested acceptance criteria for each index as:

For Rural region:

- $|FB| \leq 0.30$; the relative mean bias less than about 0.3
- $NMSE \leq 3$; the random scatter is ≤ 1.7 times the mean
- $FAC2 \geq 0.50$; the fraction of M within a factor of two of O exceeds 0.50

For urban region:

- $|FB| \leq 0.67$; the relative mean bias less than a factor of ~2
- $NMSE \leq 6$; the random scatter is ≤ 2.4 times the mean
- $FAC2 \geq 0.30$; the fraction of M within a factor of two of O exceeds 0.30

The predicted and observed data were compared using 1-hour quantile-quantile plots. Quantile-quantile plots consist of observed data on the x-axis and predicted data on the y-axis, both of which are ranked in numeric order. The purpose of the plot is to evaluate the distribution of the long-term data, especially when it is not necessary to require temporal concurrence (Chang and Hanna, 2004).

As most regulatory models emphasize the high concentrations, the evaluations with the quantile-quantile plot can be focused more on the ability of a model to reproduce the upper end of the concentration distribution (Chang and Hanna, 2004; Dresser and Huizer, 2011). The calculation for model statistics was confined to the concentrations over 13.1 $\mu g/m^3$ (~0.005 ppm) for both observed and predicted concentrations.

5.2. Pohang Case

Pohang is in Gyeongsangbuk-do, which is a southeast region of the Korean peninsula. Since there is an ASOS and a rawinsonde station, the surface and upper air meteorological measurement data from Pohang has been used for the AERMOD modeling in Wolsong and Kori. Here, the focus was on the dispersion of SO_2 from a point source to the nearby air pollution monitors.

5.2.1. Source Term

Table 5.1 summarizes the major facilities located in the Gyeongsangbuk-do region that are registered in the TMS. Among the facilities where continuous SO_2 measurements are made, the P steel mill accounts for nearly 90% of the total SO_2 emission in the region.

It is not easy to separate the total emission into individual stacks because the confirmed TMS output shows the 1-year total amount of effluents emitted from the whole facility. Thus, the emission was simplified as a single point source from a stack of 100 m height.

Table 5.1. Major facilities near Pohang registered in TMS (2019)

(Unit: kg/year)

Facility	Total	PM	SO_x	NO_x
P-Steel	17,539,924	265,560	**4,533,635**	12,739,643
G-Power	1,004,759	9,116	210,165	785,478
G-Energy	488,853	4,506	244,184	240,163
Y-Refinery	102,510	1,667	42,967	57,876
B-Zinc	86,036	1,841	58,842	25,353

5.2.2. Meteorological Data and Receptors

Meteorological data were obtained from the ASOS-138 station. The missing rate of the minute-by-minute wind speeds and directions were less than 0.1% during 2019, and the missing points were interpolated.

Figure 5.1 is the location of the point source and the receptors. The location of the ASOS-138 station is close to the receptor R4. There are five receptors in approximately a 7 km radius from the source point. The range of annual average concentrations was between 9.49 and 11.49 $\mu g/m^3$, where R1 was the highest and R5 was the lowest. The minimum hourly concentration among the five receptors was subtracted as background. The range of net concentrations was between 3.95 and 6.46 $\mu g/m^3$.

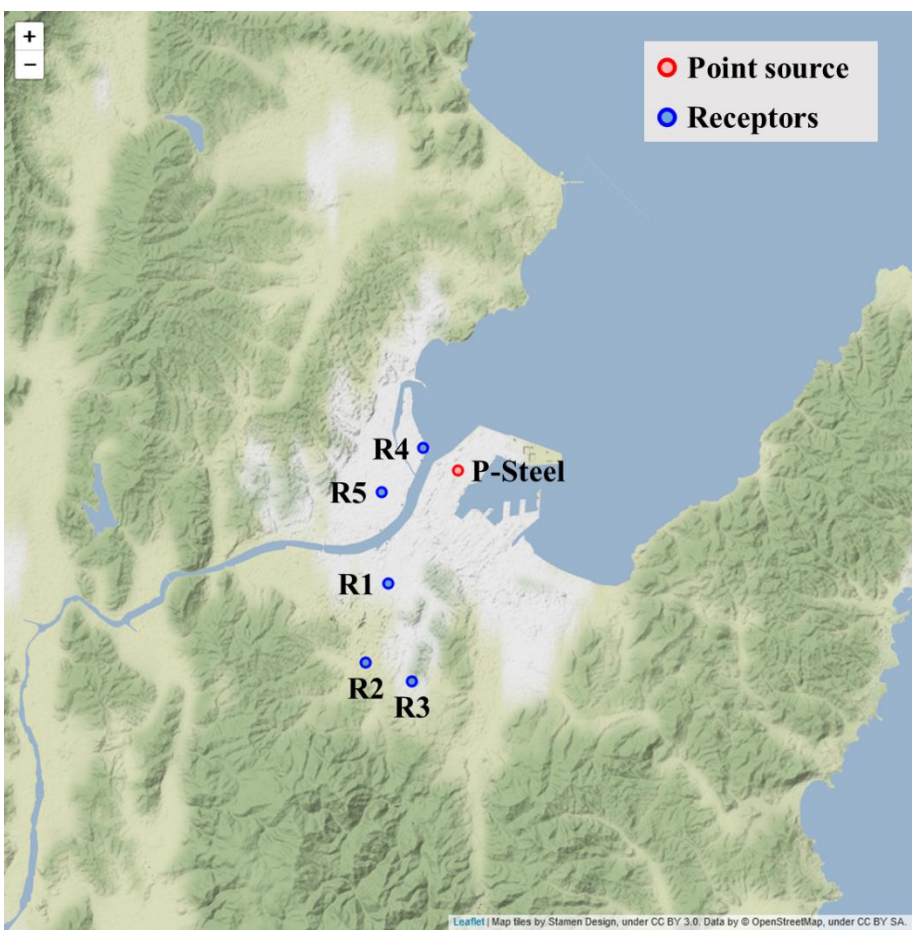

Figure 5.1. Point source and receptor locations in Pohang

Figure 5.2 is the distribution of wind speeds and directions measured in the ASOS−138 station. The prevailing winds throughout the year corresponded to the sea breeze in the WSW and WS directions. The land breeze in the NE and NNE directions formed the next most considerable fraction.

Considering the annual distribution of wind directions, the receptor locations can be grouped into two. The first group consists of the receptors R1, R2, and R3, in SSW directions. The second group includes the receptors R4 and R5, which are in WNW and WSW directions. The receptors in the first group were under the influence of frequent wind direction (NNE), while the receptors in the latter group were affected by relatively rare wind directions of ESE and ENE.

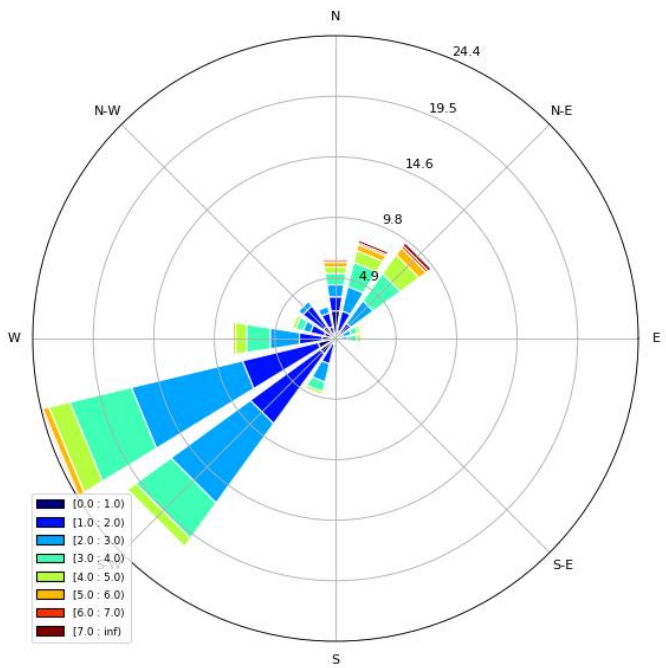

Figure 5.2. Distribution of wind speeds and directions in Pohang, 2019

5.2.3. Results and Discussions

Figures 5.3 and 5.4 are the quantile-quantile plots of 1-hour average concentrations for five receptors in Pohang. Tables 5.2 and 5.3 summarize model statistics for all the five receptors and the receptors in the prevailing wind direction (R1, R2, and R3). The ranges of statistical values and their averages and standard deviations are indicated. The model performance in terms of statistics varied between XOQDOQ and AERMOD and the terrain elevation processing methods.

When terrain elevation was not considered, both models tended to underpredict the observed concentration. XOQDOQ, on average, performed better than AERMOD. When the receptors R1, R2, and R3, were considered only, the performance of XOQDOQ was far more enhanced.

As the concentrations increased with the terrain elevation, the performance of XOQDOQ in the receptors R1 and R2 was enhanced. The difference between horizontal and adjusted plume assumptions was minimal since the terrain heights in the two receptors were not significant. In AERMOD, the difference due to terrain elevation was even more negligible, and the model statistics were slightly enhanced with terrain elevation. For the receptor R3, on the other hand, XOQDOQ resulted in overprediction for both assumptions due to elevated receptor height.

Both models displayed either overprediction (R4) or underprediction (R5) in the receptors with less frequent wind directions, leading to poor performance statistics.

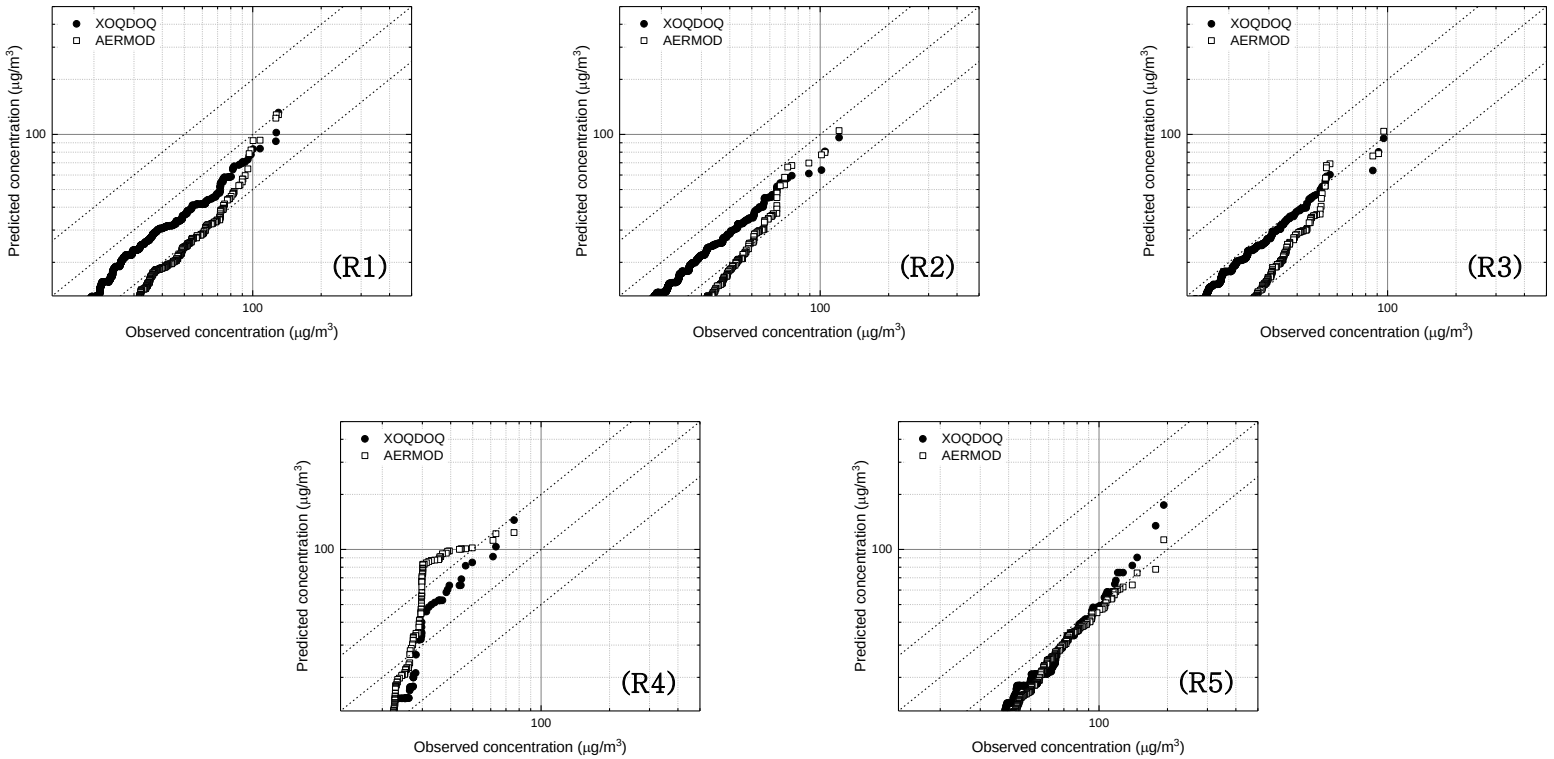

Figure 5.3. Quantile−Quantile plot based on observed and predicted data for Pohang, 2019 (no terrain)

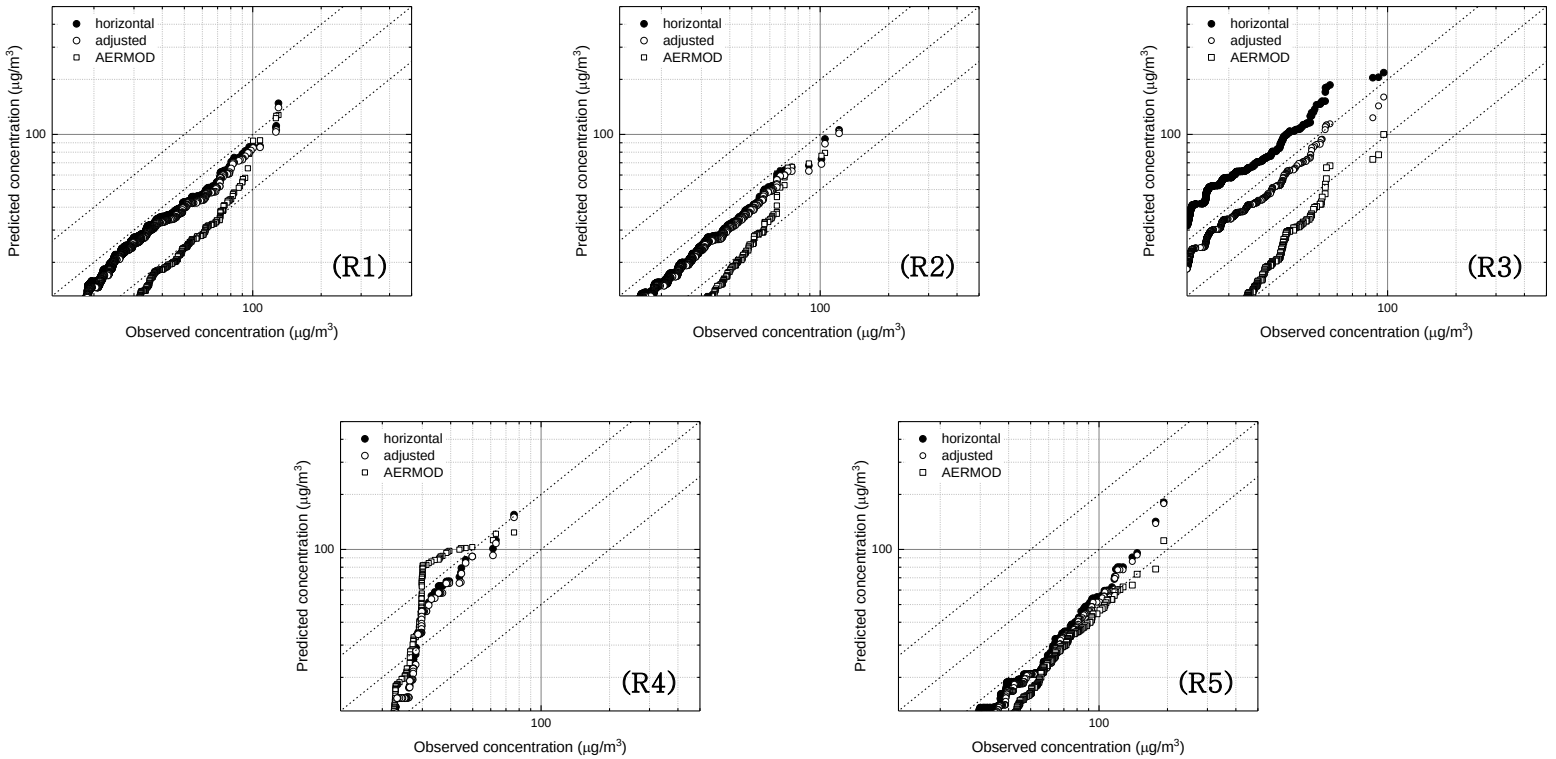

Figure 5.4. Quantile-Quantile plot based on observed and predicted data for Pohang, 2019 (with terrain)

Table 5.2. Summary of Statistical Analysis – Pohang Case (R1−R5)

Index	XOQDOQ			AERMOD	
	No terrain	Horizontal plume	Adjusted plume	No terrain	With terrain
$\mathbf{0 \le RMSE_U}$	0.23−1.02 (0.59, 0.31)	0.33−2.01 (0.89, 0.69)	0.38−1.03 (0.65, 0.27)	0.71−1.10 (0.86, 0.14)	0.66−1.10 (0.85, 0.16)
$\mathbf{-2 \le \lvert FB \rvert \le 2}$	0.20−1.09 (0.64, 0.39)	0.31−1.01 (0.68, 0.34)	0.31−1.01 (0.61, 0.34)	0.60−1.12 (0.96, 0.23)	0.62−1.13 (0.95, 0.24)
$\mathbf{0 \le NMSE}$	0.05−2.43 (0.94, 1.07)	0.12−2.22 (0.98, 0.88)	0.17−2.22 (0.82, 0.91)	0.95−2.16 (1.71, 0.49)	0.75−2.25 (1.72, 0.60)
$\mathbf{0 < FAC2 < 1}$	0.02−1.00 (0.58, 0.47)	0.00−1.00 (0.42, 0.49)	0.05−1.00 (0.61, 0.47)	0.00−0.14 (0.07, 0.07)	0.00−0.23 (0.08, 0.10)

Table 5.3. Summary of Statistical Analysis – Pohang Case (R1−R3)

Index	XOQDOQ			AERMOD	
	No terrain	Horizontal plume	Adjusted plume	No terrain	With terrain
$\mathbf{0 \leq RMSE_U}$	0.23−0.45 (0.37, 0.12)	0.33−2.01 (0.89, 0.97)	0.38−0.73 (0.50, 0.20)	0.71−0.83 (0.79, 0.07)	0.66−0.83 (0.77, 0.10)
$\mathbf{-2 \leq \lvert FB \rvert \leq 2}$	0.20−0.45 (0.22, 0.22)	0.31−0.88 (0.30, 0.36)	0.37−0.42 (0.23, 0.21)	0.87−1.12 (0.62, 0.57)	0.79−1.13 (0.61, 0.57)
$\mathbf{0 \leq NMSE}$	0.05−0.27 (0.18, 0.12)	0.12−1.17 (0.47, 0.60)	0.17−0.26 (0.20, 0.05)	0.95−2.04 (1.61, 0.58)	0.75−2.10 (1.59, 0.73)
$\mathbf{0 < FAC2 < 1}$	0.79−1.00 (0.92, 0.11)	0.00−1.00 (0.63, 0.55)	0.85−1.00 (0.95, 0.09)	0.02−0.14 (0.07, 0.06)	0.02−0.23 (0.09, 0.12)

5.3. Donghae Case

5.3.1. Source Term

Table 5.4 summarizes the major facilities located in the Gangwon-do region that are registered in the TMS. Among the facilities where continuous SO_2 measurements are made, the D-power plant accounts for more than 50% of the total SO_2 emission in the region.

D-Power includes two coal-fired power plants with a capacity of 200 MW each. As the Enforcement Rule of the Clean Air Conservation Act requires the stack heights of the coal-fired plants to be at least 100 m, the Donghae case was modeled as a single source with a stack height of 100 m.

Table 5.4. Major facilities near Donghae registered in TMS (2019)

(Unit: kg/year)

Facility	Total	PM	SO_X	NO_X
D-Power	2,561,170	27,713	**1,892,562**	632,754
G-Power	2,177,137	35,313	672,070	1,469,754
S-Power	2,708,762	133,415	658,471	1,916,876
Y-Power	480,835	17,522	51,818	411,495

5.3.2. Meteorological Data and Receptors

Meteorological data were obtained from the ASOS-106 station. The missing rate for hourly wind speeds and directions was less than 0.5% during 2019.

Figure 5.5 shows the location of the point source, the receptors, and the ASOS station. There are two receptors in approximately a 5 km radius from the source point. For the background subtraction, four more receptors in the nearby region were used. The hourly minimum among the six monitors was subtracted as a background.

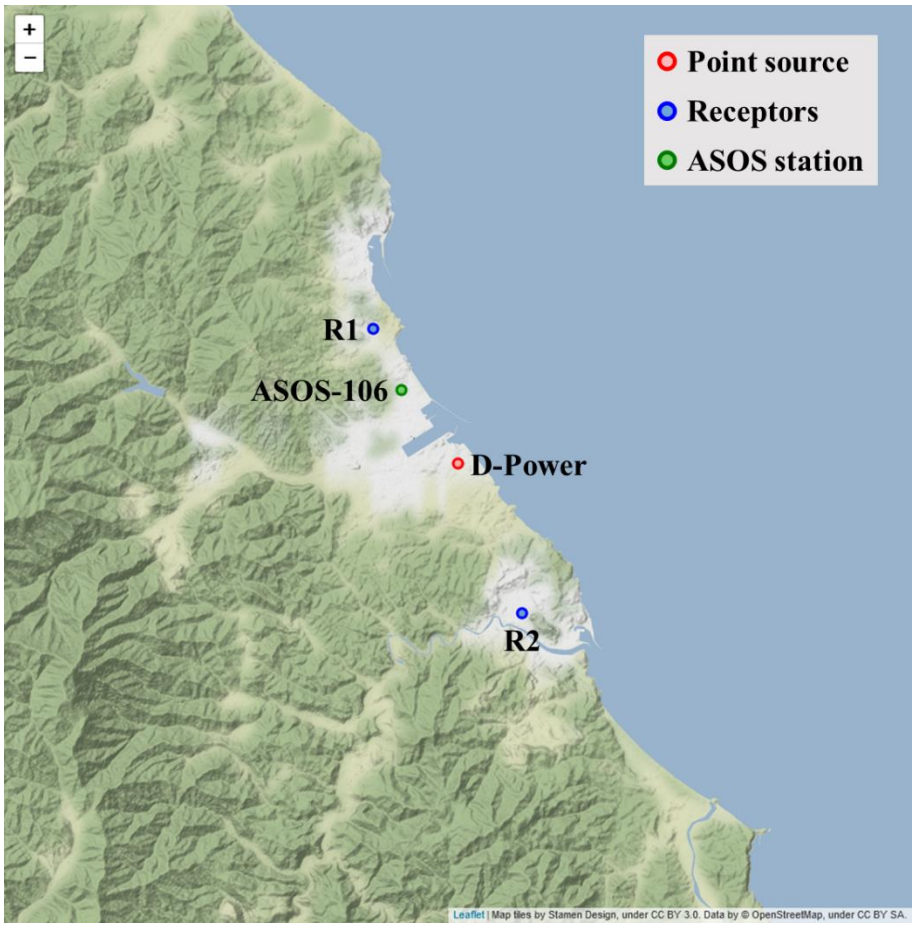

Figure 5.5. Point source and receptor locations in Donghae

Figure 5.6 is the distribution of wind speeds and directions measured in the ASOS-106 station. The prevailing winds throughout the year were in the WSW and WS directions.

The receptor locations are 5100 m to NNW direction (R1) and 5200 m to SSE direction (R2) from the point source. Both receptors were not under the influence of the prevailing winds, but the wind directions toward the receptor R1 were more frequent than the other.

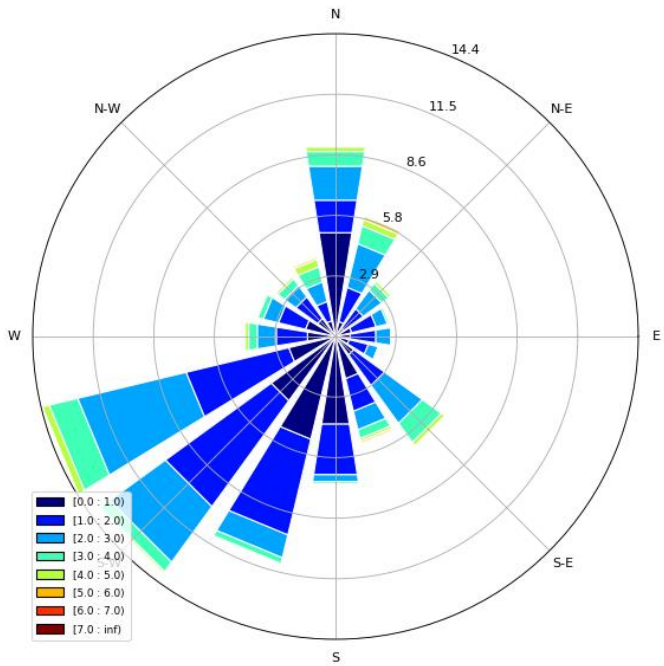

Figure 5.6. Distribution of wind speeds and directions in Donghae, 2019

5.3.3. Results and Discussions

Figures 5.7 and 5.8 are the quantile−quantile plots of 1−hour average concentrations for the receptors in Donghae. Tables 5.5 and 5.6 are the summary of model statistics for the receptors R1 and R2. The model performed well in the receptor R1, while the net concentrations in the receptor R2 were relatively low.

In the receptor R1, without terrain elevation, XOQDOQ tended to fluctuate between overprediction and underprediction. AERMOD, on the other hand, displayed better agreement with the high concentrations.

With the horizontal plume assumptions in R1, the results were shifted toward overprediction. Assuming the adjusted plume heights showed better performance with the decreased $RMSE_U$ and $NMSE$. AERMOD consistently displayed better performance measures with terrain elevation as well.

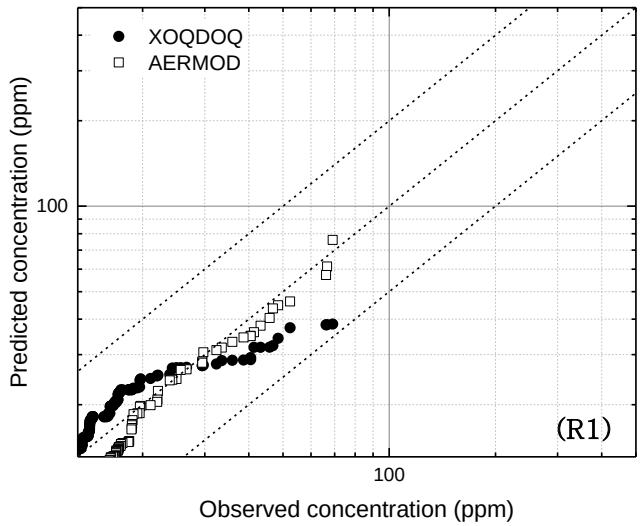

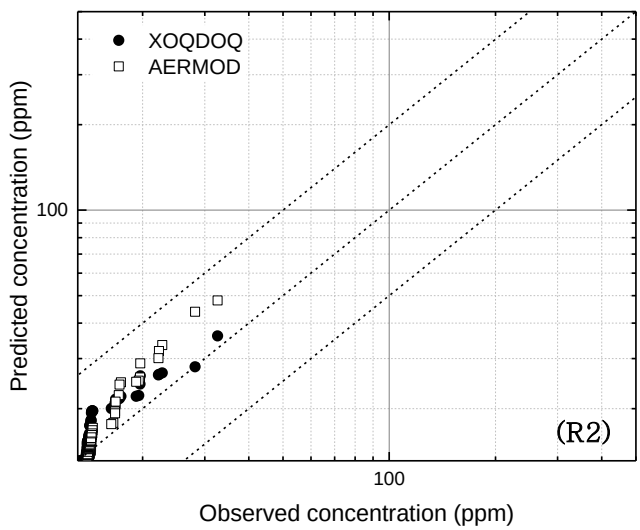

Figure 5.7. Quantile−Quantile plot based on observed and predicted concentrations for Donghae, 2019 (without terrain)

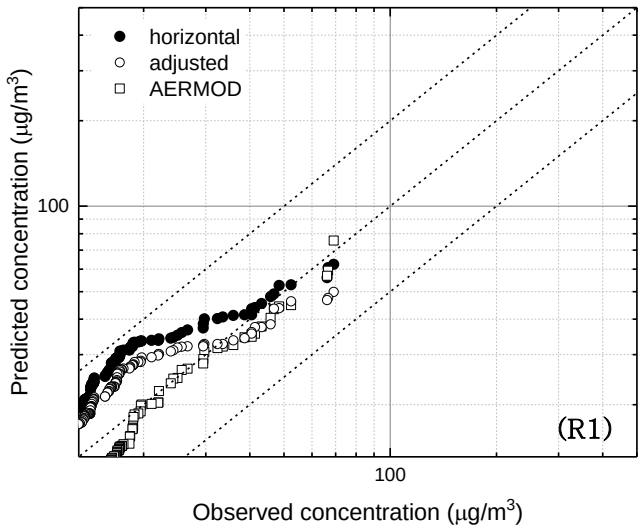

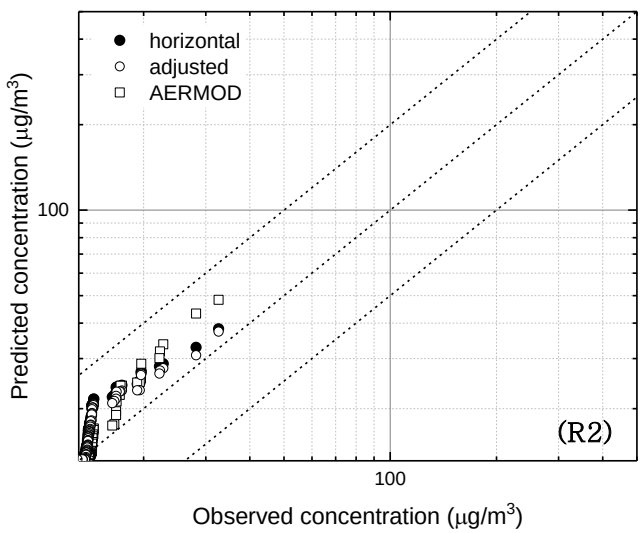

Figure 5.8. Quantile−Quantile plot based on observed and predicted concentrations for Donghae, 2019 (with terrain)

Table 5.5. Summary of statistical analysis – Donghae R1

Index	XOQDOQ			AERMOD	
	No terrain	Horizontal plume	Adjusted plume	No terrain	With terrain
$\mathbf{0 \leq RMSE_U}$	0.40	0.54	0.41	0.19	0.19
$\mathbf{-2 \leq \lvert FB \rvert \leq 2}$	−0.01	−0.35	−0.19	0.15	0.15
$\mathbf{0 \leq NMSE}$	0.13	0.16	0.11	0.03	0.04
$\mathbf{0 < FAC2 < 1}$	1.00	1.00	1.00	1.00	1.00

Table 5.6. Summary of statistical analysis – Donghae R2

Index	XOQDOQ			AERMOD	
	No terrain	Horizontal plume	Adjusted plume	No terrain	With terrain
$\mathbf{0 \leq RMSE_U}$	0.33	0.47	0.40	0.43	0.43
$\mathbf{-2 \leq \lvert FB \rvert \leq 2}$	−0.19	−0.29	−0.24	−0.16	−0.15
$\mathbf{0 \leq NMSE}$	0.06	0.10	0.08	0.10	0.10
$\mathbf{0 < FAC2 < 1}$	1.00	1.00	1.00	1.00	1.00

5.4. Boryeong Case

5.4.1. Source Term

Table 5.7 summarizes the major facilities located in the Chungcheongnam-do region that are registered in the TMS. Even though H-Steel and T-Power are more significant emitters for the SO_2 in the area, they are at least 60 km apart from the receptors R1 and R2 in Boryeong. Thus, the dispersion in the region was modeled as two sources with stack heights of 100 m.

Table 5.7. Major facilities near Boryeong registered in TMS (2019)

(Unit: kg/year)

Facility	Total	PM	SOx	NOx
B-Power1	9,240,059	307,024	**4,428,190**	4,504,845
B-Power2	2,307,475	83,863	**1,503,365**	720,247
H-Steel	17,832,384	480,926	10,310,631	7,040,426
T-Power	10,792,293	344,048	4,821,311	5,626,934
H-Oil	4,242,605	43,580	1,957,819	2,241,123

5.4.2. Meteorological Data and Receptors

Meteorological data were obtained from the ASOS-235 station. The missing rate for hourly wind speeds and directions was less than 0.5% during 2019.

Figure 5.9 shows the locations of the point sources, the receptors, and the ASOS station. There are two receptors in approximately a 10 km radius from the source point. For the background subtraction, three more receptors in the nearby region were used. The hourly minimum among the five monitors was subtracted as a background.

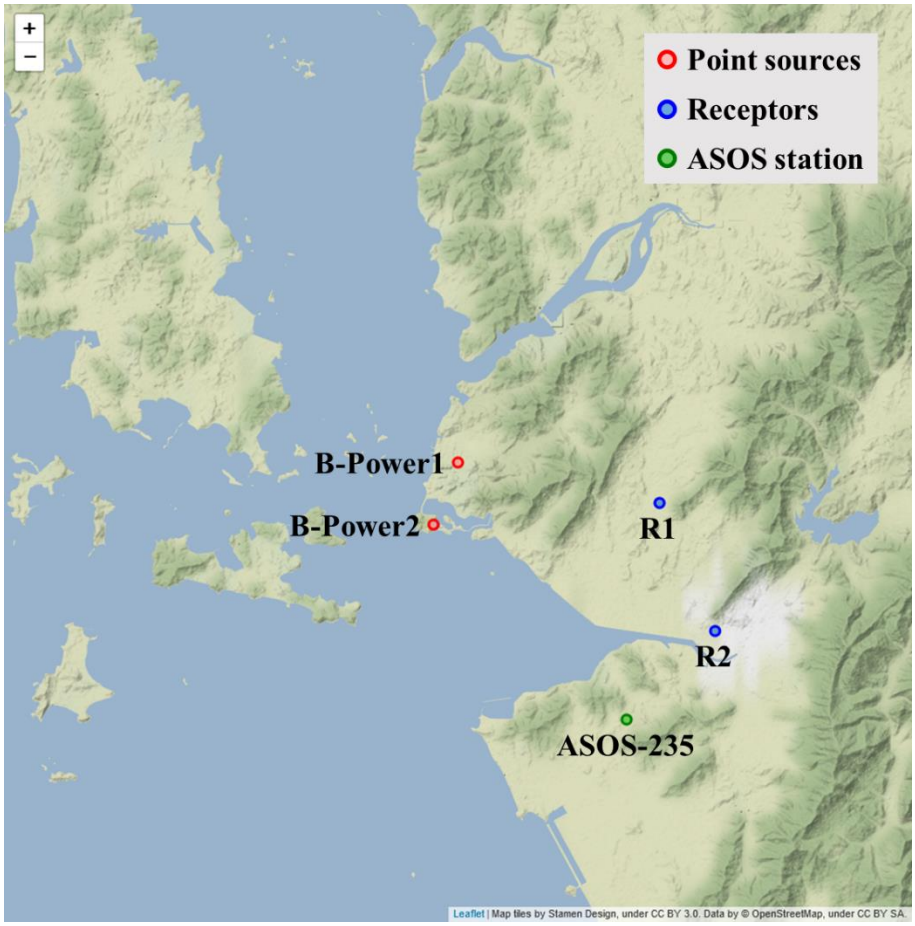

Figure 5.9. Point sources and receptor locations in Boryeong

Figure 5.10 is the distribution of wind speeds and directions measured in the ASOS-235 station. The prevailing winds throughout the year were in the N direction.

The receptor locations are 6700 m to E direction (R1) and 10000 m to ESE direction (R2) from B-Power1. The receptor locations are 7400 m to E direction (R1) and 9900 m to ESE direction (R2) from B-Power2. Both receptors were not under the influence of the prevailing winds.

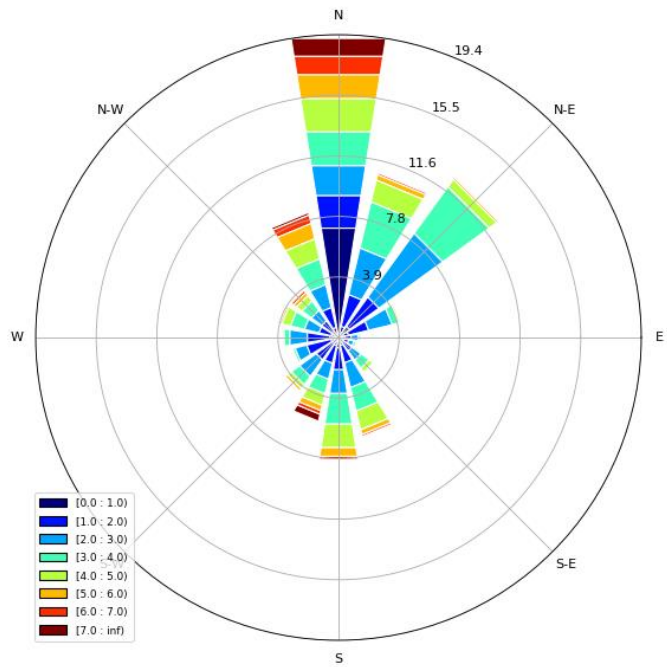

Figure 5.10. Distribution of wind speeds and directions in Boryeong, 2019

5.4.3. Results and Discussions

Figures 5.11 and 5.12 are the quantile-quantile plots of 1-hour average concentrations for the receptors in Boryeong. Tables 5.8 and 5.9 are the summary of model statistics for the receptors R1 and R2. The models performed poorly for the receptor R1, while they performed better for the receptor R2.

In the receptor R1, without terrain elevation, both XOQDOQ and AERMOD overpredicted the observed concentrations. Except for few outliers, the predicted values of XOQDOQ exceeded those of AERMOD. For the receptor R2, both models displayed better accordance between the predicted and observed concentrations.

When terrain elevation was considered in the receptor R1, the results from XOQDOQ were shifted toward overprediction. The degree of overprediction was slightly mitigated by choosing adjusted plume heights. AERMOD results showed little difference due to terrain heights. For the receptor R2, both models displayed good performance in terms of statistics. While the XOQDOQ results were biased toward overprediction, the AERMOD well performed in all the statistical indicators.

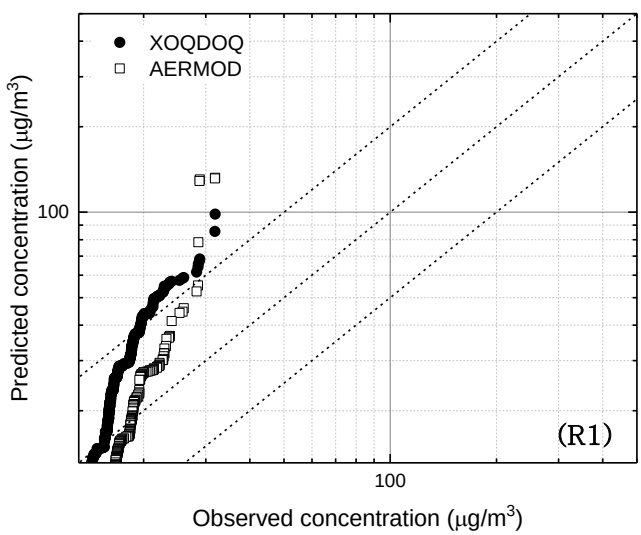

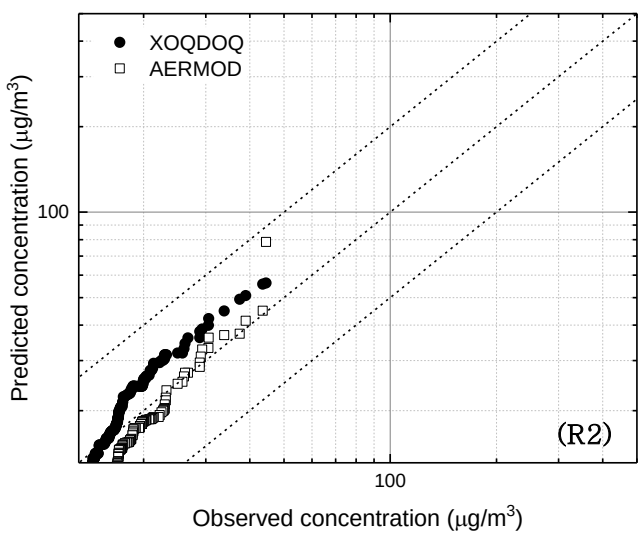

Figure 5.11. Quantile–Quantile plot based on observed and predicted concentrations for Boryeong, 2019 (without terrain)

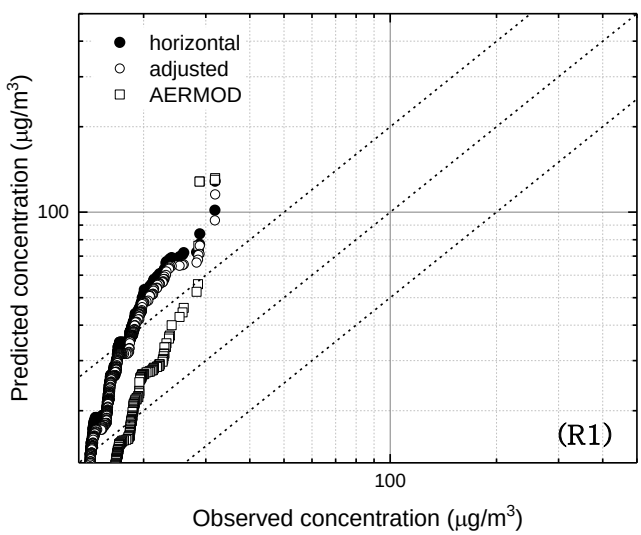

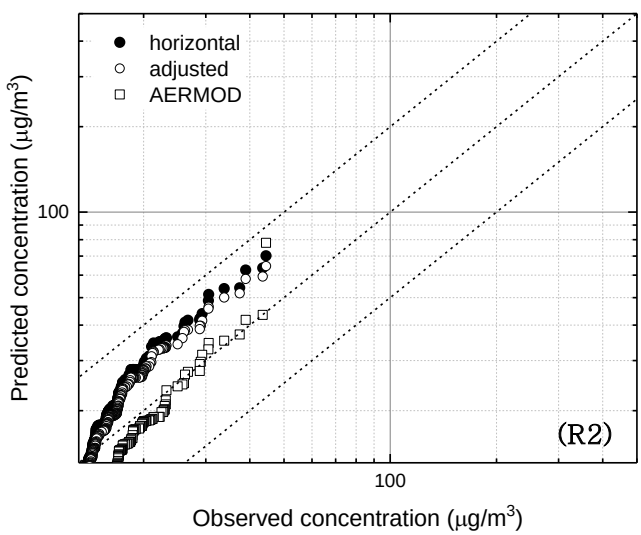

Figure 5.12. Quantile−Quantile plot based on observed and predicted concentrations for Boryeong, 2019 (with terrain)

Table 5.8. Summary of statistical analysis – Boryeong R1

Index	XOQDOQ			AERMOD	
	No terrain	Horizontal plume	Adjusted plume	No terrain	With terrain
$\mathbf{0 \leq RMSE_U}$	1.04	1.39	1.23	1.14	1.13
$\mathbf{-2 \leq \lvert FB \rvert \leq 2}$	−0.44	−0.57	−0.52	−0.23	−0.24
$\mathbf{0 \leq NMSE}$	0.42	0.66	0.55	0.63	0.62
$\mathbf{0 < FAC2 < 1}$	0.85	0.72	0.80	0.97	0.97

Table 5.9. Summary of statistical analysis – Boryeong R2

Index	XOQDOQ			AERMOD	
	No terrain	Horizontal plume	Adjusted plume	No terrain	With terrain
$\mathbf{0 \leq RMSE_U}$	0.31	0.52	0.43	0.25	0.25
$\mathbf{-2 \leq \lvert FB \rvert \leq 2}$	−0.15	−0.27	−0.23	0.06	0.07
$\mathbf{0 \leq NMSE}$	0.05	0.13	0.10	0.04	0.04
$\mathbf{0 < FAC2 < 1}$	1.00	1.00	1.00	1.00	1.00

5.5. Summary and Conclusion

Most field experiments that can be applied to validate an atmospheric dispersion model are short-term. However, since regulatory dispersion modeling focuses on annual average concentrations, validating the model based on long-term datasets is preferable.

Long-term dispersion datasets were generated by combining data from various sources. The amount of SO_2 emission from the stack was retrieved from TMS data, and hourly measurements were made in the air monitors near the emission points.

Predicted concentrations of SO_2 were compared with observed concentrations. From the annual distribution of 1-hour averaged concentrations, the models' predictability was evaluated by the statistical indicators such as $RMSE_U$, FB, $NMSE$, and $FAC2$.

It was confirmed that the current dispersion model performed well for the prevailing wind directions within the factor of 2 ranges. The XOQDOQ models tended to estimate higher concentrations compared to AERMOD in several receptors. Significant terrain elevation reinforced the overprediction in the horizontal model compared to the adjusted and AERMOD models.

It should be noted that severe uncertainties are expected in the input parameters. The uncertainties include source parameters such as the location, diameter and height of the stack, stack exit velocity, and temperature.

Chapter 6. Conclusion

In this study, the current regulatory dispersion model was evaluated for elevated release with complex terrain conditions. Preliminary assessments showed that when height information was placed in, the maximum dispersion factors increased, and their locations shifted to elevated areas. The velocity-based deposition modeling displayed more realistic results than the default approach.

The XOQDOQ results based on horizontal plume assumptions resulted in a relatively huge discrepancy with the AERMOD results. The adjusted plume height approach, on the other hand, showed comparable results.

The validation results based on the SO_2 dispersion showed that the models could predict annual high concentrations reasonably well in terms of 1-hour averages. The model showed better performance for the receptors under the influence of prevailing wind directions. Still, severe uncertainties were expected in the source locations, release heights, and emission rates.

As few domestic regulatory cases implemented dispersion modeling with terrain elevations, this study can be a reference for the future regulatory processes. Various evaluation approaches such as model intercomparison, sensitivity analysis, and long-term validation were implemented.

Future works to incorporate wet deposition and site-specific recirculation can further enhance the accuracy of the model. In addition, analyzing the modeling results in terms of seasonal and temporal variations can provide guidance on a mitigation strategy.

Bibliography

Domestic Regulatory Guides (in Korean)

- 한국원자력안전기술원, 원자로시설 부지의 기상 및 대기확산특성에 관한 조사평가, KINS/RG-N01.03, 2015.
- 한국원자력안전기술원, 경수로형 원전 안전심사지침(개정6판) 제1권, KINS/GE-N001, 2018
- 한국원자력안전기술원, 연구용 · 교육용 원자로시설 안전심사지침, KINS/GE-N10 Vol.2, 2014.

NRC Regulatory Guides

- Nuclear Regulatory Commission, Methods for Estimating Atmospheric Transport and Dispersion of Gaseous Effluents in Routine Releases from Light-Water-Cooled Reactors, Regulatory Guide 1.111 (rev. 1), 1977.
- Nuclear Regulatory Commission, NRCDose3 Code: User Guide and Technical Manual, NUREG-XXXX (DRAFT), 2019.
- Sagendorf et al., XOQDOQ: Computer Program for the Meteorological Evaluation of Routine Effluent Releases at Nuclear Power Stations, NUREG/CR-2919, 1982.

Domestic Research Reports (in Korean)

- 한국기상산업진흥원, 우리나라 대기안정도의 지역분포에 관한 연구, 기상청 기상지진기술개발사업 (CATER 2008-2107), 2009.
- 한국원자력안전기술원, 주요 국가의 제한구역에 관한 기술규정 조사분석, KINS/RR-1119, 2014.
- 한국원자력안전기술원, 원전 주요 국가의 제한구역 설정 규제기준 분석, KINS/RR-1289, 2015.
- 한국원자력안전기술원, 원자로시설의 위치제한에 대한 기술기준 개정(안) 개발, KINS/RR-1448, 2016.
- 한국원자력연구원, 하나로 시설에 대한 환경 방출물의 유도 방출한도 설정, KAERI/TR-2924, 2005.

Research Reports

- L. R. Bauer, Modelling Chronic Atmospheric Releases at the SRS: Evaluation and Verification of XOQDOQ, WSRC-RP-91-320, 1991.
- Environmental Protection Agency, AERMOD Deposition Algorithms - Science Document (Revised Draft), 2004.
- Environmental Protection Agency, Risk and Exposure Assessment to Support the Review of the SO_2 Primary National Ambient Air Quality Standards: Final Report, EPA-452/R-09-007, 2009.
- Environmental Protection Agency, Review of the Primary National Ambient Air Quality Standard for Sulfur Oxides: Risk and Exposure Assessment Planning Document, EPA-452/P-17-001, 2017.
- Environmental Protection Agency, User's Guide for the AERMOD Terrain Preprocessor (AERMAP), EPA-454/B-18-004, 2018.
- Environmental Protection Agency, AERMOD Model Formulation and Evaluation, EPA-454/R-19-014, 2019a.
- Environmental Protection Agency, User's Guide for the AMS/EPA Regulatory Model (AERMOD), EPA-454/B-19-027, 2019b.
- European Commission, Guidance on the Calculation, Presentation and Use of Collective Doses for Routine Discharges, Radiation Protection 144, 2007.
- European Commission, Assessment of the Radiological Impact on the Population of the European Union from European Union Nuclear Sites between 1987 and 1996, Radiation Protection 128, 2002.
- European Commission, Implied Doses to the Population of the EU arising from Reported Discharges from EU Nuclear Power Stations and Reprocessing Sites in the years 1997 to 2004, Radiation Protection 153, 2008.
- Health Protection Agency, The Methodology for Assessing the Radiological Consequences of Routine Releases of Radionuclides

to the Environment used in PC-CREAM 08, HPA-RPD-058, 2009.

- International Atomic Energy Agency, Site Evaluation for Nuclear Installations, Specific Safety Requirements, No. SSR-1, 2019.
- International Atomic Energy Agency, Generic Models for Use in Assessing the Impact of Discharges of Radioactive Substances to the Environment, IAEA Safety Report Series, No. 19, 2001.
- International Atomic Energy Agency, Prospective Radiological Environmental Impact Assessment for Facilities and Activities, General Safety Guide, No. GSG-10, 2018.
- National Council on Radiation Protection and Measurements, Uncertainty in NCRP Screening Models relating to Atmospheric Transport, Deposition and Uptake by Humans, NCRP Commentary, No. 8, 1993.
- National Radiological Protection Board, The Uncertainty in Dispersion Estimates Obtained from the Working Group Models, NRPB-R199, 1986.
- National Research Council, Air Quality and Stationary Source Emission Control, 1975.
- Nuclear Regulatory Commission, Regulatory Guide Periodic Review (RG 1.111), 2014.
- J. S. Scire et al., A User's Guide for the CALPUFF Dispersion Model, Earth Tech, 2000.
- J. Bluett et al., Good Practice Guide for Atmospheric Dispersion Modelling, Ministry for the Environment - New Zealand, 2004.
- M. L. Wesely et al., Deposition Parameterizations for the Industrial Source Complex (ISC3) Model, ANL/ER/TR-01/003, 2001.
- Korea Environment Institute, The Application of Air Quality Models on Environment Impact Assessment, RE-19, 2005. (in Korean)

Domestic Regulatory Documents (in Korean)

- 한국수력원자력, 최종안전성분석보고서(공개본)
- 고리 1호기, 2호기, 3, 4호기
- 신고리 1, 2호기, 3, 4호기, 5, 6호기
- 월성 2호기, 3, 4호기
- 신월성 1, 2호기
- 한빛 1, 2호기, 3, 4호기, 5, 6호기
- 한울 1, 2호기, 3, 4호기, 5, 6호기
- 한국원자력안전기술원, 기장연구로 건설허가 심사 보고서(공개본), KINS/AR-1139, 2018.
- 원자력안전전문위원회, 기장연구로 건설허가 심사보고서에 대한 검토 결과, 2019.
- 한국원자력연구원, 소형 연구로용 연료가공시설 방사선 환경영향 평가서, 2019.

Final Safety Analysis Report, received by NRC

- Dresden Units 1, 2, 3
- LaSalle Units 1, 2
- Nine Mile Point
- Oyster Creek
- Peach Bottom Units 2, 3
- Turkey Point Units 6, 7

Research Articles

- K. J. Allwine and C. D. Whiteman, Single-Station Integral Measures of Atmospheric Stagnation, Recirculation and Ventilation, Atmospheric Environment, Vol. 28, No. 4, 1994.
- N. An et al., Assessment of the Methods for Determining Net Radiation at Different Time-scales of Meteorological Variables, Journal of Rock Mechanics and Geotechnical Engineering, Vol. 9, 2017.
- L. M. Bardal et al., Evaluation of Methods for Estimating

Atmospheric Stability at Two Coastal Sites, Wind Engineering, Vol. 42, No. 6, 2018.

- M. J. Barnes et al., Spatially-varying surface roughness and ground-level air quality in an operational dispersion model, Environmental Pollution, Vol. 185, 2014.
- B. Cao et al., Development and Uncertainty Analysis of Radionuclide Atmospheric Dispersion Modeling Codes Based on Gaussian Plume Model, Energy, Vol. 194, 2020.
- L. M. T. Carbonell et al., Methodological Guide for Implementation of the AERMOD System with Incomplete Local Data, Atmospheric Pollution Research, Vol. 1, 2010.
- D. J. Carson, The Development of a Dry Inversion-capped Convectively Unstable Boundary Layer, Quarterly Journal of the Royal Meteorological Society, Vol. 99, 1973.
- J. C. Chang, and S. R. Hanna, Air Quality Model Performance Evaluation, Meteorology and Atmospheric Physics, Vol. 87, 2004.
- G. S. Choi et al., Characteristics of Regional Scale Atmospheric Dispersion around Ki-Jang Research Reactor Using the Lagrangian Gaussian Puff Dispersion Model, Nuclear Engineering and Technology, Vol. 50, 2018.
- J. Cimorelli et al., AERMOD: A Dispersion Model for Industrial Source Applications. Part I: General Model Formulation and Boundary Layer Characterization, Journal of Applied Meteorology, Vol. 44, 2005.
- A. Crawford et al., A Tracer of Opportunity Dataset for Atmospheric Transport and Dispersion Model Evaluation, 21st Joint Conference on the Applications of Air Pollution Meteorology with the A&WMA, 2020.
- L. Dresser, and R. D. Huizer, CALPUFF and AERMOD Model Validation Study in the Near Field: Martin Creek Revisited, Journal of Air & Waste Management Association, Vol. 61, 2011.
- M. D. Gibson et al., Dispersion Model Evaluation of $PM_{2.5}$, NO_X and SO_2 from Point and Major Line Sources in Nova Scotia, Canada using AERMOD Gaussian Plume Air Dispersion Model,

Atmospheric Pollution Research, Vol. 4, 2013.

- T. G. Grosch and R. F. Lee, Sensitivity of the AERMOD Air Quality Model to the Selection of Land Use Parameters, WIT Transactions on Ecology and the Environment, Vol. 37, 1999.
- S. R. Hanna, and J. C. Chang, Acceptance Criteria for Urban Dispersion Model Evaluation, Meteorology and Atmospheric Physics, Vol. 116, 2012.
- S. R. Hanna, and B. Chowdhury, Minimum Turbulence Assumptions and u* and L Estimation for Dispersion Models during Low-wind Stable Conditions, Journal of the Air & Waste Management Association, Vol. 64, 2014.
- A. A. M. Holtslag, and A. P. Van Ulden, A Simple Scheme for Daytime Estimates of the Surface Fluxes from Routine Weather Data, Journal of Applied Meteorology and Climatology, Vol. 22, 1983.
- W. T. Hwang et al., Influence of Statistical Compilation of Meteorological Data on Short-Term Atmospheric Dispersion Factors in a Hypothetical Accidental Release of Nuclear Power Plants, Journal of Radiation Protection, Vol. 37, No. 3, 2012. (in Korean)
- W. T. Hwang et al., Influence of Modelling Approaches of Diffusion Coefficients on Atmospheric Dispersion Factors, Journal of Radiation Protection, Vol. 38, No. 2, 2013. (in Korean)
- W. T. Hwang et al., Importance Analysis of Radiological Exposure by Ground Deposition in Potential Accident Consequences for the Licensing Approval of a Nuclear Power Plant, Journal of Radiation Protection, Vol. 39, No.2, 2014. (in Korean)
- H. S. Jeong et al., The Annual Averaged Atmospheric Dispersion Factor and Deposition Factor according to Methods of Atmospheric Stability Classification, Journal of Radiation Protection and Research, Vol. 41, No. 3, 2016.
- H. Jeong et al., The Effect of Calm Conditions and Wind Intervals in Low Wind Speed on Atmospheric Dispersion Factors, Annals of Nuclear Energy, Vol. 55, 2013a.

- H. Jeong et al., Analysis of Atmospheric Dispersion Factors for Building Wakes at the Wolsung Nuclear Site in Korea, Radiation Protection Dosimetry, Vol. 154, No. 4, 2013b.
- H. Jeong et al., Terrain and Building Effects on the Transport of Radioactive Material at a Nuclear Site, Annals of Nuclear Energy, Vol. 68, 2014a.
- H. Jeong et al., Numerical Simulation of Air Pollutant Dispersion Using an in situ Tracer Experiment at a Nuclear Site, Annals of Nuclear Energy, Vol. 73, 2014b.
- Jones et al., Assessing the Possible Radiological Impact of Routine Radiological Discharges from Proposed Nuclear Power Stations in England and Wales, Journal of Radiological Protection, Vol. 33, 2013.
- H. Ju et al., Long-term Trend Analysis of Key Criteria Air Pollutants over Air Quality Control Regions in South Korea using Observation Data and Air Quality Simulation, Journal of Korean Society for Atmospheric Environment, Vol. 34, No. 1, 2018. (in Korean)
- J. D. W. Khal, and H. L. Chapman, Atmospheric Stability Characterization Using the Pasquill Method: A Critical Evaluation, Atmospheric Environment, Vol. 184, 2018.
- E. H. Kim et al., Analysis of the Site Characteristics of Korean Nuclear Power Sites from the Meteorological Aspects, Annals of Nuclear Energy, Vol. 34, 2007.
- C. Langner, and O. Klemm, A Comparison of Model Performance between AERMOD and AUSTAL2000, Journal of the Air & Waste Management Association, Vol. 61, 2011.
- H. D. Lee et al., Evaluation of Concentrations and Source Contribution of PM_{10} and SO_2 Emitted from Industrial Complexes in Ulsan, Korea: Interfacing of the WRF-CALPUFF Modelling Tools, Atmospheric Pollution Research, Vol. 5, 2014.
- G. B. Lee et al., Applicability Evaluation of Gaussian Plume Model (XOQDOQ) for Assessing Radiological Impact Assessment of Radioactive Materials around the Nuclear Power Plant Site with

the Comoplex Terrain in Korea, 18th International Conference on Harmonisation within Atmospheric Dispersion Modelling for Regulatory Purposes, 2017.

- S. J. Lee et al., An Automated Monitoring of Atmospheric Mixing Height from Routine Radiosonde Profiles over South Korea using a Web-based Data Transfer Method, Environmental Monitoring and Assessment, Vol. 186, 2014.
- S. J. Lee, Source Identification of PM_{10} and SO_2 in a Multi-industrial City of Korea, Master's Thesis, UNIST, 2018.
- S. J. Lee, and S. D. Choi, Determination of PM_{10} and SO_2 Source Contribution using Emission Inventory Data in the Multi-industrial City of Ulsan, South Korea, Turkish National Committee for Air Pollution Research and Control (TUNCAP), 2019.
- A. Leelossy et al., A Review of Numerical Models to Predict the Atmospheric Dispersion of Radionuclides, Journal of Environmental Radioactivity, Vol 182, 2018.
- I. H. Lim, and S. H. Bae, A Study on Development of the Meteorological Data Preprocessing Program for Air Pollution Modeling, The Journal of the Korea Institute of Electronic Communication Sciences, Vol. 10, No. 1, 2015. (in Korean)
- G. E. Long et al., An Analysis of AERMOD Sensitivity to Input Parameters in the San Francisco Bay Area, 13th Conference on the Applications of Air Pollution Meteorology with the Air and Waste Management Assoc., 2004.
- E. R. Lutman et al., Comparison between the Prediction of a Gaussian Plume Model and a Lagrangian Particle Dispersion Model for Annual Average Calculations of Long-range Dispersion of Radionuclides, Journal of Environmental Radioactivity, Vol. 75, 2004.
- M. Mohan, and T. A. Siddiqui, Analysis of Various Schemes for the Estimation of Atmospheric Stability Classification, Atmospheric Environment, Vol. 32, No. 21, 1998.
- D. M. Moreira, T. Tirabassi, and J. C. Carvalho, Plume Dispersion Simulation in Low Wind Conditions in Stable and Convective

Boundary Layers, Atmospheric Environment, Vol. 39, 2005.

- M. G. Na et al, Atmospheric Dispersion Assessment for Potential Accidental Releases at Yonggwang Nuclear Power Plants, Journal of Radiation Protection and Research, Vol. 25, 2000.
- N. Nelson et al., Assessment of Routine Atmospheric Discharges from the Sellafield Nuclear Installation – Cumbria UK, Atmospheric Environment, Vol. 36, 2002.
- H. R. Olesen, and J. C. Chang, Consolidating Tools for Model Evaluation, International Journal of Environment and Pollution, Vol. 40, 2010.
- S. G. Perry, CTDMPLUS: A Dispersion Model for Sources near Complex Topography. Part I: Technical Formulations, Journal of Applied Meteorology and Climatology, Vol. 31, 1992.
- S. G. Perry et al., AERMOD: A Dispersion Model for Industrial Source Applications. Part II: Model Performance against 17 Field Study Databases, Journal of Applied Meteorology, Vol. 44, 2005.
- Richter, State of the Art Atmospheric Dispersion Modelling: Should the Gaussian Plume Model Still be Used? KERNTECHNIK, Vol. 81, No. 5, 2016.
- A. A. Romanov et al., Graz Lagrangian Model (GRAL) for Pollutants Tracking and Estimating Sources Partial Contributions to Atmospheric Pollution in Highly Urbanized Areas, Atmosphere, Vol. 11, 2020.
- P. Seibert et al., Review and Intercomparison of Operational Methods for the Determination of the Mixing Height, Atmospheric Environment, Vol. 34, 2000.
- B. Sportisse, A Review of Parameterizations for Modelling Dry Deposition and Scavenging of Radionuclides, Atmospheric Environment Vol. 41, 2007.
- J. M. Stockie et al., The Mathematics of Atmospheric Dispersion Modelling, Siam Review, Vol. 53, No. 2, 2011.
- R. Stull, A Reevaluation of Two Dispersion Theories, Journal of Atmospheric Sciences, Vol. 45, 1988.

- D. Tartakovsky et al., Evaluation of AERMOD and CALPUFF for Predicting Ambient Concentrations of Total Suspended Particulate Matter (TSP) Emissions from a Quarry in Complex Terrain, Environmental Pollution, Vol. 179, 2013.
- P. Thunis et al., Performance Criteria to Evaluate Air Quality Modeling Applications, Atmospheric Environment, Vol. 59, 2012.
- B. Turner, The Long Lifetime of the Dispersion Methods of Pasquill in U.S. Regulatory Air Modeling, Journal of Applied Meteorology, Vol. 36, 1996.
- Venkatram et al., A Complex Terrain Dispersion Model for Regulatory Applications, Atmospheric Environment, Vol. 35, 2001.
- 김정미 외, 한울원전 대기확산모델 부지적합성 검증 실험 설계, 대한방사선방어학회 추계 학술발표회 논문요약집, 2017. (in Korean)
- 김정미 외, 야외추적자 확산실험을 이용한 대기확산모델 부지적합성 예비 검증, 대한방사선방어학회 춘계 학술발표회 논문요약집, 2018. (in Korean)
- 이갑복 외, 월성원전 주변 삼중수소 농도 측정값을 이용한 XOQDOQ 전산코드의 부지 적용성 검토, 한국방사성폐기물학회 추계학술논문요약집, 2014a. (in Korean)
- 이갑복 외, 삼차원 모델 결과 비교를 통한 XOQDOQ 전산코드의 월성원전 부지 적용성 검토, 대한방사성방어학회 추계 학술발표회 논문요약집, 2014b. (in Korean)
- 황원태 외, 방사성유출물에 의한 주민선량평가시 강우에 의한 습침적 영향, 대한방사선방어학회 춘계 학술발표회 논문요약집, 2016. (in Korean)

국문 초록

연구로와 소형 원전은 시설 규모가 작아 기존 원전에 비해 제한구역경계 거리를 짧게 설정할 수 있다. 단축된 경계거리에서 기체 방사성물질 방출에 따른 지표면에서의 농도를 평가하는데 있어서, 사업자는 지표면방출보다 고공방출 시나리오를 선호한다. 그러나 현행 규제지침에서 정하는 대기확산평가 모델은 고공방출 및 복잡 지형에 대한 평가에는 부적합하다는 지적이 있었고, 관련된 국내 적용 사례도 부족한 상황이다. 향후 규제 혼선을 방지하기 위해서는 현행 대기확산평가 방식에 대한 정비와 신규 모델로의 채용 가능성에 대한 검토가 필요하다. 본 연구는, 현행 대기확산평가 모델을 검증하여 개선 사항의 도출과 방안을 제시하는데 목적이 있다.

현행 대기확산평가 모델의 분석을 위해 XOQDOQ에 기반한 평가 코드를 작성하였다. 일정한 수평 방향의 플룸 이동만을 가정했던 기존 코드와는 달리, 플룸 중심선의 높이가 대기안정도와 지형 고도를 반영하여 재조정될 수 있도록 하는 모듈을 추가하였다. 침적인자 계산 시에는 상대 침적률 함수를 적용하는 대신, 부지 기상 인자로부터 침적 속도를 산정함으로써 대기확산인자와 침적인자가 연계되도록 하였다.

예비 평가는 월성과 고리 부지를 대상으로 2016-2018년의 기상자료에 근거하여 수행하였다. 재순환 인자의 적용과 풍속 측정 고도의 보정 방식에 따라 대기확산인자가 변화하는 경향을 확인하고, 혼합방출을 가정했을 때의 결과를 고공방출 시 결과와 비교하였다. 고공방출 시 지형 고도를 반영할 경우, 대기확산인자의 최댓값이 증가하고 최댓값 지점은 지형 고도가 높은 지점으로 이동하였다. 혼합방출 상황에서 300 m 지점의 대기확산인자 최댓값은 고공방출 시의 최댓값들보다 항상 더 큼을 확인하였다.

환경영향평가 목적의 대기확산평가 모델인 AERMOD와의 비교 분석을 수행하였다. AERMOD 입력 인자 계산을 위해 원전 부지에서 측정된 기상자료와 기상청이 제공하는 지상 및 고공에서 관측한 기상자료를 결합하는 전처리 코드를 작성하였다. 지형 고도를 반영하지 않았을 때 XOQDOQ와 AERMOD 두 모델의 평가 결과가 큰 차이를 보이지 않았으나 지형 고도를 반영한 결과 XOQDOQ 평가치가 최댓값 기준 약 8배에서 27배까지 증가한 반면, AERMOD 평가치의 증가폭은 약 2배 이내로 제한되었다. 지형 정보를 반영하여 플룸 높이를 조정한 경우에는 XOQDOQ 평가치의 증가폭이 약 4배 이내로 제한되었고, 최대

지점이 형성되는 위치도 AERMOD 평가치에 근접함을 확인하였다.

새로 정비한 대기확산평가 모델에 대한 검증을 위해, 대기오염물질 확산을 평가하고 장기간 국내 대기오염 모니터링 자료와 비교하였다. 관찰 지점에서 측정된 대기오염물질의 1시간 평균 농도 자료로부터 도출한 연간 농도 분포를 기준으로 비교한 결과, 현행 대기확산모델은 풍향 발생 빈도가 큰 주풍향 지점에 대해서는 2배 이내 범위 결과를 산출하였다. 모델의 과대/과소 예측과 관련한 특이성은 없었으나, 몇 개 관찰 지점에서는 지형 고도의 반영에 의해 오염도가 높게 평가됨을 확인하였다. 정확한 방출 위치와 지형 고도 값의 불확실성과 연간 방출량이 일정하다는 가정으로 전산 모사가 수행되었다는 점에서 본 검증은 한계를 갖는다.

본 연구를 통해 첫째, 현행 규제지침이 제시하는 바의 고공방출 및 지형 고도 반영 방법에 따라 대기확산 평가를 실시하였다. 국내 적용 사례가 드물었던 고공방출 상황에 대해 모델 요소 분석을 수행하였고, 지형 고도 반영에 의한 확산 분포의 변화를 확인하였다. 향후 고공방출 방식의 채용 여부를 결정하는데 참고가 될 수 있으리라고 생각된다.

둘째, 현행 대기확산 모델에 대한 다각도의 평가 즉, 모델 간 비교, 민감도 분석, 장기간 검증 등을 수행하였다. 대기오염물질의 환경 영향 평가를 목적으로 개발된 확산 평가 모델과 비교할 때, 지형 고도를 반영하지 않을 경우 두 모델의 확산 농도 계산 결과가 작은 차이를 보이고, 지형 고도를 반영할 경우에는 현행 모델에 기반한 확산농도 평가치가 큼을 확인하였다.